SAPIENZA
UNIVERSITÀ DI ROMA

Study on the Benefits of Lattice Structures within the Framework of High-Performance Structural Design: A Case Study.

Ph.D. Thesis.

Doctorate Degree in Industrial and Management Engineering.

Doctoral Student: ***Abas Ahmad.***
(Matricola: 1773063)

Advisor: ***Prof. Francesca Campana, PhD.***

Co-advisor: ***Ing. Valerio Pettinacci, (INFN).***

Faculty of Civil and Industrial Engineering
Department of Mechanical and Aerospace Engineering

(Academic Year 2022/2023)

SAPIENZA
UNIVERSITÀ DI ROMA

Faculty of Civil and Industrial Engineering.
Department of Mechanical and Aerospace Engineering.

Study on the Benefits of Lattice Structures within the Framework of High-Performance Structural Design: A Case Study.

Ph.D. Thesis.

Doctorate Degree in Industrial & Management Engineering.

Doctoral Student
Abas Ahmad.
(Matricola: 1773063)

Advisor
Prof. Francesca Campana, PhD.

Co-advisor
Ing. Valerio Pettinacci, (INFN).

(Academic Year 2022/2023)

Preface

The work presented in this thesis for the Ph.D. degree pertains to the Ph.D. course: Industrial and Management Engineering (36th Cycle). The basic aim of this project is to study the benefits of lattice structures within the framework of high-performance structural design. This research work concludes that the effective application of lattice structures may help to obtain innovative and high-performance structures. This is done by proposing a design-development workflow, which abridges the gap between the design and manufacturing workflows of the structural design concerning the innovative structures, and subsequently facilitate the development of the innovative structures with virtual prototyping and additive manufacturing (AM). The validation case study (a real application) for this project is provided by the industrial partner INFN (Istituto Nazionale di Fisica Nucleare/National Institute for Nuclear Physics) Rome (Italy). This case study is a part of the BULLKID project, which is developing the next-generation cryogenic detectors for Particle Physics research, in the field of neutrino and dark matter.

This work was carried out at the Department of Mechanical and Aerospace Engineering (DIMA), University of Rome (Italy), and INFN (Department of Physics), Sapienza University of Rome (Italy). The Ph.D. project was supervised by the academic advisor Prof. Francesca Campana (Department of Mechanical and Aerospace Engineering), and the industrial co-advisor Ing. Valerio Pettinacci (INFN, Rome). I would like to express my sincere thanks to my both advisors for inspiring me to do this work, and for their helpful advice, suggestions, support, encouragement, and patience when I needed it.

The design work was carried out at DIMA (Sapienza) and INFN (Rome). The production of the prototype pertaining to additive manufacturing (AM) was carried out at the LNGS department of INFN, Gran Sasso (Italy), and so I would also like to thank to Dr.-ing. Daniele Cortis (In-charge of the Additive Manufacturing–LNGS Gran Sasso) for his guidance and cooperation.

I would also like to thank Prof. Marco Vignati (Department of Physics, Sapienza University of Rome), and his research team for their valuable ideas and insightful collaboration throughout the entire processes of design, production, assembly, and physical testing/functional validation.

This work was financially supported by the mutual collaboration of Regione Lazio (Italy), and INFN Rome (Italy). This support is gratefully acknowledged.

Last but not least, I would also like to thank my colleagues in my Research Group for their technical support, and my family & friends for their moral and social support through the years.

Roma (Italy), October 2023
Abas Ahmad

Abstract

The design and development of the innovative structures require rigorous and robust efforts when they are based on complex geometries, involving multi-physics functionalities/behavior, subjected to other assembly components, and to be prototyped with additive manufacturing. Additive manufacturing allows us to explore new topologies that may fulfill many functional requirements. Lattice structures are part of these new topologies, providing abundant promising advantages, such as lightweight design, functional graded solutions, etc. In this work we investigate the state of the art of lattice structures in respect of their related field of applications and we apply this knowledge to support the design of a high-performance device, such as next-generation cryogenic detectors for particle physics research. Lattice structures pose many challenges in the field of the CAD-CAE approaches, since it requires managing a multiscale modelling domain. This may reduce the capability of young engineers to completely accomplish the design workflow with efficiency. This thesis aims to investigate a design-development workflow suitable to guarantee this efficiency, and subsequently facilitates the development of innovative structures with virtual prototyping and additive manufacturing.

The followed approach was:

- To investigate the state of the art of lattice design modelling and simulation.
- To define a design-development workflow suitable to accomplish functional, performance and process requirements.
- To test the design-development workflow through the design of a high-performance device.

The proposed design-development workflow is based on a comprehensive list of requirements engulfing all the design, functional, assembly, and manufacturing requirements to fulfill the desired objectives. This list of requirements is then successfully translated into the initial design phase to facilitate the subsequent 3D modelling, manufacturing, and assembly phases.

The validation case study is a real application of BULLKID Project, provided by the industrial partner INFN (Istituto Nazionale di Fisica Nucleare/Italian National Institute of Nuclear Physics) Rome (Italy). BULLKID is developing the next-generation cryogenic detectors for Particle Physics research, in the field of neutrino and dark matter. The detectors are operated at 10 mK temperature in a

high vacuum and light-tight environment. This case study is basically a multi-physics problem, and it is based on multi-objective design optimization. Main challenges concerning the research work are to hold the detector with the least possible mechanical vibrations, excellent thermal contact, and stacking up several of them in a closely packed structure. In addition, the proposed design should be lightweight, thermal efficient, and the protype of the wafer holders and the wafer holding ring should be developed with additive manufacturing (AM) technology (SLM technique) to ensure maximum flexibility in the design and to obtain the fine features required for the final structure.

The design optimization is carried out in two stages: first without the lattice structure, and second with the lattice structure. In the first optimization stage, it is ensured that the optimized design (without lattice) has the capability to stack up three wafer assemblies successfully in the prototype, withstand a fail-safe cryogenic operation (ensuring an improved rigidity with respect to vibration issues detected during the experimental run of the previous design), and the prototyping of complex components with AM in accordance with the stipulated requirements. In the second optimization stage, the infill volume lattice (with an optimal cell structure) is employed in the wafer holding ring, under the consideration of the assembly constraints, to further reduce the structural weight, reduce the mechanical vibrations, and improve the thermal efficiency. In addition, to facilitate the AM of the desired component and minimize the possible thermal distortion, the support structure for the AM is also designed with an optimized lattice structure.

The proposed design is initially validated through numerical simulations (structural, modal, and thermomechanical analysis), and virtual 3D CAD assembly. However, it is physically validated through prototyping and subsequent experimental tests. In addition, 3D scanning of the additively manufactured components is also performed through the reverse engineering technique of photogrammetry, as a quality check of the AM process.

In conclusion, the proposed design successfully supports up to three detector assemblies. It also reduced the structural weight, mechanical vibrations, and improved thermal efficiency, as warranted by the design requirements.

Contents

Preface iii

Abstract v

1. Chapter: Lattice Structure in Mechanical Design. 1

1.1. Lattice Structures. 1

1.2. Classification of Lattice Structures. 2

1.2.1. Unit Cell Characteristics. 3

1.2.2. Characteristics of the Cell Replication Pattern. 6

1.3. Mechanical Behavior. 9

1.4. Applications of Lattice Structures. 11

1.5. References. 14

2. Chapter: Issues on Design and Manufacturing of Lattice Structures. 19

2.1. Manufacturing of Lattice Structures. 19

2.2. Designing and Modelling of Lattice Structures. 21

2.3. Conclusion of the Literature Review. 22

2.4. References. 23

3. Chapter: Test Case Study. 27

3.1. Introduction to the PhD Project. 27

3.2. Test Case Study. 27

3.3. Details of the Stakeholders. 30

4. Chapter: Methodology and Workflow. 31

4.1. Methodology and Materials. 31

4.2. Aim and Objectives. 36

4.3. Design and Manufacturing Details of the New Design. 36

5. Chapter: Design via Virtual Prototyping. 38

5.1. Design of the Wafer Holding Ring. 38

5.2. Design of the Wafer Holders. 40

5.3. Design of the Thermalization Rods. 41

5.4. Design of the Aluminium Casings. 42
5.5. Design of the Aluminium Casings' Bolt. 45
5.6. Design Modification of the Cryogenic Device Mounting Plates. 46
5.7. Virtual Assembly 47
5.7.1. Wafer Assembly (WA) 48
5.7.2. DA Stage-1. 49
5.7.3. DA Stage-2. 50
5.7.4. Final Assembly 51
5.8. Mass Details of the New DA (without Lattice) 55
6. Chapter: Structural Performance Assessment via FEA. 56
6.1. FEA Modelling. 56
6.2. Materials & Properties. 57
6.3. Meshing. 57
6.4. Loads and Boundary Conditions. 59
6.5. FEA Simulations. 61
6.5.1. Structural Analysis. 61
6.5.2. Modal Analysis. 64
6.5.3. Thermomechanical Analysis 66
6.5.4. Transient Thermal Analysis 70
7. Chapter: Physical Prototyping, Assembly, and 3D Scanning. 74
7.1. Prototyping via Additive Manufacturing (SLM). 74
7.2. Prototyping via Conventional Manufacturing. 79
7.3. Physical Assembly. 81
7.4. 3D Scanning of the Wafer Holding Ring. 83
7.5. Physical Experimentation 85
8. Chapter: Optimization Study via Lattice. 86
8.1. Design of the Lattice Structure 86
8.2. FEA Simulations. 88

8.2.1. Structural Analysis 89
8.2.2. Modal Analysis of the Lattice Structure 90
8.2.3. Thermomechanical Analysis of the Lattice Structure 90
8.2.4. Transient Analysis of the Lattice Structure 91
9. Chapter: Results & Discussion, Conclusions & Future Work. 93
9.1. Results and Discussion. 93
9.1.1. Comparison of the Structural Analysis. 93
9.1.2. Comparison of the Modal Analysis. 94
9.1.3. Comparison of the Thermomechanical Analysis. 95
9.1.4. Comparison of the Transient Thermal Analysis. 95
9.1.5. Comparison of Total Mass. 96
9.2. Conclusions 97
9.3. Future Work 98
List of Figures 100
List of Tables 102
List of Symbols and Acronym 103

1. Chapter: Lattice Structure in Mechanical Design.

This chapter describes the first part of the literature review, which is related to the lattice structures, its classification, and its state-of-the-art applications in various engineering fields, particularly in Mechanical Design.

1.1. Lattice Structures.

A lattice structure is made by a unit cell that is repeated in the space, making a larger functional structure; thus, it is a peculiar kind of cellular structure. The basic idea of cellular structures evolved from natural organic structures such as bamboo, bone, cork, etc. For the very first time, the concept of cellular structures was introduced by Gibson and Ashby [1,2]. Initially, they classified cellular structures into foam (open cell and closed cell, ***Figure 1-1****a,b*) and honeycomb. Foam's cell shape and pattern are usually defined by random distributions, while the honeycomb structure has a regular 2D hexagonal unit cell, and the cell walls are uniformly oriented in the space (as shown in ***Figure 1-1****c*) [1,2,5]. In open-cell foam, the cells are not totally enclosed by their walls, while in closed-cell foam, the cells are entirely enclosed by their walls. Despite these differences, the component is always defined from a micro/mesoscale cell, replicated to fill the overall macroscale volume. However, the cellular structures were later classified [3,4] into three main categories: foam, honeycomb, and lattice.

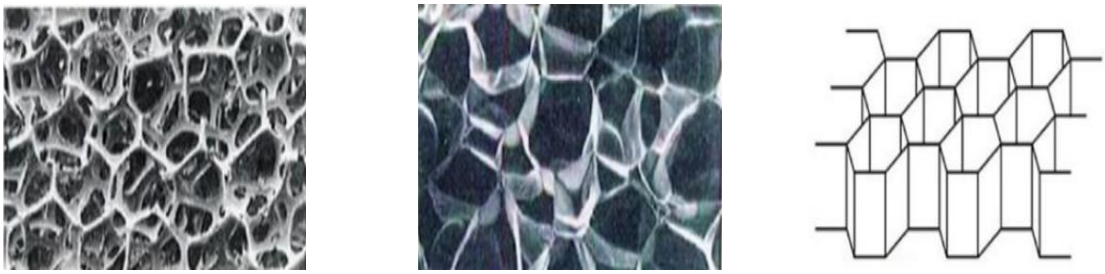

(a). Open Cell Foam. (b). Open Cell Foam. (c). Honeycomb.

Figure 1-1. *Cellular Structures.*

According to the literature, in many applications, lattice structures have been found to be superior to their other cellular counterparts, such as foam and honeycomb structures. A more in detail strength-to-weight ratio and mechanical performance, such as energy absorption or compliance, is generally better due to the tailored shape of the cell and the replication pattern [6,7]. Moreover, they can support functional designs, such as heat exchangers or fluid conveyors, as demonstrated in [8]. More recently, taking inspiration from natural organic structures such as bones and plant stems, the concept of graded densities increased the spread of lattice structures, for example, being used to optimize load distributions [9,10]. It also furthers the evolution towards multigrade lattice structures, coupled with different materials. From this, the concept of multigrade and multifunction lattices arises. These are the solutions in which not only the type

of unit cells but also the cell's density and materials are distributed to gain a specific performance or function. Multigrade lattice structures have numerous applications, i.e., to enhance stiffness [11], to increase energy absorption capability [12–17], to improve thermal exchange efficiency [18,19], to tailor specific behaviors such as a negative Poisson's ratio [20–22], etc.

From the manufacturing point of view, Additive Manufacturing (AM) is often considered as a specific technology to manufacture lattice structures; indeed, the capability of reproducing specific cell designs and distribution through AM increases the fields of investigation pertaining to lattice structures in the respect of foams. Nevertheless, foams obtained by blowing agents (in batch foaming, extrusion, or injection molding) may have a superior reliability concerning the mechanical characteristics since the AM interlayer interfaces may present delamination and, thus, crack propagation [23]. Besides this aspect, the advancements in AM with multigrade materials for lattice structures have gained immense popularity, providing an extraordinary performance and array of functions [24,25].

Due to these promising characteristics, lattice structures have been extensively studied and they are still undergoing rigorous research to support numerous industrial applications. Research on lattice structures ranges in many fields, such as mechanical characterization, manufacturing processes and its final shape control, and cell and pattern designs in respect of their applications.

1.2. Classification of Lattice Structures.

According to [23], lattice structures may be classified based on:

- The unit cell's characteristics, which include topology, cell's element geometry, and cell's size.
- The characteristics of the cell's replication pattern.

However, in [26,27], the classification of the lattice structure has been discussed in more detail; therefore, the latest classification of lattice structure can be shown as ***Figure 1-2.***

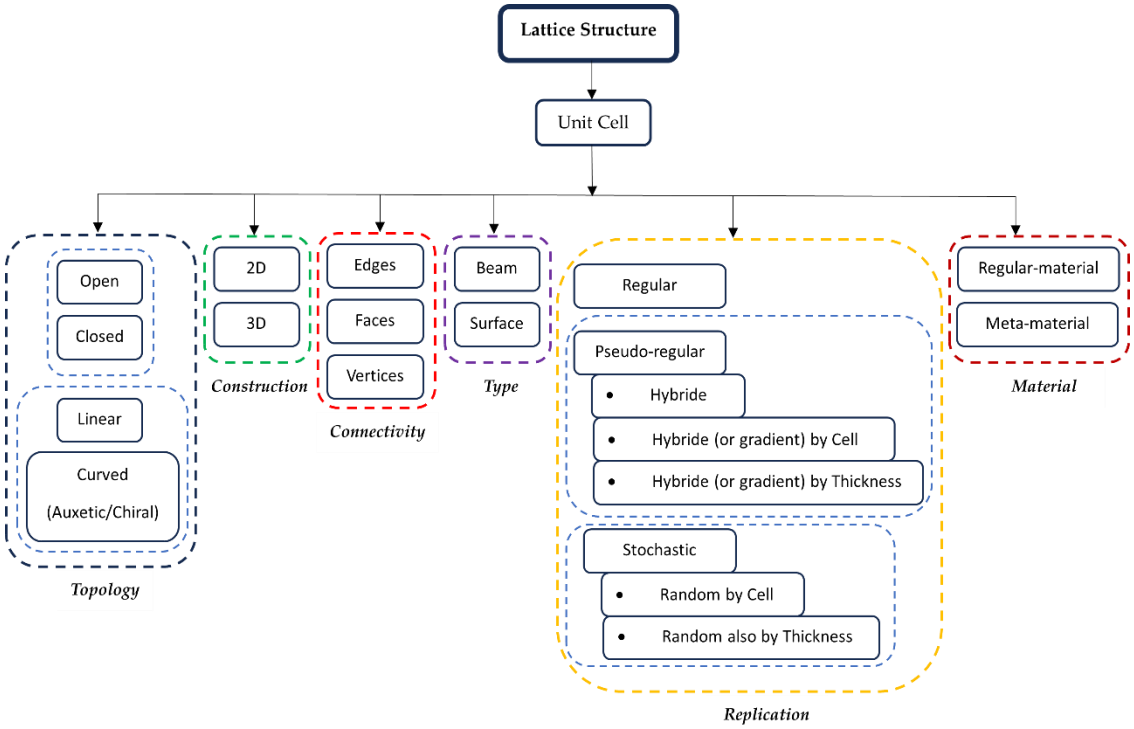

Figure 1-2. *Classification of Lattice Structure.*

1.2.1. Unit Cell Characteristics.

A topology-based classification defines whether the cells are closed or open and how many cells' faces are open, while a cell's element geometry, according to [2], distinguishes between cells made of struts and cells made of plates or shells, introducing a structural behavior classification of the cells. A cell's element geometry includes a geometrical definition of the structural elements (sections, number of edges, etc.) [6,7,23,28], and the size, including all the dimensional elements that define a cell (e.g., section size and axial length for struts, length, width, and thickness for plate/shell). The cell's element geometry, indeed, may also constrain the topology of the cell (e.g., strut cells are always open, shells and plates may be open with different geometrical shapes). Concerning the cell's size, the distinction between homogeneous and heterogeneous defines whether the structural elements of the cell are constant or not. ***Figure 1-3*** and ***Figure 1-4*** show an overview of strut-based and surface-based lattice cells, respectively.

Concerning strut-based unit cells, Simple Cubic (SC), Body-Centered (BC), and Body-Centered Cubic (BCC) are derived from the same cubic cell, just with an increasing number of beams [23,29–31]. The Octet Truss (OT) cell comes from the face-centered cell [32]. Other frequently used cells are the modified Gibson–Ashby (GA) and the modified Wallach–Gibson (WG) cells [6,7,23,28]. ***Figure 1-3****h* shows an example of a re-entrant cell.

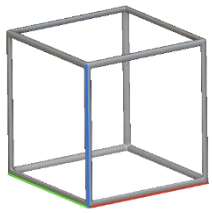

(a). Simple Cubic Cell.

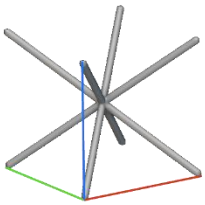

(b). Body Centered Cubic Cell.

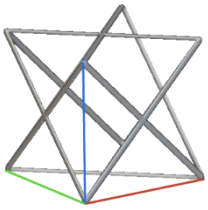

(c). Face Centered Cubic Cell.

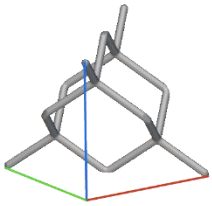

(d). Diamond Cell.

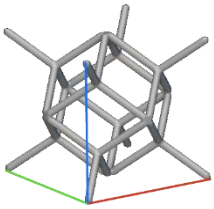

(e). Fluorite Cell.

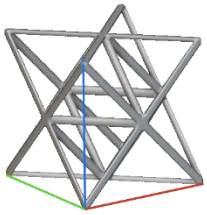

(f). Octet Cell.

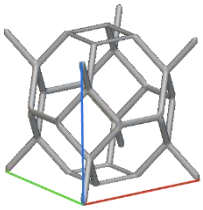

(g). Truncated Octahedron Cell.

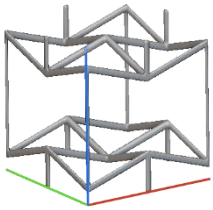

(h). Re-entrant Cell.

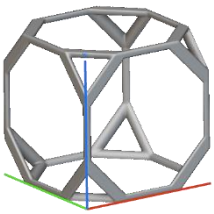

(i). Truncated Cubic Cell.

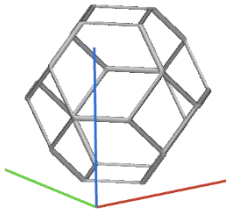

(j). Kelvin Cell.

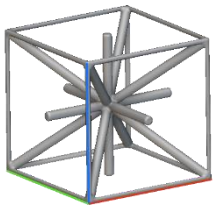

(k). Iso Truss Cell.

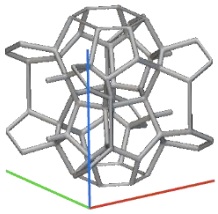

(l). Weair-Phelan Cell.

Figure 1-3. *Beam Lattice (generated with nTop).*

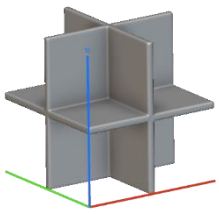

(a). Surface-based lattice.

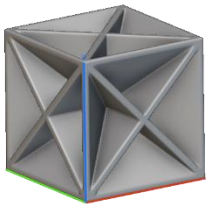

(b). Body Centered Cubic Foam Cell.

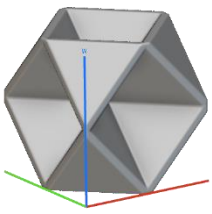

(c). Face Centered Cubic Foam Cell.

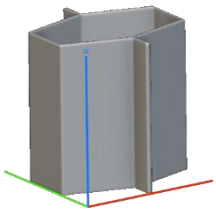

(d). Hexagonal Honeycomb Cell.

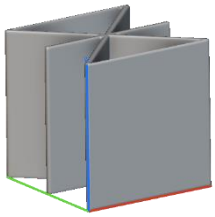

(e). Triangular Honeycomb Cell.

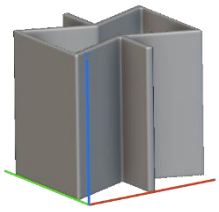

(f). Re-entrant Honeycomb Cell.

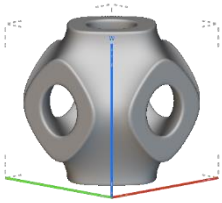

(g). Schwartz Cell.

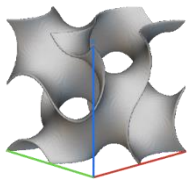

(h). Gyroid Cell.

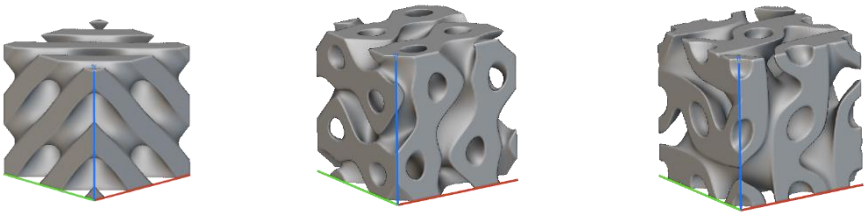

(i). Diamond Cell. *(j). Split-P Cell.* *(k). Lidinoid Cell.*

Figure 1-4. *Surface-based Lattice (generated with nTop).*

It is an auxetic cell designed to present a negative Poisson's ratio, which means that the cell enlarges when stretched and contracts when compressed [33-36].

Concerning surface-based unit cells, we can distinguish between plate and shell cells, and more generally the surface-based cells like Triply Periodic Minimal Surface (TPMS). In [37], according to Gibson, plate cells were investigated connecting some struts of ***Figure 1-3*** with plates, as shown for example in ***Figure 1-4****a-c*. These solutions, although may be replicated as periodic and regular, are often considered a type of closed foam, as said in [38]. Honeycomb lattice [28], in ***Figure 1-4****d-f*, may have unit cells hexagonal, triangular, and recently also the re-entrant configurations have been studied.

Triply Periodic Minimal Surface (TPMS) are being widely investigated. They are bio-inspired cells with boundary surfaces with zero-mean curvature at every point [39,40]. TPMS are relevant as functionally graded structures, since their geometric characteristics allow them to reach different surface-related properties (e.g., manufacturability, fluid permeability, electrical and thermal conductivity) . According to the procedure adopted to model them, they can be classified in skeletal and sheet TPMS. In the first case, a volume is trimmed by the TPMS, and the remaining part is thinned (skeletonized) with assigned thickness. In the second case, the TPMS surface represents the shell sheet that is subsequently thickened.

TPMS Formulation:

From the mathematical point of view, a TPMS is an infinite surface, periodic along three mutually orthogonal directions, that satisfies the following conditions:

$$H(x,y,z) = 0, H = \frac{K_1+K_2}{2} \qquad \textbf{Equation 1-1}$$

where *k1* and *k2* stand for the principal curvatures of the surface at a general point *P*. Many authors studied the theoretical formulations of TPMS starting from different mathematical points of view. In [39], the level set method, an approach applied in mechanical engineering to optimize topology in accordance with structural requirements, is adopted to study five TPMS, namely Primitive, Gyroid, IWP, Diamond, and Fisher-Koch. Assuming that a TPMS may

be described by a sum of Fourier terms, and that its leading term is the basis function of TPMS i.e., *φ(x,y,z)*, TPMS can be achieved as iso-level curves:

$$\varphi(x,y,z) = const \qquad \textbf{Equation 1-2}$$

Subjected to Equation (1-2). Equations from (1-3) to (1-5) show three formulations achieved according to such reasoning and reported in ***Figure 1-4****g-i***.**

Schwartz primitive:

$$\varphi(x,y,z) = (cosx) + (cosy) + (cosz) \qquad \textbf{Equation 1-3}$$

Schwartz diamond:

$$\varphi(x,y,z) = (cosx)(cosy)(cosz) - (sinx)(siny)(sinz) \qquad \textbf{Equation 1-4}$$

Gyroid:

$$\varphi(x,y,z) = (sinx)(cosy) + (siny)(cosz) + (sinz)(cosx) \qquad \textbf{Equation 1-5}$$

where:

$$\mathrm{X} = 2\pi\frac{X}{L_x}, \qquad \textbf{Equation 1-6}$$

$$\mathrm{Y} = 2\pi\frac{Y}{L_y},$$

and

$$Z = 2\pi\frac{Z}{L_z}.$$

The L_x, L_y, and L_z are the unit cell size in *x, y* and *z* directions. x, y, and z are the periodicities, while the X, Y, and Z are the cell's repetitions.

1.2.2. Characteristics of the Cell Replication Pattern.

Characteristics of the replication pattern are concerned with the cell's connection, orientation, and density in the space, as discussed in [7,41,42]. It also pertains to the cell size in the sense that the cell's length may also change along the replication pattern randomly, or according to a gradient as a request of the design intent (e.g., functionally graded lattice structures) [43-46].

Replication patterns can be:

- Regular.
- Pseudo-regular.

  Hybrid,
  Warped (or gradient) by cell size,
  Warped (or gradient) by thickness,

  Conformal.
- Stochastic.

Random by cell size,
Random also by thickness.

In a regular replication pattern, no changes regarding the unit cell characteristics occur at all (***Figure 1-5***). Hybrid patterns include different unit cells that may also have different geometric characteristics (***Figure 1-6***). They can be considered as a part of pseudo-regular patterns that provide several replications based on the variation of unit cell's size.

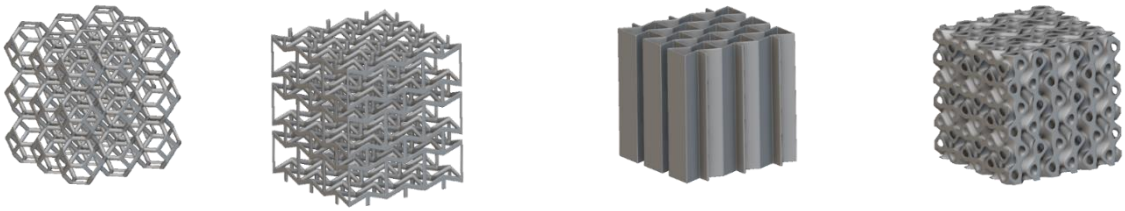

(a). Kelvin Cell. *(b). Re-entrant Cell.* *(c). Re-entrant Honeycomb Cell.* *(d). Split-p Cell.*

Figure 1-5. *Examples of Regular Replication Patterns (generated with nTop).*

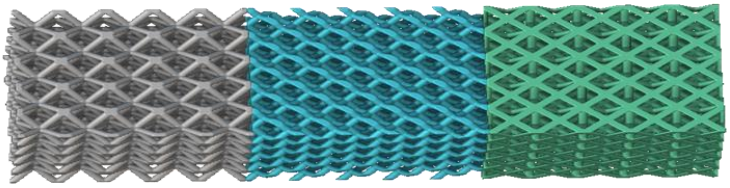

(a). BCC Lattice + Diamond Lattice + FCC Lattice.

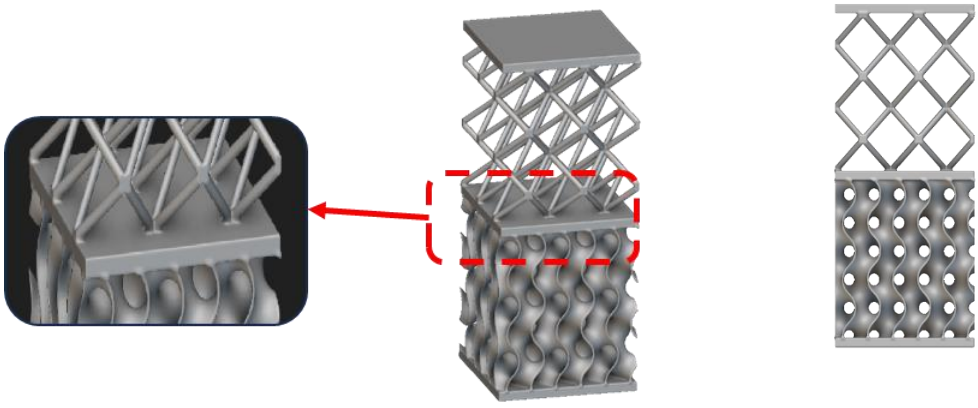

(b). BCC Lattice + Gyroid TMPS.

Figure 1-6. *Examples of Hybrid Replication Patterns: Unit Cells Variation (generated with nTop).*

Pseudo-regular patterns include also the warped (gradient) and conformal structures (***Figure 1-7***). The gradient by cell size is a replication pattern that provides a structure in which the unit cell's size varies gradually along a specified direction, while the thickness of the elements remains the same (***Figure 1-7****a*). In the case of the gradient by thickness, the structure maintains a constant cell's size,

but its thickness is changed (***Figure 1-7****b*). Conformal lattice structures consist of cells changing in length and shapes not homogeneously so that the replication pattern may follow the boundaries of the part (***Figure 1-7****c*) [47,48].

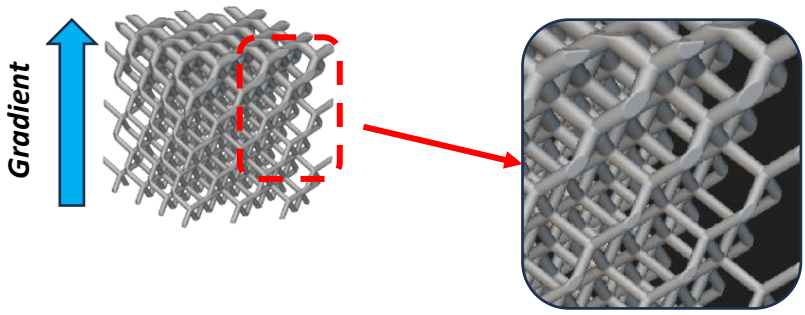

(a). BCC Cells with Gradient by Thickness.

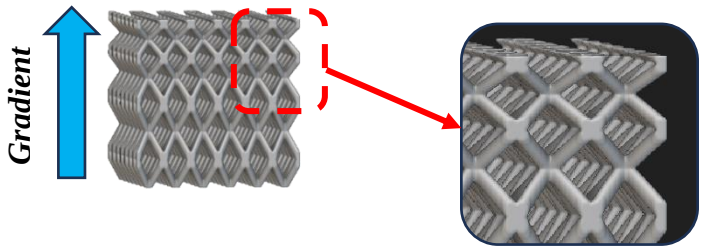

(b). BCC Cells with Gradient by Cell Size.

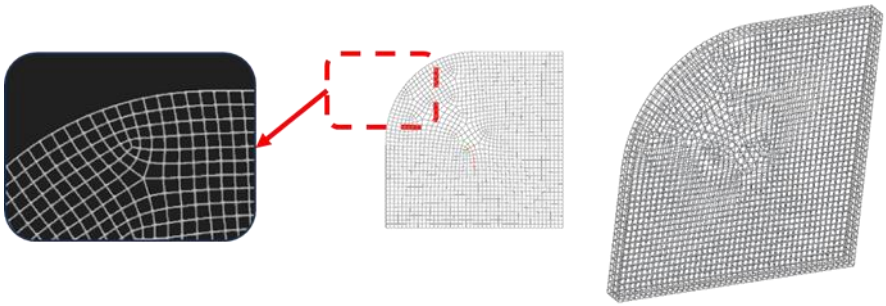

(c). Simple cubic Cells Conformal.

Figure 1-7. *Examples of Pseudo-regular Pattern Replications (generated with nTop).*

In stochastic patterns, the cell size varies randomly while the thickness remains the same. However, in stochastic random patterns, even the thickness varies randomly or along a gradient throughout the structure (***Figure 1-8***).

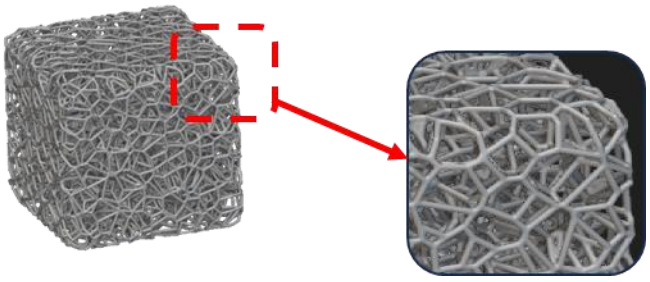

(a). Cell's Size Variation.

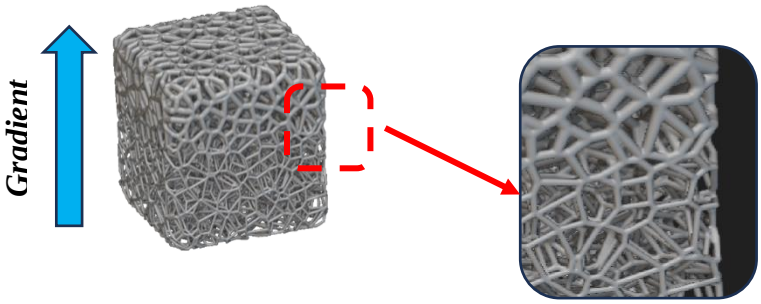

(b). Thickness Variation by Gradient.

Figure 1-8. *Examples of Stochastic Replication Patterns (generated with nTop).*

1.3. Mechanical Behavior.

The mechanical behavior of cellular materials is affected by the micro/mesoscale characteristics (unit cell and replication pattern), besides the macroscale topology and shape of the overall component [49,50]. This means that the local behaviors determine the global mechanical response and its related performance. Based on their local mechanical response, lattice structure is generally classified into [51]:

- Bending-dominated.
- Stretch-dominated.

Bending-dominated structures react locally with a bending deformation. This makes them extremely useful (such as compliant structures) for the applications related to mechanical energy absorption, especially in crashworthiness design [52,53]. Stretch-dominated structures experience a stretch deformation under the action of a uniaxial compression or tension within their material linear elastic limit (e.g., yielding strength, ultimate strength). This makes them useful for the lightweight design without losing the global stiffness of the component.

The Maxwell stability criterion may help to determine the local behavior of a truss-based cell by its Maxwell number (*M*), that is:

$$M = s\text{-}3n+6 \qquad \textbf{Equation 1-7}$$

where *s* is the number of struts, *n* is the number of joints in the unit cell, and 6 is the *d.o.f.* in case of three-dimensional structures. When *M* equals zero or is greater than zero, it means that the isostatic or over-constrained solutions undertake a stretch dominated category. The condition of *M* as less than zero means that the structure is a mechanism assumed to weld the joints (as it will be in a real lattice cell) and it undertakes a bending dominated category.

According to this reasoning, the bending dominated cells are BCC and Kelvin structures; while honeycomb (if axially loaded) and Octet cells are stretched dominated (concerning the application of *M* to the honeycomb, it is worthwhile to remember that shell-based cells are derived from the truss-based cells, assuming to close them with walls).

In [54], the classification between stretch and bending dominated is enriched by proposing a third class, named "programmable active", able to actively merge the two categories. Active structures are functionally graded materials, such as auxetic cells, which have the ability to switch their behavior from stretched dominated to bending dominated. This is extremely suitable for crashworthiness design when the defined impact loads may activate the plastic bending.

According to Gibson and Ashby power criterion [51], the elastic modulus of the unit cell can be calculated with the help of following equations:

For bending-dominated lattice,

$$\left(\frac{E^*}{E_s}\right) = C\left(\frac{\rho^*}{\rho_s}\right)^2 \qquad \textbf{Equation 1-8}$$

For stretch-dominated lattice,

$$\left(\frac{E^*}{E_s}\right) = C\left(\frac{\rho^*}{\rho_s}\right) \qquad \textbf{Equation 1-9}$$

where E^* is the elastic modulus of the cellular structure and E_s is the elastic modulus of the equivalent solid. Similarly, ρ^* is the density of the cellular structure and ρ_s is the density of the equivalent solid. *C* is the Gibson and Ashby constant which depends on the unit cell's topology and is determined by experimental tests. From Equations (8) and (9), the modulus-density chart of the lattice cells can be defined to assess performance of the cells in respect to the ideal behaviors. In addition, similar equations are available for finding the strength-density chart.

Lattice structures made by AM are currently studied from the resistance point of view, to validate both the structures and the technological process. More in detail, data are necessary to assess the repeatability of the stress-strain behavior to be used in the integrated product-process design. The AM discontinuities at small scale may penalize the fatigue behavior, as discussed in [55]. In literature, many other examples

of mechanical characterization on lattice structures are provided. Reference [56], studies the compression and three-point bending resistance of 3D Kagome lattice, while [57] provides a comparative study of the auxetic cells that are systematically compared in terms of Poisson ratio, maximum volume or area reductions, and equivalent Young's modulus by CAD-CAE tools. In [40], five TPMS structures are characterized from the dynamic point of view with Hopkinson bar, finding the strain-rate effect on the stress-strain response. This result is also discussed in terms of strain-rate sensitivity of the base material and accuracy of the AM process.

1.4. Applications of Lattice Structures.

Querying the Scopus database about research fields and applications related to lattice structures, published in journals in the last decade, an exponential trend can be clearly seen, confirmed also by the provisional data of 2023. More in details, ***Figure 1-9****a* shows relative percentage bars for five main topics related to specific technological and design fields (additive manufacturing, lightweight design, energy absorption, biomedical, and heat dissipations) and the two emerging keywords related to functionally graded materials that fit well the lattice structure classification we made, such as TPMS and Auxetic. ***Figure 1-9****b* shows the overall number of papers per topic found by the queries. As predicted, the TPMS and auxetic are still limited in respect of AM (the most populated topic), lightweight, and energy absorption design. In the middle of the rank, there are the biomedical applications and studies, partially related to TPMS, and the heat dissipation that also includes heat exchangers and sinks.

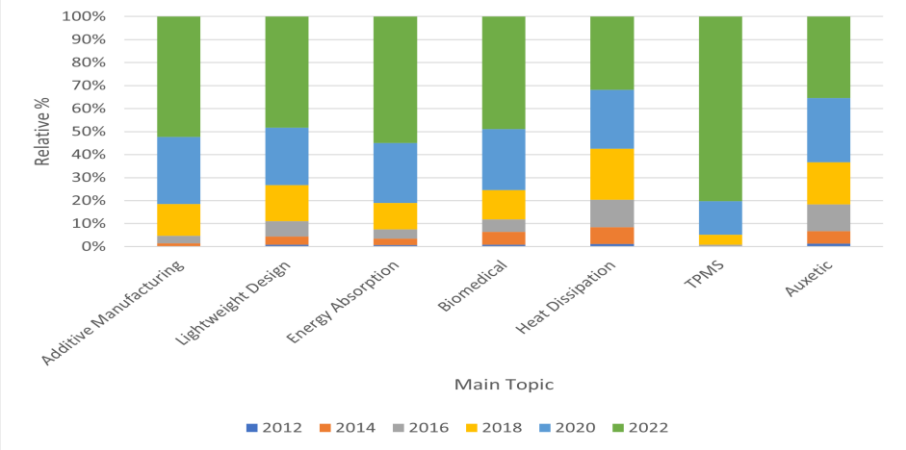

(a). Timeline Relative Percentage Distribution of Journal Papers in Scopus Sorted by Topic (subject limited to "Engineering").

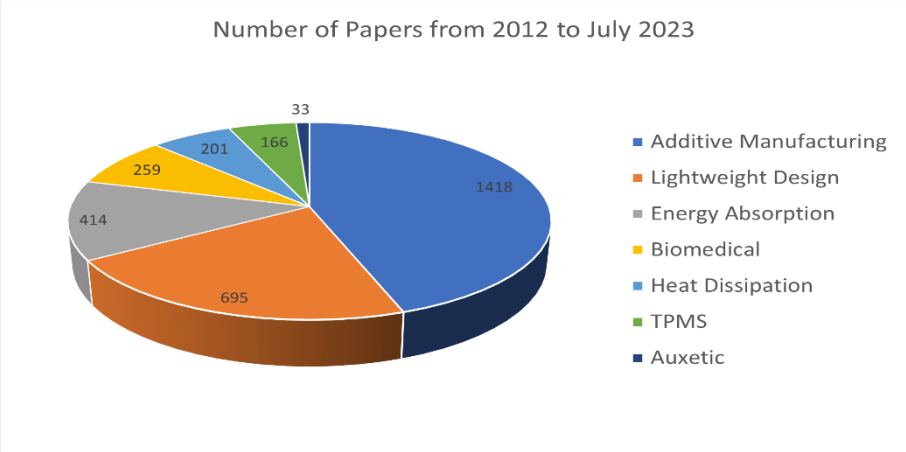

(b). Amount of Journal Papers per Topic (subject limited to "Engineering").

Figure 1-9. *Query Results from Scopus.*

Being part of the class of cellular materials, lattice structures may be adopted to design functional structures. In the respect of foams, lattice structures have more characteristics to be tailored to both meso and macroscale level, according to the description made in Section 2. A design optimization suitable to make a fine tuning of these characteristics allows to achieve better performances, as highlighted, for example, in [44], discussing the lightweight design. According to this, one of the most recent overviews concerning lattice structure applications, presented in [58], classifies the applications in the respect of the relevant design property that the lattice structure may help to achieve.

The ability to tailor the stiffness of a structure via cell topology and pattern [59] allows to control stress and strain for energy absorption, both in static and dynamic conditions at high strain rate [60]. This makes them appropriate for crashworthiness design, shock absorption, vibration, and acoustic noise control, useful for fields such as automotive, aerospace, ergonomics, ballistic, packaging, robotics, manufacturing tools [12,13,16,17,20,38,61]. According to [33,62], Kelvin cells must be mentioned as the structures derived from the basic beam cells with the best performance for damping vibration.

A clear example of how lattice structure may be tailored in the respect of assigned design requirements is provided by auxetic lattice structures. They can realize structures with negative Poisson's ratio, which could be utilized in the aerospace sector for the design of morphing wings for next generation aircraft [63-65]. Similarly, in biomedical applications, such as the bones based on TPMS cells, they allow to tailor structures suitable to match bone's stiffness, surface roughness and material compatibility for bone's growth, as demonstrated in [66,67].

Another class of applications is related to their capability of achieving a high surface/volume ratio or proper thermal conduction characteristics that make the lattice structures suitable for thermal insulation, heat pipe wicks, exchangers, sinks. In [68], applications related to thermal systems are reviewed and encouraged, thanks

to AM advancements. They involve both metallic and non-metallic lattice structures. Heat transfer media made of lattice structure increases the efficiency of the process, as demonstrated in [69].

Concerning the correlation among applications and the characteristics of the lattice structures according to unit cells and replication patterns, ***Table 1-1*** provides an overview of references in terms of the industrial sectors and related applications.

Table 1-1. *Applications of Lattice Structures by Field of Expertise.*

Sectors	Unit Cell/Replication Pattern	Applications	References
Aerospace Engineering	▪ BCC ▪ Auxetic ▪ Rhombic ▪ Chiral ▪ Honeycomb ▪ Pyramidal	o Heat Exchanger, o Wings o Gas Turbine Fan Blades o Airfoil o Drone Structure o Satellite Structure o Rocket Body o Landing Gear	[18, 70-76]
Biomedical Engineering	▪ Diamond Cubic ▪ Stochastic ▪ Octet-truss ▪ Tetrahedral ▪ BCC ▪ TPMS ▪ Honeycomb Lattice	o Hip Implant o Orthopedic Implant o Bone Scaffold o Femoral Stem	[77-86]
Mechanical Engineering: Automotive	▪ Honeycomb ▪ Truss-based ▪ TPMS ▪ Auxetic	o Crash Box o Bumper o Engine Hood o Crash Absorber o Chassis Frame o Heat Exchanger	[87-92]
Mechanical Engineering: Defense	▪ BCC ▪ Honeycomb ▪ Auxetic	o Military Armor Body o Helmet Liner o Military Seat Shock Panel	[93-95]
Mechanical Engineering: Heat Exchanger	▪ Truss-based ▪ TPMS	o Natural Convection	[96,97]
Mechanical Engineering	▪ BCC ▪ Cubic ▪ FCC ▪ TPMS	o AM Supporting Structure o AM Volume Infills	[98-103]
Product Design: Sports	▪ Auxetic ▪ Honeycomb ▪ Truss-base Random	o Football helmet o Sports Shoes o Horse saddle	[104-106]

Civil Engineering: Building Construction	▪ BCC ▪ Conformal ▪ Stochastic ▪ BCC	o Canton Tower o Beijing National Stadium (Bird's Nest) o The Atomium	[107-109]

1.5. References.

1. Gibson, L.J. Modelling the mechanical behavior of cellular materials. *Mater. Sci. Eng. A* 1989, *110*, 1–36. https://doi.org/10.1016/0921-5093(89)90154-8.
2. Gibson, L.J.; Ashby, M.F. *Cellular Solids: Structure and Properties*, 2nd ed.; Cambridge University Press: Cambridge, UK, 1997; pp. 16–21. https://doi.org/10.1017/CBO9781139878326.
3. Bhate, D. Four Questions in Cellular Material Design. *Materials* 2019, *12*, 1060. https://doi.org/10.3390/ma12071060.
4. Tao, W.; Leu, M.C. Design of lattice structure for additive manufacturing. In Proceedings of the 2016 International Symposium on Flexible Automation Cleveland (ISFA 2016), Cleveland, OH, USA, 1–3 August 2016; pp. 326–332. https://doi.org/10.1109/ISFA.2016.7790182.
5. Mancini, E.; Campana, F.; Pilone, D.; Amodio, D.; Sasso, M. Definition of a unified material model for cellular materials with high morphological and topological dispersion: Application to an AA7075-T6 aluminium foam. *Mater. Sci. Eng. A* 2022, *833*, 142346. https://doi.org/10.1016/j.msea.2021.142346.
6. Pan, C.; Han, Y.; Lu, J. Design and optimization of lattice structures: A review. *Appl. Sci.* 2020, *10*, 6374. https://doi.org/10.3390/app10186374.
7. Suethao, S.; Shah, D.U.; Smitthipong, W. Recent progress in processing functionally graded polymer foams. *Materials* 2020, *13*, 4060. https://doi.org/10.3390/ma13184060.
8. Bici, M.; Brischetto, S.; Campana, F.; Ferro, C.G.; Seclì, C.; Varetti, S.; Mazza, A. Development of a multifunctional panel for aerospace use through SLM additive manufacturing. *Procedia CIRP* 2018, *67*, 215–220. https://doi.org/10.1016/j.procir.2017.12.202.
9. Ghouse, S.; Reznikov, N.; Boughton, O.R.; Babu, S.; Ng, K.G.; Blunn, G.; Jeffers, J.R. The design and in vivo testing of a locally stiffness-matched porous scaffold. *Appl. Mater. Today* 2019, *15*, 377–388. https://doi.org/10.1016/j.apmt.2019.02.017.
10. de Wild, M.; Schumacher, R.; Mayer, K.; Schkommodau, E.; Thoma, D.; Bredell, M.; Weber, F.E. Bone regeneration by the osteoconductivity of porous titanium implants manufactured by selective laser melting: A histological and micro computed tomography study in the rabbit. *Tissue Eng. Part A* 2013, *19*, 2645–2654. https://doi.org/10.1089/ten.tea.2012.0753.
11. Saxena, K.K.; Das, R.; Calius, E.P. 3D printable multimaterial cellular auxetics with tunable stiffness. *arXiv* 2017, arXiv:1707.04486.
12. Zhang, J.; Huang, H.; Liu, G.; Zong, H.; Zhang, C. Stiffness and energy absorption of additive manufactured hybrid lattice structures. *Virtual Phys. Prototyp.* 2021, *16*, 428–443. https://doi.org/10.1080/17452759.2021.1954405.
13. Yin, H.; Zhang, W.; Zhu, L.; Meng, F.; Liu, J.; Wen, G. Review on lattice structures for energy absorption properties. *Compos. Struct.* 2022, *304*, 116397. https://doi.org/10.1016/j.compstruct.2022.116397.
14. Shan, S.; Kang, S.H.; Raney, J.R.; Wang, P.; Fang, L.; Candido, F.; Bertoldi, K. Multistable architected materials for trapping elastic strain energy. *Adv. Mater.* 2015, *27*, 4296–4301. https://doi.org/10.1002/adma.201501708.
15. Brennan-Craddock, J.; Brackett, D.; Wildman, R.; Hague, R. The design of impact absorbing structures for additive manufacture. *J. Phys. Conf. Ser.* 2012, *382*, 012042. IOP Publishing. https://doi.org/10.1088/1742-6596/382/1/012042.
16. Ozdemir, Z.; Tyas, A.; Goodall, R.; Askes, H. Energy absorption in lattice structures in dynamics: Nonlinear FE simulations. *Int. J. Impact Eng.* 2017, *102*, 1–15. https://doi.org/10.1016/j.ijimpeng.2016.11.016.
17. Habib, F.N.; Iovenitti, P.; Masood, S.H.; Nikzad, M. Fabrication of polymeric lattice structures for optimum energy absorption using Multi Jet Fusion technology. *Mater. Des.* 2018, *155*, 86–98. https://doi.org/10.1016/j.matdes.2018.05.059.
18. Maloney, K.J.; Fink, K.D.; Schaedler, T.A.; Kolodziejska, J.A.; Jacobsen, A.J.; Roper, C.S. Multifunctional heat exchangers derived from three-dimensional micro-lattice structures. *Int. J. Heat Mass Transf.* 2012, *55*, 2486–2493. https://doi.org/10.1016/j.ijheatmasstransfer.2012.01.011.
19. Son, K.N.; Weibel, J.A.; Kumaresan, V.; Garimella, S.V. Design of multifunctional lattice-frame materials for compact heat exchangers. *Int. J. Heat Mass Transf.* 2017, *115*, 619–629. https://doi.org/10.1016/j.ijheatmasstransfer.2017.07.073.

20. Chen, Y.; Li, T.; Scarpa, F.; Wang, L. Lattice metamaterials with mechanically tunable Poisson's ratio for vibration control. *Phys. Rev. Appl.* 2017, *7*, 024012. https://doi.org/10.1103/PhysRevApplied.7.024012.
21. Chen, D.; Zheng, X. Multi-material additive manufacturing of metamaterials with giant, tailorable negative Poisson's ratios. *Sci. Rep.* 2018, *8*, 9139. https://doi.org/10.1038/s41598-018-26980-7.
22. Yuan, S.; Shen, F.; Bai, J.; Chua, C.K.; Wei, J.; Zhou, K. 3D soft auxetic lattice structures fabricated by selective laser sintering: TPU powder evaluation and process optimization. *Mater. Des.* 2017, *120*, 317–327. https://doi.org/10.1016/j.matdes.2017.01.098.
23. Savio, G.; Rosso, S.; Meneghello, R.; Concheri, G. Geometric modeling of cellular materials for additive manufacturing in biomedical field: A review. *Appl. Bionics Biomech.* 2018, *2018*, 1654782. https://doi.org/10.1155/2018/1654782.
24. Chan, Y.C.; Shintani, K.; Chen, W. Robust topology optimization of multi-material lattice structures under material and load uncertainties. *Front. Mech. Eng.* 2019, *14*, 141–152. https://doi.org/10.1007/s11465-019-0531-4.
25. Stanković, T.; Mueller, J.; Egan, P.; Shea, K. A generalized optimality criteria method for optimization of additively manufactured multimaterial lattice structures. *J. Mech. Des.* 2015, *137*, 111405. https://doi.org/10.1115/1.4030995.
26. Ramirez-Chavez, I.E.; Anderson, D.; Sharma, R.; Lee, C.; Bhate, D. A classification of aperiodic architected cellular materials. *Designs* 2022, *6*, 63. https://doi.org/10.3390/designs6040063.
27. Álvarez-Trejo, A.; Cuan-Urquizo, E.; Bhate, D.; Roman-Flores, A. Mechanical metamaterials with topologies based on curved elements: An overview of design, additive manufacturing and mechanical properties. *Mater. Des.* 2023, *233*, 112190. https://doi.org/10.1016/j.matdes.2023.112190.
28. Zhang, Q.; Yang, X.; Li, P.; Huang, G.; Feng, S.; Shen, C.; Lu, T.J. Bioinspired engineering of honeycomb structure-Using nature to inspire human innovation. *Prog. Mater. Sci.* 2015, *74*, 332–400. https://doi.org/10.1016/j.pmatsci.2015.05.001.
29. Yan, C.; Hao, L.; Hussein, A.; Bubb, S.L.; Young, P.; Raymont, D. Evaluation of light-weight AlSi10Mg periodic cellular lattice structures fabricated via direct metal laser sintering. *J. Mater. Process. Technol.* 2014, *214*, 856–864. https://doi.org/10.1016/j.jmatprotec.2013.12.004.
30. Hunt, C.J.; Morabito, F.; Grace, C.; Zhao, Y.; Woods, B.K. A review of composite lattice structures. *Compos. Struct.* 2022, *284*, 115120. https://doi.org/10.1016/j.compstruct.2021.115120.
31. Luxner, M.H.; Stampfl, J.; Pettermann, H.E. Finite element modeling concepts and linear analyses of 3D regular open cell structures. *J. Mater. Sci.* 2005, *40*, 5859–5866. https://doi.org/10.1007/s10853-005-5020-y.
32. Deshpande, V.S.; Fleck, N.A.; Ashby, M.F. Effective properties of the octet-truss lattice material. *J. Mech. Phys. Solids* 2001, *49*, 1747–1769. https://doi.org/10.1016/S0022-5096(01)00010-2.
33. Lakes, R. Foam structures with a negative Poisson's ratio. *Science* 1987, *235*, 1038–1040. https://doi.org/10.1126/science.235.4792.1038.
34. Wang, F. Systematic design of 3D auxetic lattice materials with programmable Poisson's ratio for finite strains. *J. Mech. Phys. Solids* 2018, *114*, 303–318. https://doi.org/10.1016/j.jmps.2018.01.013.
35. Kumar, S.; Vyavahare, S.; Teraiya, S.; Kootikuppala, J.; Bogala, H. A state of the art review of additively manufactured auxetic structures. In *Recent Advances in Manufacturing Processes and Systems: Select Proceedings of RAM 2021*; Springer: Singapore, 2022; pp. 69–84. https://doi.org/10.1007/978-981-16-7787-8_6.
36. Xue, Y.; Gao, P.; Zhou, L.; Han, F. An enhanced three-dimensional auxetic lattice structure with improved property. *Materials* 2020, *13*, 1008. https://doi.org/10.3390/ma13041008.
37. Berger, J.B.; Wadley, H.N.G.; McMeeking, R.M. Mechanical metamaterials at the theoretical limit of isotropic elastic stiffness. *Nature* 2017, *543*, 533–537. https://doi.org/10.1038/nature21075.
38. Xue, R.; Cui, X.; Zhang, P.; Liu, K.; Li, Y.; Wu, W.; Liao, H. Mechanical design and energy absorption performances of novel dual scale hybrid plate-lattice mechanical metamaterials. *Extrem. Mech. Lett.* 2020, *40*, 100918. https://doi.org/10.1016/j.eml.2020.100918.
39. Al-Ketan, O.; Abu Al-Rub, R.K. Multifunctional mechanical metamaterials based on triply periodic minimal surface lattices. *Adv. Eng. Mater.* 2019, *21*, 1900524. https://doi.org/10.1002/adem.201900524.
40. AlMahri, S.; Santiago, R.; Lee, D.W.; Ramos, H.; Alabdouli, H.; Alteneiji, M.; Alves, M. Evaluation of the dynamic response of triply periodic minimal surfaces subjected to high strain-rate compression. *Addit. Manuf.* 2021, *46*, 102220. https://doi.org/10.1016/j.addma.2021.102220.
41. Song, J.; Tang, Q.; Feng, Q.; Ma, S.; Guo, F.; Han, Q. Investigation on the modelling approach for variable-density lattice structures fabricated using selective laser melting. *Mater. Des.* 2021, *212*, 110236. https://doi.org/10.1016/j.matdes.2021.110236.
42. Al Khalil, M.; Lebaal, N.; Demoly, F.; Roth, S. A design and optimization framework of variable-density lattice structures for additive manufacturing. *Mech. Adv. Mater. Struct.* 2022, *29*, 4711–4725. https://doi.org/10.1080/15376494.2021.1936704.
43. Sienkiewicz, J.; Płatek, P.; Jiang, F.; Sun, X.; Rusinek, A. Investigations on the mechanical response of gradient lattice structures manufactured via SLM. *Metals* 2020, *10*, 213. https://doi.org/10.3390/met10020213.

44. Seharing, A.; Azman, A.H.; Abdullah, S. A review on integration of lightweight gradient lattice structures in additive manufacturing parts. *Adv. Mech. Eng.* 2020, *12*, 1687814020916951. https://doi.org/10.1177/1687814020916951.
45. Li, D.; Liao, W.; Dai, N.; Xie, Y.M. Anisotropic design and optimization of conformal gradient lattice structures. *Comput.-Aided Des.* 2020, *119*, 102787. https://doi.org/10.1016/j.cad.2019.102787.
46. Seharing, A.; Azman, A.H.; Abdullah, S. Finite element analysis of gradient lattice structure patterns for bone implant design. *Int. J. Struct. Integr.* 2020, *11*, 535–545. https://doi.org/10.1108/IJSI-03-2020-0028.
47. Fabbro, P.D.; Rosso, S.; Ceruti, A.; Meneghello, R.; Concheri, G.; Savio, G. Conformal Lattice Structures: Modeling and Optimization. In *Design Tools and Methods in Industrial Engineering II, Proceedings of the International Conference on Design, Simulation, Manufacturing: The Innovation Exchange, ADM 2021, Rome, Italy, 9–10 September 2021*; Springer International Publishing: Cham, Switzerland, 2021; pp. 474–485. https://doi.org/10.1007/978-3-030-91234-5_48.
48. Nguyen, J.; Park, S.I.; Rosen, D.W.; Folgar, L.; Williams, J. Conformal lattice structure design and fabrication. In Proceedings of the 2012 International Solid Freeform Fabrication Symposium, Austin, TX, USA, 6–8 August 2012; University of Texas at Austin: Austin, TX, USA, 2012.
49. D'Angelo, C.; Ortona, A.; Colombo, P. Influence of the loading direction on the mechanical behavior of ceramic foams and lattices under compression. *Acta Mater.* 2013, *61*, 5525–5534. https://doi.org/10.1016/j.actamat.2013.06.009.
50. Singamaneni, S.; Bertoldi, K.; Chang, S.; Jang, J.H.; Young, S.L.; Thomas, E.L.; Tsukruk, V.V. Bifurcated mechanical behavior of deformed periodic porous solids. *Adv. Funct. Mater.* 2009, *19*, 1426–1436. https://doi.org/10.1002/adfm.200801675.
51. Ashby, M.F.; Gibson, L.J. Cellular solids: Structure and properties. Press Syndicate of the University of Cambridge: Cambridge, UK, 1997; pp. 175–231.
52. Tumino, D.; Alaimo, A.; Orlando, C.; Valvano, S. A Preliminary Study on the Effect of Strut Waviness on the Mechanical Properties of BCC Lattice Unit Cells. In *Design Tools and Methods in Industrial Engineering II, Proceedings of the International Conference on Design, Simulation, Manufacturing: The Innovation Exchange, ADM 2021, Rome, Italy, 9–10 September 2021*; Springer: Cham, Switzerland, 2021; pp. 431–441. https://doi.org/10.1007/978-3-030-91234-5_44.
53. Graziosi, S.; Ballo, F.M.; Libonati, F.; Senna, S. 3D printing of bending-dominated soft lattices: Numerical and experimental assessment. *Rapid Prototyp. J.* 2022, *28*, 51–64.
54. Wagner, M.A.; Lumpe, T.S.; Chen, T.; Shea, K. Programmable, active lattice structures: Unifying stretch-dominated and bending-dominated topologies. *Extrem. Mech. Lett.* 2019, *29*, 100461. https://doi.org/10.1016/j.eml.2019.100461.
55. Benedetti, M.; Du Plessis, A.; Ritchie, R.O.; Dallago, M.; Razavi, S.M.J.; Berto, F. Architected cellular materials: A review on their mechanical properties towards fatigue-tolerant design and fabrication. *Mater. Sci. Eng. R Rep.* 2021, *144*, 100606. https://doi.org/10.1016/j.mser.2021.100606.
56. Wei, K.; Yang, Q.; Ling, B.; Xie, H.; Qu, Z.; Fang, D. Mechanical responses of titanium 3D kagome lattice structure manufactured by selective laser melting. *Extrem. Mech. Lett.* 2018, *23*, 41–48. https://doi.org/10.1016/j.eml.2018.07.001.
57. Elipe, J.C.Á.; Lantada, A.D. Comparative study of auxetic geometries by means of computer-aided design and engineering. *Smart Mater. Struct.* 2012, *21*, 105004. https://doi.org/10.1088/0964-1726/21/10/105004.
58. du Plessis, A.; Razavi, N.; Benedetti, M.; Murchio, S.; Leary, M.; Watson, M.; Berto, F. Properties and applications of additively manufactured metallic cellular materials: A review. *Prog. Mater. Sci.* 2022, *125*, 100918. https://doi.org/10.1016/j.pmatsci.2021.100918.
59. Wu, G.; Cho, Y.; Choi, I.S.; Ge, D.; Li, J.; Han, H.N.; Yang, S. Directing the deformation paths of soft metamaterials with prescribed asymmetric units. *Adv. Mater.* 2015, *27*, 2747–2752. https://doi.org/10.1002/adma.201500716.
60. Niknam, H.; Akbarzadeh, A.H. Graded lattice structures: Simultaneous enhancement in stiffness and energy absorption. *Mater. Des.* 2020, *196*, 109129. https://doi.org/10.1016/j.matdes.2020.109129.
61. Ji, J.C.; Luo, Q.; Ye, K. Vibration control based metamaterials and origami structures: A state-of-the-art review. *Mech. Syst. Signal Process.* 2021, *161*, 107945. https://doi.org/10.1016/j.ymssp.2021.107945.
62. Wei, Y.; Yu, B.; Yang, Q.; Gao, P.; Miao, Z.; Cheng, J.; Sun, X. Damping behaviors of steel-based Kelvin lattice structures fabricated by indirect additive manufacture combining investment casting. *Smart Mater. Struct.* 2020, *29*, 055001. https://doi.org/10.1088/1361-665X/ab78b8.
63. Spadoni, A.; Ruzzene, M. Static aeroelastic response of chiral-core airfoils. *J. Intell. Mater. Syst. Struct.* 2007, *18*, 1067–1075. https://doi.org/10.1177/1045389X06072361.
64. Alderson, A.; Alderson, K.L. Auxetic materials. *Proc. Inst. Mech. Eng. Part G J. Aerosp. Eng.* 2007, *221*, 565–575. https://doi.org/10.1243/09544100JAERO185.
65. Xia, Y.; Friswell, M.I.; Flores, E.S. Equivalent models of corrugated panels. *Int. J. Solids Struct.* 2012, *49*, 1453–1462. https://doi.org/10.1016/j.ijsolstr.2012.02.023.

66. El-Sayed, M.A.; Essa, K.; Ghazy, M.; Hassanin, H. Design optimization of additively manufactured titanium lattice structures for biomedical implants. *Int. J. Adv. Manuf. Technol.* 2020, *110*, 2257–2268. https://doi.org/10.1007/s00170-020-05982-8.
67. Murr, L.E.; Gaytan, S.M.; Medina, F.; Lopez, H.; Martinez, E.; Machado, B.I.; Bracke, J. Next-generation biomedical implants using additive manufacturing of complex, cellular and functional mesh arrays. *Philos. Trans. R. Soc. A Math. Phys. Eng. Sci.* 2010, *368*, 1999–2032. https://doi.org/10.1098/rsta.2010.0010.
68. Sajjad, U.; Rehman, T.U.; Ali, M.; Park, C.W.; Yan, W.M. Manufacturing and potential applications of lattice structures in thermal systems: A comprehensive review of recent advances. *Int. J. Heat Mass Transf.* 2022, *198*, 123352. https://doi.org/10.1016/j.ijheatmasstransfer.2022.123352.
69. Shabgard, H.; Allen, M.J.; Sharifi, N.; Benn, S.P.; Faghri, A.; Bergman, T.L. Heat pipe heat exchangers and heat sinks: Opportunities, challenges, applications, analysis, and state of the art. *Int. J. Heat Mass Transf.* 2015, *89*, 138–158. https://doi.org/10.1016/j.ijheatmasstransfer.2015.05.020.
70. Moon, S.K.; Tan, Y.E.; Hwang, J.; Yoon, Y.J. Application of 3D printing technology for designing light-weight unmanned aerial vehicle wing structures. *Int. J. Precis. Eng. Manuf.-Green Technol.* 2014, *1*, 223–228. https://doi.org/10.1007/s40684-014-0028-x.
71. Magerramova, L.; Volkov, M.; Afonin, A.; Svinareva, M.; Kalinin, D. Application of light lattice structures for gas turbine engine fan blades. In Proceedings of the 31st Congress of the International Council of the Aeronautical Sciences, ICAS, Belo Horizonte, Brazil, 9–14 September 2018.
72. Spadoni, A.; Ruzzene, M. Numerical and experimental analysis of the static compliance of chiral truss-core airfoils. *J. Mech. Mater. Struct.* 2007, *2*, 965–981. https://doi.org/10.2140/jomms.2007.2.965.
73. Aabid, A.; Parveez, B.; Parveen, N.; Khan, S.A.; Zayan, J.M.; Shabbir, O. Reviews on design and development of unmanned aerial vehicle (drone) for different applications. *J. Mech. Eng. Res. Dev.* 2022, *45*, 53–69.
74. Zhang, X.; Zhou, H.; Shi, W.; Zeng, F.; Zeng, H.; Chen, G. Vibration tests of 3D printed satellite structure made of lattice sandwich panels. *AIAA J.* 2018, *56*, 4213–4217. https://doi.org/10.2514/1.J057241.
75. Vasiliev, V.V.; Barynin, V.A.; Razin, A.F. Anisogrid composite lattice structures-Development and aerospace applications. *Compos. Struct.* 2012, *94*, 1117–1127. https://doi.org/10.1016/j.compstruct.2011.10.023.
76. Khorrami, M.R.; Humphreys, W.M.; Lockard, D.P. An assessment of flap and main landing gear noise abatement concepts. In Proceedings of the 21st AIAA/CEAS Aeroacoustics Conference, Dallas, TX, USA, 22–26 June 2015; p. 2987. https://doi.org/10.2514/6.2015-2987.
77. Jetté, B.; Brailovski, V.; Dumas, M.; Simoneau, C.; Terriault, P. Femoral stem incorporating a diamond cubic lattice structure: Design, manufacture and testing. *J. Mech. Behav. Biomed. Mater.* 2018, *77*, 58–72. https://doi.org/10.1016/j.jmbbm.2017.08.034.
78. Heinl, P.; Müller, L.; Körner, C.; Singer, R.F.; Müller, F.A. Cellular Ti-6Al-4V structures with interconnected macro porosity for bone implants fabricated by selective electron beam melting. *Acta Biomater.* 2008, *4*, 1536–1544. https://doi.org/10.1016/j.actbio.2008.03.013.
79. Challapalli, A.; Ju, J. Continuum model for effective properties of orthotropic octet-truss lattice materials. In Proceedings of the ASME International Mechanical Engineering Congress and Exposition, Montreal, QC, Canada, 14–20 November 2014; American Society of Mechanical Engineers: New York, NY, USA, 2015; Volume 46583, p. V009T12A051. https://doi.org/10.1115/IMECE2014-38925.
80. Dumas, M.; Terriault, P.; Brailovski, V. Modelling and characterization of a porosity graded lattice structure for additively manufactured biomaterials. *Mater. Des.* 2017, *121*, 383–392. https://doi.org/10.1016/j.matdes.2017.02.021.
81. Stevenson, G.; Rehman, S.; Draper, E.; Hernández-Nava, E.; Hunt, J.; Haycock, J.W. Combining 3D human in vitro methods for a 3Rs evaluation of novel titanium surfaces in orthopaedic applications. *Biotechnol. Bioeng.* 2016, *113*, 1586–1599. https://doi.org/10.1002/bit.25919.
82. Chen, W.M.; Lee, S.J.; Lee, P.V.S. Failure analysis of an additive manufactured porous titanium structure for orthopedic implant applications. *Mater. Sci. Forum* 2016, *863*, 45–49. https://doi.org/10.4028/www.scientific.net/MSF.863.45.
83. Gorguluarslan, R.M.; Choi, S.K.; Saldana, C.J. Uncertainty quantification and validation of 3D lattice scaffolds for computer-aided biomedical applications. *J. Mech. Behav. Biomed. Mater.* 2017, *71*, 428–440. https://doi.org/10.1016/j.jmbbm.2017.04.011.
84. Soro, N.; Attar, H.; Brodie, E.; Veidt, M.; Molotnikov, A.; Dargusch, M.S. Evaluation of the mechanical compatibility of additively manufactured porous Ti-25Ta alloy for load-bearing implant applications. *J. Mech. Behav. Biomed. Mater.* 2019, *97*, 149–158. https://doi.org/10.1016/j.jmbbm.2019.05.019.
85. Rahmani, R.; Antonov, M.; Kollo, L.; Holovenko, Y.; Prashanth, K.G. Mechanical behavior of Ti6Al4V scaffolds filled with CaSiO3 for implant applications. *Appl. Sci.* 2019, *9*, 3844. https://doi.org/10.3390/app9183844.
86. Jia, D.; Li, F.; Zhang, C.; Liu, K.; Zhang, Y. Design and simulation analysis of Lattice bone plate based on finite element method. *Mech. Adv. Mater. Struct.* 2021, *28*, 1311–1321. https://doi.org/10.1080/15376494.2019.1665759.
87. Wang, C.; Li, Y.; Zhao, W.; Zou, S.; Zhou, G.; Wang, Y. Structure design and multi-objective optimization of a novel crash box based on biomimetic structure. *Int. J. Mech. Sci.* 2018, *138*, 489–501. https://doi.org/10.1016/j.ijmecsci.2018.01.032.

88. Wang, C.; Wang, W.; Zhao, W.; Wang, Y.; Zhou, G. Structure design and multi-objective optimization of a novel NPR bumper system. *Compos. Part B Eng.* 2018, *153*, 78–96. https://doi.org/10.1016/j.compositesb.2018.07.024.
89. Yin, S.; Chen, H.; Wu, Y.; Li, Y.; Xu, J. Introducing composite lattice core sandwich structure as an alternative proposal for engine hood. *Compos. Struct.* 2018, *201*, 131–140. https://doi.org/10.1016/j.compstruct.2018.06.038.
90. Niutta, C.B.; Ciardiello, R.; Tridello, A. Experimental and Numerical Investigation of a Lattice Structure for Energy Absorption: Application to the Design of an Automotive Crash Absorber. *Polymers* 2022, *14*, 1116. https://doi.org/10.3390/polym14061116.
91. Mantovani, S.; Campo, G.A.; Ferrari, A.; Cavazzuti, M. Optimization methodology for automotive chassis design by truss frame: A preliminary investigation using the lattice approach. In *Transdisciplinary Engineering Methods for Social Innovation of Industry 4.0*; IOS Press: Amsterdam, The Netherlands, 2018; pp. 984–992.
92. Kumar, V.; Manogharan, G.; Cormier, D.R. Design of periodic cellular structures for heat exchanger applications. In *2009 International Solid Freeform Fabrication Symposium*; University of Texas at Austin: Austin, TX, USA, 2009.
93. Pannikottu, A.; Bandaru, S. *Flexible Honeycomb Composite Vehicle Armor (No. 2009-01-0601)*; SAE Technical Paper: 2009, Pennsylvania, USA. https://doi.org/10.4271/2009-01-0601.
94. Harris, J.A. Additively Manufactured Metallic Cellular Materials for Blast and Impact Mitigation. Ph.D. Thesis, University of Cambridge, Cambridge, UK, 2018.
95. Acanfora, V.; Corvino, C.; Saputo, S.; Sellitto, A.; Riccio, A. Application of an additive manufactured hybrid metal/composite shock absorber panel to a military seat ejection system. *Appl. Sci.* 2021, *11*, 6473. https://doi.org/10.3390/app11146473.
96. Luo, J.W.; Chen, L.; Xia, Y.; Zheng, X.; Tao, W.Q. Topology optimization of natural convection using porous metal foam based on the adjoint lattice Boltzmann method and level set method. *Comput. Fluids* 2023, *265*, 106007. https://doi.org/10.1016/j.compfluid.2023.106007.
97. Baobaid, N.; Ali, M.I.; Khan, K.A.; Al-Rub, R.K.A. Fluid flow and heat transfer of porous TPMS architected heat sinks in free convection environment. *Case Stud. Therm. Eng.* 2022, *33*, 101944. https://doi.org/10.1016/j.csite.2022.101944.
98. Hussein, A.; Hao, L.; Yan, C.; Everson, R.; Young, P. Advanced lattice support structures for metal additive manufacturing. *J. Mater. Process. Technol.* 2013, *213*, 1019–1026. https://doi.org/10.1016/j.jmatprotec.2013.01.020.
99. Vaissier, B.; Pernot, J.P.; Chougrani, L.; Véron, P. Genetic-algorithm based framework for lattice support structure optimization in additive manufacturing. *Comput.-Aided Des.* 2019, *110*, 11–23. https://doi.org/10.1016/j.cad.2018.12.007.
100. Cheng, L.; Liang, X.; Bai, J.; Chen, Q.; Lemon, J.; To, A. On utilizing topology optimization to design support structure to prevent residual stress induced build failure in laser powder bed metal additive manufacturing. *Addit. Manuf.* 2019, *27*, 290–304. https://doi.org/10.1016/j.addma.2019.03.001.
101. Alejandrino, J.D.; Concepcion, R.S., II; Lauguico, S.C.; Tobias, R.R.; Venancio, L.; Macasaet, D.; Dadios, E.P. A machine learning approach of lattice infill pattern for increasing material efficiency in additive manufacturing processes. *Int. J. Mech. Eng. Robot. Res.* 2020, *9*, 1253–1263. https://doi.org/10.18178/ijmerr.9.9.1253-1263.
102. Ntintakis, I.; Stavroulakis, G.E. Infill Microstructures for Additive Manufacturing. *Appl. Sci.* 2022, *12*, 7386. https://doi.org/10.3390/app12157386.
103. Dong, G.; Tang, Y.; Li, D.; Zhao, Y.F. Design and optimization of solid lattice hybrid structures fabricated by additive manufacturing. *Addit. Manuf.* 2020, *33*, 101116. https://doi.org/10.1016/j.addma.2020.101116.
104. Ahmad, A.; Elamana, S.; Adam, K.; Bici, M.; Campana, F. Lightweight Horse Saddletree Through Reverse Engineering and Lattice Structure Design. *Comput. Des. Appl.* 2023, *20*, 923–935. https://doi.org/10.14733/cadaps.2023.923-935.
105. Hanna, B.; Adams, R.; Townsend, S.; Robinson, M.; Soe, S.; Stewart, M.; Theobald, P. Auxetic metamaterial optimisation for head impact mitigation in American football. *Int. J. Impact Eng.* 2021, *157*, 103991. https://doi.org/10.1016/j.ijimpeng.2021.103991.
106. Ren, X.; Das, R.; Tran, P.; Ngo, T.D.; Xie, Y.M. Auxetic metamaterials and structures: A review. *Smart Mater. Struct.* 2018, *27*, 023001. https://doi.org/10.1088/1361-665X/aaa61c.
107. ARUP. Canton Tower. Available online: https://www.arup.com/projects/guangzhou-tv-tower (accessed on 27 June 2023).
108. ARUP. Beijing National Stadium (Bird's Nest). Available online: https://www.arup.com/services/buildings/structural-engineering (accessed on 27 June 2023).
109. Atomium. The Atomium (The Symbol of Brussels and Belgium). Available online: https://atomium.be/home/Index (accessed on 27 June 2023).

2. Chapter: Issues on Design and Manufacturing of Lattice Structures.

This chapter pertains to the second part of the literature review, which describes the design and manufacturing techniques related to lattice structures. It also highlights the glaring issues pertinent to these design and manufacturing techniques. In the end of this chapter, the whole literature is concluded to produce the summary related to the benefits of lattice structures, to highlight the deficiencies pertaining to the design workflow of the lattice structure, and to furnish some recommendations for the future works.

2.1. Manufacturing of Lattice Structures.

From the design point of view, unit cell selection is strongly affected by the functional requirements to be accomplished but it is also constrained by the manufacturing feasibility. Manufacturing feasibility may be related to the type of structure (according to the classifications of Section 1.2), or to process limits such as range of accuracy, lengths, necessity of post-processing, etc. According to this, Table 2 and 3 show a glance of manufacturing methods versus base materials and major limitations together with references, where such limitations are exploited. More in detail, ***Table 2-1*** refers to the traditional manufacturing processes and ***Table 2-2*** refers to AM processes.

Table 2-1. *Overview of the Lattice Structures via Traditional Manufacturing Methods.*

Manufacturing Method	Base Material	Issues	References
Direct Foaming	▪ Metals	○ Cell Replication Pattern: Only stochastic structure can be obtained.	[1,2]
Investment Casting	▪ Metals	○ Low accuracy for fine structures. ○ Long production time.	[3–5]
Stamping Forming	▪ Metals	○ Cell's characteristics. ○ Post-processing is required. ○ Difficult to produce fine structures.	[6,7]
Interlocking Grid Assembly	▪ Metals ▪ Composites ▪ Polymer Fibers	○ Cell's characteristics. . ○ Difficult to produce fine structures.	[8–10]
Extrusion Wire Cutting	▪ Metals	○ Cell's characteristics. ○ Costly Processes.	[11]
Lap Assembly	▪ Metals	○ Cell's characteristics. ○ Post-processing is required.	[12]
Wire-Woven Method	▪ Metals	○ Cell's characteristics. ○ Post-processing is required.	[13–15]

Table 2-2. *Overview of the Lattice Structures via Additive Manufacturing (AM) Methods.*

AM Method	Base Material	Issues	References
Binder jetting (BJ)	▪ Metals ▪ Ceramics ▪ Polymers	○ Part shrinkage 2-3% ○ Low accuracy and tolerance	[16–18]
Cold Spray Additive Manufacturing (CSAM)	▪ Metals ▪ Ceramics	○ Loss of ductility due to plastic deformation. ○ Post-processing	[19–21]
Direct Energy Deposition (DED)	▪ Metals ▪ Ceramics	○ Low resolution ○ Poor surface finish ○ Costly	[22–24]
Direct Ink Writing (DIW)	▪ Ceramics ▪ Metal s ▪ Slurries ▪ Polymers ▪ Sol-gel inks	○ Fine surface finish just in case of ceramics.	[25–27]
Fused Deposition Modelling (FDM)	▪ Metals ▪ Thermoplastics ▪ Wax	○ Slow Speed ○ Low Accuracy	[28–30]
Liquid Metal Additive Manufacturing	▪ Metals	○ Melting and cooling of the printing material influence the final geometry	[31–33]
Laminated Object Manufacturing (LOM)	▪ Papers ▪ Plastics ▪ Metals	○ Poor surface finish	[34–36]
Powder Bed Fusion (PBF)	▪ Metals ▪ Ceramics ▪ Thermoplastics ▪ Wax	○ Volumetric Expansion ○ Low accuracy and tolerance	[37–39]

Generally speaking, the traditional manufacturing methods have severe limitations concerning the type of cells that can be built. In particular, a limited set of cells may be obtained through joining the manufactured details achieved on relevant planes (e.g., honeycombs are manufactured by joining hexagonal cells between plates). In some cases, also the replication patterns may be limited (e.g., direct foaming). It is clearly shown how AM processes may overcome the limit on the unit cell characteristics as well as on the capability to fill in uniformly complex shapes and volumes. The traditional manufacturing processes are mostly limited to the base materials (mostly available in metals), few types of unit cells, mandatory post-processing, high production time, and unavailability of the fine structures. However, AM solutions are limited to the mandatory postprocessing (in the most cases), high production time, weak performance against fatigue loading, low aesthetic, build direction, residual stresses, support/sacrificial structures, etc. Particularly, the job orientation on the building platform of the printer, during the AM process should be meticulously defined to avoid the geometrical errors, and to minimize the residual stresses and the presence of supports [40,41].

2.2. *Designing and Modelling of Lattice Structures.*

According to the literature [42-47], the researchers have mostly defined the development workflows for the design and manufacturing of the lattice structure, separately. Most of these development workflows are based on very few basic requirements that pertain only to the lattice structure design and the manufacturing process, without taking care (more often) about the overall optimization requirements on weight reduction, assembly efforts, reliability, post-processing issues regarding the mechanical performance (in general) and the support structure removal in case of AM, and so on.

Pattern replications may be defined by topological optimization [48] to improve the component performances, also considering other manufacturing constraints, that are:

- For AM: working volume, support and infill design, post-processing.
- For traditional manufacturing processes: die design, extra and complex tooling/attachments, multiple machining/manufacturing processes, precise manufacturing process control, complex assembly/bonding process, post-processing and/or set up by other design criteria such as aesthetics, assembly, etc.

In [48], AM lattice for biomedical applications related to implant design are studied and three design workflows are discussed to optimize this kind of design.

In any case, the micro/meso scale of the cell must be replicated at the macro scale to fulfill the component volumes.

From the CAD modelling point of view, it is computationally expensive, often requiring the adoption of dedicated tools and/or a change of the modelling approach. ***Table 2-3*** shows a summary of current tools available to support the CAD-CAE development of known lattice structures. Only a few of them provide the opportunity for obtaining a diversity of lattice shapes, and design freedom.

Table 2-3. *3D CAD Modelling of Lattice Structures.*

Design Tools	Software	Lattice Type	References
CAD Software / Numerical Solvers	▪ Solid Works ▪ nTopology ▪ Optistruct ▪ Inspire ▪ Rhinoceros Grasshopper ▪ Fusion 360 ▪ Netfabb ▪ Materialize ▪ Free CAD ▪ Ansys	○ Beam Lattice ○ TPMS ○ Honeycomb ○ Voronoi ○ Auxetic ○ Conformal ○ Gradient Lattice	[44, 49–64]

Special Tools	▪ MS Lattice ▪ FLatt Pack	○ TPMS	[65,66]

In the case of cells defined by the shell elements, many CAD solutions (such as nTopology, Rhinoceros, Surface Design in Catia, etc.) adopted Implicit CAD Modelling (ICM) to vary the cell characteristics and the pattern distribution analytically. This allows to drive results via optimization criteria, since, through ICM, the geometry is directly described by a mathematical equation. Although ICM may produce formulas not physically realistic (e.g., non-manifold solutions), in case of lattice structures it can use the data points to influence the design with instant change and therefore facilitates the designer for any change in the geometry [67,68]. Through the field-driven design, ICM may simplify the pattern definitions, also for conformal, stochastic, and hybrid structures by utilizing a scalar field that represents the unit cell replication, as a weight of the ICM set of data points. Changes of the field drive the geometry and alter the characteristics of the pattern. Commonly, it helps to optimize the lattice structure based on the stress field [67].

In [68], a hybrid geometric modelling method is proposed in which the selected unit cell is replicated by a voxelization approach of the complex volume to be fulfilled, through the geometrical functions suitable to describe the cell. Generally, the computation loop includes one or more steps for filling the inner volume with cells, and steps to constrain the boundary surface. It allows good transferability to the CAE analysis, closing the information loop between CAD modelling and FEA analysis that often may limit the actions of the designer when she/he adopts commercial software. Moreover, it can provide both regular and stochastic replications, also in conformal configurations, thanks to a Voronoi-based approach [69,70]. In [71], a NURBS-Free Form Deformation (FFD) approach is proposed and validated by FEA, to build and optimize conformal truss-based lattice structures. Other methods to build conformal lattice are Twin Curve Division Method (TCD), Arc Division Method (AD), Curvature Division Method (CD), and NURBS Free Form Deformation Method (NFFD).

2.3. Conclusion of the Literature Review.

The literature review in Chapter 1 and 2, provides some insights into the design capabilities of the lattice structures with subsequent achievable properties in the context of the engineering requirements and applications, with a wide range of materials, from metal to plastic. Since a few decades, the researchers have extensively worked to unfold the amazing unique characteristics of the lattice structures such as auxetic structures, negative thermal expansions, active stiffness, etc. These functional properties are derived from the lattice cell characteristic, and for this reason, starting from them, the literature linked the design and manufacturing issues, such as replication patterns, cell mechanical response, manufacturability, to the most relevant engineering applications found in the research literature. Moreover, to

provide also the design practice point of view, CAD-CAE issues related to their modelling and optimization are also discussed.

This literature review also highlighted that the lattice structures benefit many engineering sectors in the context of engineering requirements ranging from lightweight structures to energy absorption structures, to conduction/convection heat management, to sound/vibration energy minimization, to electromagnetic wave shielding, biomedical bone implants, etc. However, based on the above discussions, the following few recommendations are furnished for the future research work:

- In order to Investigate the mechanical properties of a structure derived from the multiscale properties of the component(s), and from the mesoscale cell characteristics, a proper functional behavior may be tailored. CAD-CAE approach may massively help this study by virtual testing.

- CAD-CAE approaches are also affected by the multiscale domains involved in the problem, with increasing computational costs. This gives impetus to adopt new modelling approaches, such as the Implicit Geometric Modelling and/or homogenization techniques for CAE analysis.

- In the case of AM, the mechanical characteristics related to stress-strain curves must be investigated and validated to distinguish between the lattice structure properties and AM set-up conditions.

- Metallic AM lattice structures suffer with fatigue loads due to the limited process conditions and/or set-up. In addition, the post-processing treatments may be infeasible due to the complexity of the structures. Therefore, a suitable workflow engulfing all the design, assembly, manufacturing (including post-processing) requirements may be defined in order to minimize these concerns and facilitate the functional requirements of the lattice structures.

2.4. References.

1. Huang, R.; Ma, S.; Zhang, M.; Xu, J.; Wang, Z. Dynamic deformation and failure process of quasi-closed-cell aluminum foam manufactured by direct foaming technique. *Mater. Sci. Eng. A* 2019, *756*, 302–311. https://doi.org/10.1016/j.msea.2019.04.050.
2. Luukkonen, T.; Yliniemi, J.; Sreenivasan, H.; Ohenoja, K.; Finnilä, M.; Franchin, G.; Colombo, P. Ag-or Cu-modified geopolymer filters for water treatment manufactured by 3D printing, direct foaming, or granulation. *Sci. Rep.* 2020, *10*, 7233. https://doi.org/10.1038/s41598-020-64228-5.
3. Singh, S.; Singh, R. Precision investment casting: A state of art review and future trends. *Proc. Inst. Mech. Eng. Part B J. Eng. Manuf.* 2016, *230*, 2143–2164. https://doi.org/10.1177/0954405415597844.
4. Barnett, S.O. Investment Casting—The Multi-Process Technology. *Foundry Trade J. Int.* 1988, *11*, 33.
5. Jones, S.; Yuan, C. Advances in shell moulding for investment casting. *J. Mater. Process. Technol.* 2003, *135*, 258–265. https://doi.org/10.1016/S0924-0136(02)00907-X.
6. Wadley, H.N. Multifunctional periodic cellular metals. *Philos. Trans. R. Soc. A Math. Phys. Eng. Sci.* 2006, *364*, 31–68. https://doi.org/10.1098/rsta.2005.1697.

7. Ablat, M.A.; Qattawi, A. Investigating the design and process parameters of folded perforated sheet metal. *Int. J. Adv. Manuf. Technol.* 2019, *102*, 615–633. https://doi.org/10.1007/s00170-018-3149-5.
8. Cheung, K.C.; Gershenfeld, N. Reversibly assembled cellular composite materials. *Science* 2013, *341*, 1219–1221. https://doi.org/10.1126/science.1240889.
9. Jiang, S.; Sun, F.; Zhang, X.; Fan, H. Interlocking orthogrid: An efficient way to construct lightweight lattice-core sandwich composite structure. *Compos. Struct.* 2017, *176*, 55–71. https://doi.org/10.1016/j.compstruct.2017.05.029.
10. Cheung, K.C.W. Digital Cellular Solids: Reconfigurable Composite Materials. Ph.D. Thesis, Massachusetts Institute of Technology, Cambridge, MA, USA, 2012.
11. Queheillalt, D.T.; Murty, Y.; Wadley, H.N. Mechanical properties of an extruded pyramidal lattice truss sandwich structure. *Scr. Mater.* 2008, *58*, 76–79. https://doi.org/10.1016/j.scriptamat.2007.08.041.
12. Kang, K.J. Wire-woven cellular metals: The present and future. *Prog. Mater. Sci.* 2015, *69*, 213–307. https://doi.org/10.1016/j.pmatsci.2014.11.003.
13. Simovski, C.R.; Belov, P.A.; Atrashchenko, A.V.; Kivshar, Y.S. Wire metamaterials: Physics and applications. *Adv. Mater.* 2012, *24*, 4229–4248. https://doi.org/10.1002/adma.201200931.
14. Khoda, B.; Ahsan, A.N. A novel rapid manufacturing process for metal lattice structure. *3d Print. Addit. Manuf.* 2021, *8*, 111–125. https://doi.org/10.1089/3dp.2020.0184.
15. Li, M.; Du, W.; Elwany, A.; Pei, Z.; Ma, C. Metal binder jetting additive manufacturing: A literature review. *J. Manuf. Sci. Eng.* 2020, *142*, 090801. https://doi.org/10.1115/1.4047430.
16. Du, W.; Ren, X.; Pei, Z.; Ma, C. Ceramic binder jetting additive manufacturing: A literature review on density. *J. Manuf. Sci. Eng.* 2020, *142*, 040801. https://doi.org/10.1115/1.4046248.
17. Mirzababaei, S.; Pasebani, S. A review on binder jet additive manufacturing of 316L stainless steel. *J. Manuf. Mater. Process.* 2019, *3*, 82. https://doi.org/10.3390/jmmp3030082.
18. Prashar, G.; Vasudev, H. A comprehensive review on sustainable cold spray additive manufacturing: State of the art, challenges and future challenges. *J. Clean. Prod.* 2021, *310*, 127606. https://doi.org/10.1016/j.jclepro.2021.127606.
19. Yin, S.; Cavaliere, P.; Aldwell, B.; Jenkins, R.; Liao, H.; Li, W.; Lupoi, R. Cold spray additive manufacturing and repair: Fundamentals and applications. *Addit. Manuf.* 2018, *21*, 628–650. https://doi.org/10.1016/j.addma.2018.04.017.
20. Pathak, S.; Saha, G.C. Development of sustainable cold spray coatings and 3D additive manufacturing components for repair/manufacturing applications: A critical review. *Coatings* 2017, *7*, 122. https://doi.org/10.3390/coatings7080122.
21. Dass, A.; Moridi, A. State of the art in directed energy deposition: From additive manufacturing to materials design. *Coatings* 2019, *9*, 418. https://doi.org/10.3390/coatings9070418.
22. Yao, X.X.; Ge, P.; Li, J.Y.; Wang, Y.F.; Li, T.; Liu, W.W.; Zhang, Z. Controlling the solidification process parameters of direct energy deposition additive manufacturing considering laser and powder properties. *Comput. Mater. Sci.* 2020, *182*, 109788. https://doi.org/10.1016/j.commatsci.2020.109788.
23. Heigel, J.C.; Michaleris, P.; Reutzel, E.W. Thermo-mechanical model development and validation of directed energy deposition additive manufacturing of Ti-6Al-4V. *Addit. Manuf.* 2015, *5*, 9–19. https://doi.org/10.1016/j.addma.2014.10.003.
24. Behera, D.; Cullinan, M. Current challenges and potential directions towards precision microscale additive manufacturing-Part I: Direct ink writing/jetting processes. *Precis. Eng.* 2021, *68*, 326–337. https://doi.org/10.1016/j.precisioneng.2020.12.009.
25. Costakis, W.J., Jr.; Rueschhoff, L.M.; Diaz-Cano, A.I.; Youngblood, J.P.; Trice, R.W. Additive manufacturing of boron carbide via continuous filament direct ink writing of aqueous ceramic suspensions. *J. Eur. Ceram. Soc.* 2016, *36*, 3249–3256. https://doi.org/10.1016/j.jeurceramsoc.2016.06.002.
26. Tu, R.; Sodano, H.A. Additive manufacturing of high-performance vinyl ester resin via direct ink writing with UV-thermal dual curing. *Addit. Manuf.* 2021, *46*, 102180. https://doi.org/10.1016/j.addma.2021.102180.
27. Ning, F.; Cong, W.; Hu, Y.; Wang, H. Additive manufacturing of carbon fiber-reinforced plastic composites using fused deposition modeling: Effects of process parameters on tensile properties. *J. Compos. Mater.* 2017, *51*, 451–462. https://doi.org/10.1177/0021998316646169.
28. Singh, S.; Ramakrishna, S.; Singh, R. Material issues in additive manufacturing: A review. *J. Manuf. Process.* 2017, *25*, 185–200. https://doi.org/10.1016/j.jmapro.2016.11.006.
29. Chacón, J.M.; Caminero, M.A.; García-Plaza, E.; Núnez, P.J. Additive manufacturing of PLA structures using fused deposition modelling: Effect of process parameters on mechanical properties and their optimal selection. *Mater. Des.* 2017, *124*, 143–157. https://doi.org/10.1016/j.matdes.2017.03.065.
30. Sukhotskiy, V.; Vishnoi, P.; Karampelas, I.H.; Vader, S.; Vader, Z.; Furlani, E.P. Magnetohydrodynamic drop-on-demand liquid metal additive manufacturing: System overview and modelling. In Proceedings of the 5th International Conference of Fluid Flow, Heat and Mass Transfer (FFHMT'18), Niagra Falls, ON, Canada, 7–9 June 2018. https://doi.org/10.11159/ffhmt18.155.

31. Gan, Z.; Yu, G.; He, X.; Li, S. Surface-active element transport and its effect on liquid metal flow in laser-assisted additive manufacturing. *Int. Commun. Heat Mass Transf.* 2017, *86*, 206–214. https://doi.org/10.1016/j.icheatmasstransfer.2017.06.007.
32. Li, A.; Liu, X.; Wan, X.; Yang, Y. Thermal behaviors and fluid flow controlling the geometry of 7075 aluminum alloy single tracks during liquid metal flow rapid cooling additive manufacturing. *Int. Commun. Heat Mass Transf.* 2020, *116*, 104664. https://doi.org/10.1016/j.icheatmasstransfer.2020.104664.
33. Dermeik, B.; Travitzky, N. Laminated object manufacturing of ceramic-based materials. *Adv. Eng. Mater.* 2020, *22*, 2000256. https://doi.org/10.1002/adem.202000256.
34. Tao, Y.; Yin, Q.; Li, P. An additive manufacturing method using large-scale wood inspired by laminated object manufacturing and plywood technology. *Polymers* 2020, *13*, 144. https://doi.org/10.3390/polym13010144.
35. Luong, D.X.; Subramanian, A.K.; Silva, G.A.L.; Yoon, J.; Cofer, S.; Yang, K.; Tour, J.M. Laminated object manufacturing of 3D-printed laser-induced graphene foams. *Adv. Mater.* 2018, *30*, 1707416. https://doi.org/10.1002/adma.201707416.
36. King, W.E.; Anderson, A.T.; Ferencz, R.M.; Hodge, N.E.; Kamath, C.; Khairallah, S.A.; Rubenchik, A.M. Laser powder bed fusion additive manufacturing of metals; physics, computational, and materials challenges. *Appl. Phys. Rev.* 2015, *2*, 041304. https://doi.org/10.1063/1.4937809.
37. Snow, Z.; Nassar, A.R.; Reutzel, E.W. Invited Review Article: Review of the formation and impact of flaws in powder bed fusion additive manufacturing. *Addit. Manuf.* 2020, *36*, 101457. https://doi.org/10.1016/j.addma.2020.101457.
38. Ladani, L.; Sadeghilaridjani, M. Review of powder bed fusion additive manufacturing for metals. *Metals* 2021, *11*, 1391. https://doi.org/10.3390/met11091391.
39. Cheng, L.; To, A. Part-scale build orientation optimization for minimizing residual stress and support volume for metal additive manufacturing: Theory and experimental validation. *Comput.-Aided Des.* 2019, *113*, 1–23. https://doi.org/10.1016/j.cad.2019.03.004.
40. Zanini, F.; Sorgato, M.; Savio, E.; Carmignato, S. Uncertainty of CT dimensional measurements performed on metal additively manufactured lattice structures. In Proceedings of the 10th Conference on Industrial Computed Tomography, Wels, Austria, 4–7 February 2020. https://doi.org/10.58286/25084.
41. Tamburrino, F.; Graziosi, S.; Bordegoni, M. The design process of additively manufactured mesoscale lattice structures: A review. *J. Comput. Inf. Sci. Eng.* 2018, *18*, 040801. https://doi.org/10.1115/1.4040131.
42. Koch, P.; Korn, H.; Kordass, R.; Holtzhausen, S.; Schoene, C.; Mueller, B.; Stelzer, R. A CAD-based workflow and mechanical characterization for additive manufacturing of tailored lattice structures. In *2018 International Solid Freeform Fabrication Symposium*; University of Texas at Austin: Austin, TX, USA, 2018.
43. Daynes, S.; Feih, S.; Lu, W.F.; Wei, J. Design concepts for generating optimised lattice structures aligned with strain trajectories. *Comput. Methods Appl. Mech. Eng.* 2019, *354*, 689–705. https://doi.org/10.1016/j.cma.2019.05.053.
44. Rosso, S.; Uriati, F.; Grigolato, L.; Meneghello, R.; Concheri, G.; Savio, G. An optimization workflow in design for additive manufacturing. *Appl. Sci.* 2021, *11*, 2572. https://doi.org/10.3390/app11062572.
45. Panagiotidou, V.; Koerner, A.; Cruz, M.; Parker, B.; Beyer, B.; Giannakopoulos, S. 3D extrusion of multi-biomaterial lattices using an environmentally informed workflow. *Front. Archit. Res.* 2022, *11*, 691–708. https://doi.org/10.1016/j.foar.2022.06.010.
46. Hudak, Y.F.; Li, J.S.; Cullum, S.; Strzelecki, B.M.; Richburg, C.; Kaufman, G.E.; Aubin, P.M. A novel workflow to fabricate a patient-specific 3D printed accommodative foot orthosis with personalized latticed metamaterial. *Med. Eng. Phys.* 2022, *104*, 103802. https://doi.org/10.1016/j.medengphy.2022.103802.
47. Al-Tamimi, A.A.; Almeida, H.; Bartolo, P. Structural optimisation for medical implants through additive manufacturing. *Prog. Addit. Manuf.* 2020, *5*, 95–110. https://doi.org/10.1007/s40964-020-00109-7.
48. Nguyen, D.S.; Vignat, F. A method to generate lattice structure for additive manufacturing. In Proceedings of the 2016 IEEE International Conference on Industrial Engineering and Engineering Management (IEEM), Bali, Indonesia, 4–7 December 2016; IEEE: 2016, USA; pp. 966–970. https://doi.org/10.1109/IEEM.2016.7798021.
49. Jafferson, J.M.; Sharma, H. Design of 3D printable airless tyres using NTopology. *Mater. Today Proc.* 2021, *46*, 1147–1160. https://doi.org/10.1016/j.matpr.2021.02.058.
50. Nguyen, D.S. Design of lattice structure for additive manufacturing in CAD environment. *J. Adv. Mech. Des. Syst. Manuf.* 2019, *13*, JAMDSM0057–JAMDSM0057. https://doi.org/10.1299/jamdsm.2019jamdsm0057.
51. Moreno Nieto, D.; Moreno Sánchez, D. Design for additive manufacturing: Tool review and a case study. *Appl. Sci.* 2021, *11*, 1571. https://doi.org/10.3390/app11041571.
52. Dragoni, E.; Ciace, V.A. Mechanical design and modelling of lightweight additively manufactured lattice structures evolved from regular three-dimensional tessellations. *Proc. Inst. Mech. Eng. Part C J. Mech. Eng. Sci.* 2021, *235*, 1759–1773. https://doi.org/10.1177/0954406219885959.
53. Abdulhadi, H.S.; Mian, A. Effect of strut length and orientation on elastic mechanical response of modified body-centered cubic lattice structures. *Proc. Inst. Mech. Eng. Part L J. Mater. Des. Appl.* 2019, *233*, 2219–2233. https://doi.org/10.1177/1464420719841084.

54. Al Rifaie, M.; Mian, A.; Srinivasan, R. Compression behavior of three-dimensional printed polymer lattice structures. *Proc. Inst. Mech. Eng. Part L J. Mater. Des. Appl.* 2019, *233*, 1574–1584. https://doi.org/10.1177/1464420718770475.
55. Lu, Y.; Birol, E.B.; Johnson, C.; Hernandez, C.; Sabin, J.E. A Method for Load-responsive Inhomogeneity and Anisotropy in 3D Lattice Generation Based on Ellipsoid Packing. In Proceedings of the 25th International Conference of the Association for Computer-Aided Architectural Design Research in Asia (CAADRIA), Bangkok, Thailand, 5–8 August 2020; pp. 395–404. https://doi.org/10.52842/conf.caadria.2020.1.395.
56. Robles-Linares, J.A.; Ramírez-Cedillo, E.; Siller, H.R.; Rodríguez, C.A.; Martínez-López, J.I. Parametric modeling of biomimetic cortical bone microstructure for additive manufacturing. *Materials* 2019, *12*, 913. https://doi.org/10.3390/ma12060913.
57. Fantini, M.; Curto, M. Interactive design and manufacturing of a Voronoi-based biomimetic bone scaffold for morphological characterization. *Int. J. Interact. Des. Manuf. (IJIDeM)* 2018, *12*, 585–596. https://doi.org/10.1007/s12008-017-0416-x.
58. Nazir, A.; Arshad, A.B.; Jeng, J.Y. Buckling and post-buckling behavior of uniform and variable-density lattice columns fabricated using additive manufacturing. *Materials* 2019, *12*, 3539. https://doi.org/10.3390/ma12213539.
59. Jin, X.; Li, G.; Gong, J. Optimal design and modeling of 3D variable-density lattice structures. In Proceedings of the 2017 8th International Conference on Mechanical and Aerospace Engineering (ICMAE), Prague, Czech Republic, 22–25 July 2017; IEEE: 2017, USA; pp. 320–325. https://doi.org/10.1109/ICMAE.2017.8038664.
60. Fragassa, C. Electric city buses with modular platform: A design proposition for sustainable mobility. In *Sustainable Design and Manufacturing 2017: Selected papers on Sustainable Design and Manufacturing 4*; Springer International Publishing: Cham, Switzerland, 2017; pp. 789–800. https://doi.org/10.1007/978-3-319-57078-5_74.
61. Abate, K.M.; Nazir, A.; Yeh, Y.P.; Chen, J.E.; Jeng, J.Y. Design, optimization, and validation of mechanical properties of different cellular structures for biomedical application. *Int. J. Adv. Manuf. Technol.* 2020, *106*, 1253–1265. https://doi.org/10.1007/s00170-019-04671-5.
62. Dakshnamoorthy, V. Automated Lattice Optimization of Hinge Fitting with Displacement Constraint. Ph.D. Thesis, The university of Texas, Texas, USA, 2016.
63. He, Y.; Burkhalter, D.; Durocher, D.; Gilbert, J.M. Solid-lattice hip prosthesis design: Applying topology and lattice optimization to reduce stress shielding from hip implants. In Proceedings of the Frontiers in Biomedical Devices, 2018 Design of Medical Devices Conference, Minneapolis, MN, USA, 9–12 April 2018; American Society of Mechanical Engineers: New York, NY, USA, 2018; Volume 40789, p. V001T03A001. https://doi.org/10.1115/DMD2018-6804.
64. Al-Ketan, O.; Abu Al-Rub, R.K. MSLattice: A free software for generating uniform and graded lattices based on triply periodic minimal surfaces. *Mater. Des. Process. Commun.* 2021, *3*, e205. https://doi.org/10.1002/mdp2.205.
65. Maskery, I.; Parry, L.A.; Padrão, D.; Hague, R.J.M.; Ashcroft, I.A. FLatt Pack: A research-focussed lattice design program. *Addit. Manuf.* 2022, *49*, 102510. https://doi.org/10.1016/j.addma.2021.102510.
66. Li, Q.; Hong, Q.; Qi, Q.; Ma, X.; Han, X.; Tian, J. Towards additive manufacturing oriented geometric modeling using implicit functions. *Vis. Comput. Ind. Biomed. Art* 2018, *1*, 9. https://doi.org/10.1186/s42492-018-0009-y.
67. Ahmad, A.; Elamana, S.; Adam, K.; Bici, M.; Campana, F. Lightweight Horse Saddletree Through Reverse Engineering and Lattice Structure Design. *Comput. Des. Appl.* 2023, *20*, 923–935. https://doi.org/10.14733/cadaps.2023.923-935.
68. Tang, Y.; Dong, G.; Zhao, Y.F. A hybrid geometric modeling method for lattice structures fabricated by additive manufacturing. *Int. J. Adv. Manuf. Technol.* 2019, *102*, 4011–4030. https://doi.org/10.1007/s00170-019-03308-x.
69. Lei, H.Y.; Li, J.R.; Xu, Z.J.; Wang, Q.H. Parametric design of Voronoi-based lattice porous structures. *Mater. Des.* 2020, *191*, 108607. https://doi.org/10.1016/j.matdes.2020.108607.
70. Bici, M.; Campana, F.; De Michelis, M. Mesoscale geometric modeling of cellular materials for finite element analysis. *Comput. -Aided Des. Appl.* 2017, *14*, 760–769. https://doi.org/10.1080/16864360.2017.1287678.
71. Dal Fabbro, P.; Rosso, S.; Ceruti, A.; Boscolo Bozza, D.; Meneghello, R.; Concheri, G.; Savio, G. Analysis of a Preliminary Design Approach for Conformal Lattice Structures. *Appl. Sci.* 2021, *11*, 11449. https://doi.org/10.3390/app112311449.

3. Chapter: Test Case Study.

This chapter introduces the Ph.D. project and briefly explains the test case study. It also highlights the main issues related to the existing DA and defines the scope of the Ph.D. work. In addition, it also describes the contributions of different teams being involved in this research work with specific responsibilities.

3.1. Introduction to the PhD Project.

This research work is financially supported by the mutual collaboration of Regione Lazio (Italy) and INFN Rome (Italy). The aim of this PhD project is to support the research activities of INFN Rome, which is a public research institution.

The test case study pertaining to this Ph.D. work is called the BULLKID (Bulky and Low-threshold Kinetic Inductance Detectors) project and provided by INFN. BULLKID is developing the next-generation cryogenic detectors for particle physics research, in the field of neutrinos and dark matter. It is an experimental setup, in which a high beam of photon is bombarded on the silicon single wafer crystal, which produces a shower of high energy physics particles. Among these high energy particles, neutrinos are the particles of interest which are absorbed by the KIDS (an array of 8x8 of the kinetic inductance detectors) of the silicon single crystal wafer at cryogenic temperature (ranging from 10mK to 40mK). This whole experiment is performed inside the cryostat which provides a high vacuum, light-tight environment, and shielding against electromagnetic waves.

Currently, the DA supports only one wafer crystal, therefore, INFN proposed to optimize the existing DA such that to use more than one wafer crystal (up to three) at a time in order to enhance its operational capability. However, in the future, the number of the DAs will be extended to an array of 20. The geometry of the final pure copper frame is to be additively manufactured using the L-PBF 3D-printer SISMA MySint 100 of INFN LNGS site (in the framework of the HAMMER collaboration - https://hammer.lngs.infn.it/), hence its structure is very small and with very complex topologies. In addition, the existing design is suffering with the mechanical vibrations of the experimental setup and particularly during the transportation, therefore, this Ph.D. work will also take care of this aspect to improve the structural stiffness against the mechanical vibrations. Moreover, the new design should be lightweight and should also improve the thermal efficiency of the DA.

3.2. Test Case Study.

The detector assembly (DA) is composed of several components, involving 5 multi-materials, varying from metallic to non-metallic (***Figure 3-1***, ***Table 3-1***). DA has multiple functions, such as to firmly hold the silicon single crystal wafer, to suffice the purpose of the cooling of silicon single crystal wafer within the operational temperature range, to allow the bombardment of the operational high photon beam on the top surface of the wafer (where an array of 64 sensors are mounted for the

desired operation) through the optical fibers passing inside the top aluminium casing, and to support the electronic harnesses. The DA is mounted inside the cryogenic device (***Figure* 3-2**). The wafer crystal is held firmly inside the aluminium (Al) casings by the wafer holding ring and the wafer holders. The two vertical thermalization rods connect the DA inside the cryogenic device. The cryogenic device transmits the desired cryogenic temperature to the DA through thermalization rods. The whole system is initially assembled at an ambient temperature (298 K), installed inside the cryostat experimental volume and then cooled down until reaching the base temperature ranging from 10mK to 40mK.

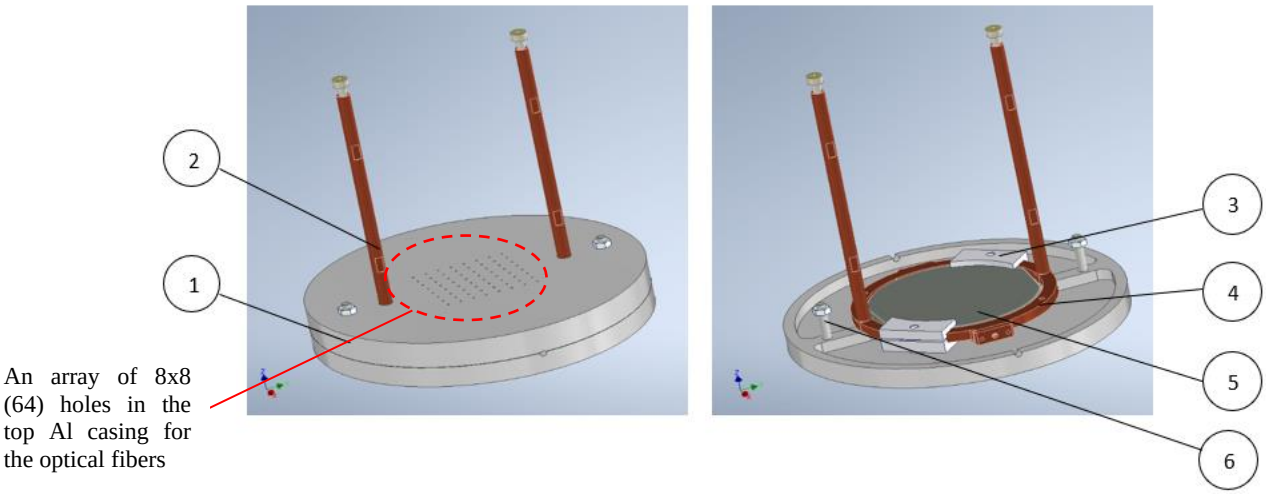

(a). Complete 3D CAD Model. *(b). 3D CAD Model without Upper Al Casing.*

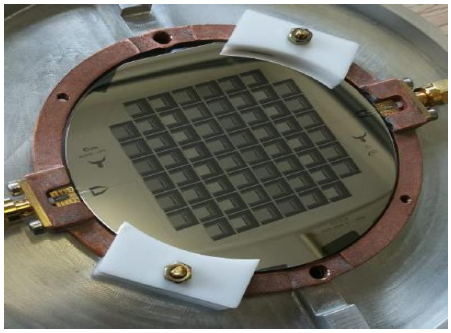

(c). Physical Wafer Assembly (WA).

Figure 3-1. *Original 3D Design of the Detector Assembly.*

Table 3-1. *Case Study: Assembly Details.*

Number	Component	Quantity	Material
1	Lower/Upper Aluminium Casing	02	Pure Aluminium
2	Thermalization Rod	02	Pure Copper
3	Wafer Holders	02	Pure Copper/Teflon
4	Wafer Holding Ring	01	Pure Copper
5	Wafer	01	Silicon Single Crystal
6	Screws/Nut & Bolts	06	Brass

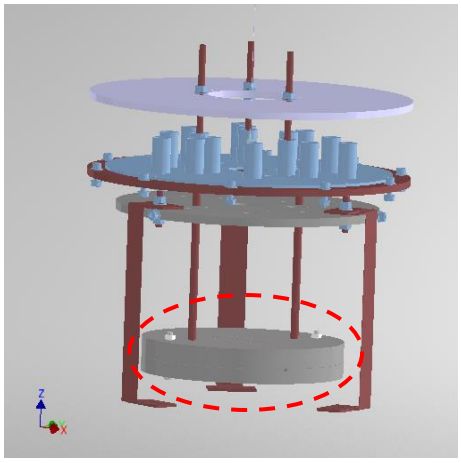

(a). 3D CAD Model without outer Shell.

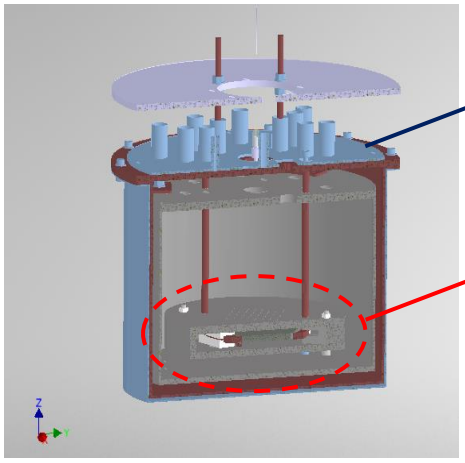

(b). 3D CAD Model with Outer Shell- Half Sectional View.

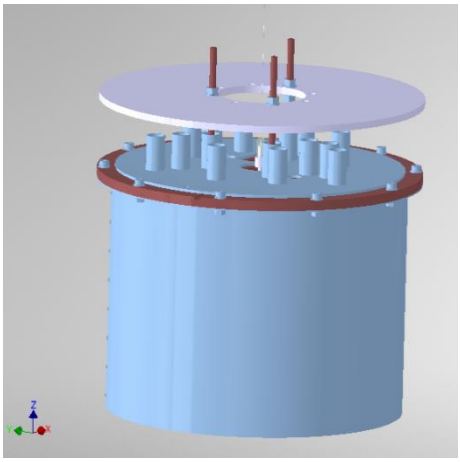

(c). 3D CAD Model with Outer Shell.

Figure 3-2. *DA inside the Cryogenic System.*

The DA is a very small structural assembly, for example, the wafer crystal is 75mm in diameter and 5mm in thickness, similarly the wafer holding ring is 98mm in diameter and 6mm in thickness. Therefore, it is a challenging case study with respect to the design for AM and design for assembly.

The DA also consists of some electronic harnesses, such as components and wiring (***Figure 3-4***). The wafer crystal has an array of 64 sensors (***Figure 3-4****a*) that are connected to the wafer connector through optical fibers and wafer launcher electronic PCB (***Figure 3-4****b*). The optical fibers are soldered on the wafer launcher, which connects it further to the wafer connector. The wafer connector is made of copper, and it exchanges the electronic data between the wafer crystal and the external source.

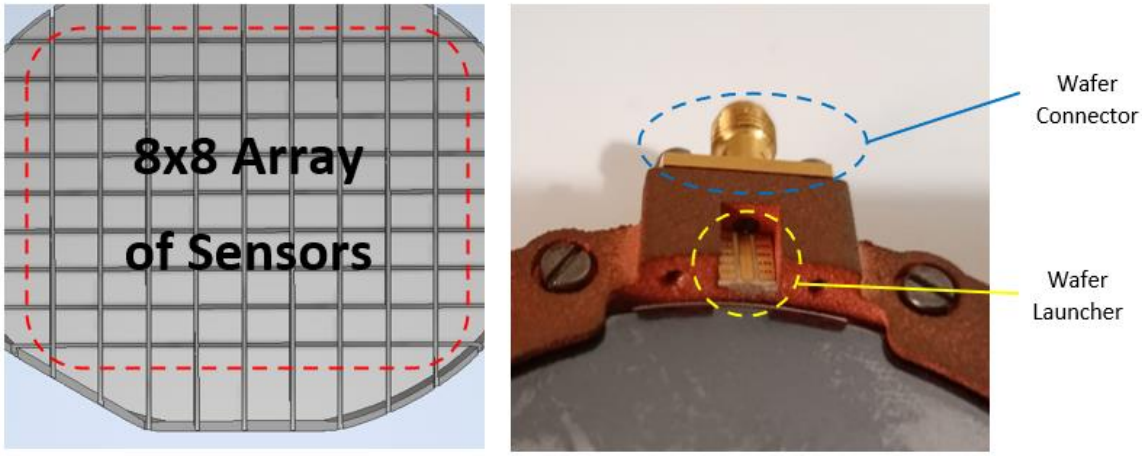

(a). Array of the Sensors. *(b). Wafer Launcher and Connector.*

Figure 3-3. *Electronics of the Detector Holder.*

3.3. Details of the Stakeholders.

The following stakeholders (***Figure 3-4***) with respective responsibilities make their contribution in this Ph.D. project.

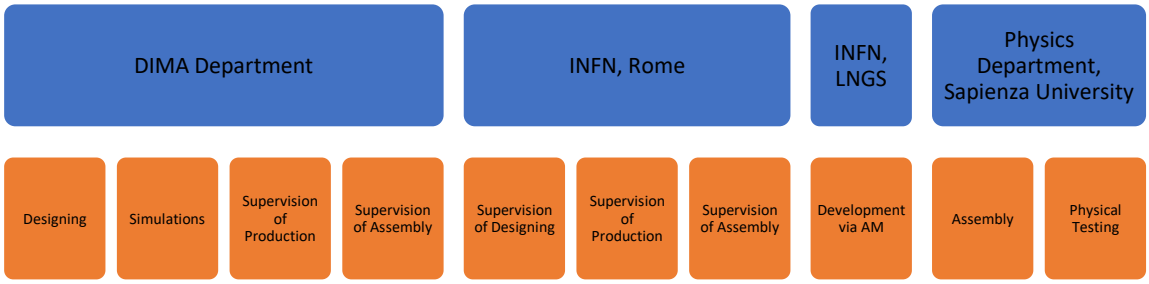

Figure 3-4. *Details of the Stakeholders.*

4. Chapter: Methodology and Workflow.

In this chapter, a list of requirements (pertaining to the design, functions, assembly, and manufacturing requirements) is furnished which facilitates the CAD-CAE process, prototyping, and the physical assembly. It also explains the basic approach being adopted for design optimization pertaining to heat transfer and mechanical vibrations. In addition, a design-development workflow is developed that works properly with the test case study and the goals, and which is subsequently applied to obtain the main results within this Ph.D. work. It also highlights the important data related to the materials of the DA like mechanical properties, thermal properties, and mass that are utilized during the finite element analysis (FEA) and for the validation of the proposed design. It also explains the main goal and relevant objectives of the Ph.D. project.

4.1. Methodology and Materials.

The original design of the DA is utilized to produce the new optimized design. The design optimization is performed in accordance with a list of requirements, that was prepared in mutual collaboration with INFN, which encapsulates all the design, functional, assembly, and manufacturing constraints (***Table 4-1***) to facilitate the subsequent initial design (3D modelling), assembly, and manufacturing phases. However, this list of requirements has the flexibility to be updated according to the feedback provided by the manufacturing and assembly stages.

Table 4-1. *List of Requirements.*

Number	Requirements	Target Value
1	The Aluminium casings should be modified such that to support **more than one DA**.	≤ 03
2	The proposed design with more than one DA should be supported by the existing cryogenic system **with least possible modifications**.	-
3	The **overall height** of the DA structure should not exceed the internal height of cryogenic system.	< 125 mm
4	To **reduce the Teflon material** of the wafer holders/or better to **replace it with the pure copper material**.	≥ 10%
5	The wafer crystal may be modified **with least possible modifications** to accommodate the new design of the wafer holders.	-
6	The new holders should not lock the wafer crystal firmly, it should provide a small room for the **vertical/lateral translation** inside the wafer ring to facilitate the thermal contraction and avoid excessive thermal stresses.	≥ 0.2 mm/≥ 01 mm
7	The wafer connectors between two consecutive wafer crystals should not be aligned and are required **to be rotated**.	$90^0 \pm 0.5^0$
8	**Gap/clearance** between two consecutive wafer crystals is required to avoid any possible electronic interference.	≥ 01 mm
9	The wafer holding rings should be provided with the **minimum set of special locking arrangement** to lock the relative rotation and translation between the two consecutive wafer crystals to facilitate	02/≤ 0.5^0

	the assembly and ensure the desired alignment within the **minimum tolerance**.	
10	**Additional thermalization points** should be provided inside the wafer holding ring for the wire mesh/thermalization strip.	≥ 4
11	The additional thermalization points should be aligned within the **minimum tolerance**.	$\leq 2^0$
12	The **wafer holding ring should be universal** for all the DAs to facilitate the assembly and life cycle support of the product.	-
13	The modified top Al casing should also **support the additional thermalization strips.**	-
14	**A gap/clearance** between the wafer crystal and the wafer holding ring is required to facilitate the assembly.	≥ 0.5 mm
15	There should be **no intermediate coupling plates** between the upper and lower aluminium casings.	-
16	**A gap/clearance** between the thermalization rod and the upper aluminium casing is required.	≥ 0.2 mm
17	**A gap/clearance** between the bottom surface of the aluminium upper casing and the top surface of the wafer crystal is required.	≥ 4 mm
18	The lower and upper aluminium casings **should be locked with independent bolts**.	-
19	**A gap/clearance** between the lower and upper aluminium casings is required	0.1 to 0.2 mm
20	The array of holes (8x8) on the top of the upper aluminium casing should be concentric with the cells (8x8) of the wafer crystal within the **minimum tolerance** to perform the operation precisely.	≤ 0.2 mm
21	The prototype of the wafer holders and the wafer holding ring is required to be developed with **AM (SLM technique).**	-
22	Any post-processing step may be added to facilitate the AM and final assembly.	-
23	The new design of the DA should reduce the structural weight.	≥ 10%
24	The new design of the DA should **improve thermal efficiency.**	≥ 10%
25	The new design of DA should **minimize the mechanical vibrations.**	≥ 10%

Based on the list of requirements (***Table 4-1***), the original design of the DA is optimized accordingly. The geometrical features of the new design are mainly decided based on the assembly constraints to successfully accommodate the DA components and the subsequent DA assemblies. Due to the air-tight environment of the cryogenic system for the DA operation, the thermal exchange is carried out only through the heat condition process. In addition, the excessive part of the heat flow occurs along the longitudinal direction of each component, therefore, for the decision point of view regarding the geometrical dimensions, this heat transfer is considered to be one dimensional, however, in thermal analysis the 3D heat transfer is performed to achieve the maximum accuracy.

According to the Fourier's law (law of heat conduction), the rate of heat transfer (q) through a material is proportional to the negative temperature gradient ($-\nabla T$) and to the normal cross-sectional area (A), i.e.,

$$q = AK(-\nabla T) \qquad \textbf{Equation 4-1}$$

$$\nabla T = \frac{\partial T}{\partial x} \qquad \textbf{Equation 4-2}$$

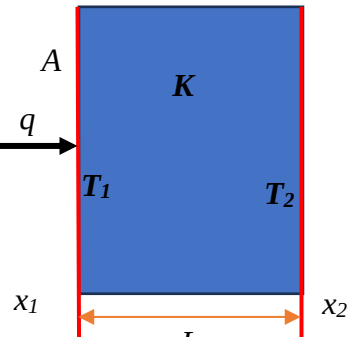

Figure 4-1. *Heat Conduction.*

Where K is the thermal conductivity of the material, T is the temperatures at the boundaries, and x is the total length across the boundaries (as shown in ***Figure 4-1***). Therefore,

$$q = -AK\frac{\partial T}{\partial x} \qquad \textbf{Equation 4-3}$$

Which means that the heat exchange can be improved by reducing the L across the boundaries, therefore, significant attention is paid to the reduction of the heights/thicknesses of the components in order to improve the thermal efficiency.

Hence the DA is suspended through the thermalization rods, therefore, mechanical vibration also occurred (***Figure 4-2***). As there is no external excitation, and the cryogenic system is air-tight, therefore, there a free vibration is occurred without damping. It can be mathematically expressed as,

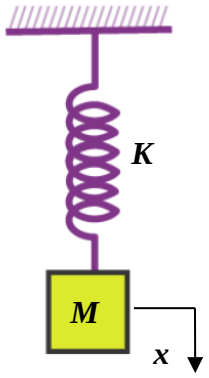

Figure 4-2. *Free Vibration.*

$$M\ddot{x} + Kx = 0 \qquad \textbf{Equation 4-4}$$

Where M is the mass of the DA, $\ddot{x}$ is acceleration, x is the displacement, and K is the stiffness of the thermalization rod. The mathematical expression can also be written in the Frequency response as,

$$Mw^2 + K = 0 \qquad \textbf{Equation 4-5}$$

$$w_n = \sqrt{\frac{k}{M}} \qquad \textbf{Equation 4-6}$$

Where w_n is the natural frequency of the structure, and the mathematical expression shows that if we reduce the structural weight of the DA, it will minimize the mechanical vibrations. We also know that,

$$k = EA/l \qquad \textbf{Equation 4-7}$$

Where E is the young modulus of the material, A is the cross-sectional area, and l is the length of the thermalization rod, therefore, reducing the lengths of the thermalization rods will also contribute to minimize the mechanical vibrations.

In addition, it is emphasized to provide direct contact (with a larger contact surface) between the wafer crystal and the wafer holding ring, to improve the thermal exchange between the two components.

In addition, the following material properties (***Table 4-2*** and ***Table 4-3***) will be used for the simulation and analysis purpose.

Table 4-2. *Case Study: Material Properties.*

Properties	**Materials**				
	Pure Copper	**Silicon Single Crystal**	**Teflon**	**Pure Aluminium**	**Brass**
Density (Kg/m^3)	8940	2329	2170	2700	8490
Youngs Modulus (Pa)	115e^9	129e^9	0.599e^9	68.9 e^9	97 e^9
Poisson Ratio	0.31	0.278	0.46	0.33	0.31
Yield/*Tensile Strength (Pa)	365e^6	*950e^6	131e^6	275e^6	124 e^6
Coefficient of linear Thermal Expansion (K^{-1})	17e^{-6}	2.6e^{-6}	10e^{-6}	-	-
Thermal Conductivity (W/mK)	391	149	0.3	-	-
Heat Capacity (J/KgK)	385	713	1500	-	-

Table 4-3. *Case Study: DA Mass Details.*

Number	**Component**	**Mass (kg)**	**Quantity**	**Total Mass (kg)**
1	Upper Aluminium Casing	0.338	01	0.338
2	Lower Aluminium Casing	0.279	01	0.279
3	Thermalization Rod	0.029	02	0.058
4	Wafer Holder	0.003	04	0.012
5	Wafer Holding Ring	0.076	01	0.076
6	Wafer Crystal	01	01	0.071
7	Aluminium Casings' Bolt	0.004	02	0.008
	Total Mass of the Detector Assembly (kg)			**0.842**

In this research work, a design-development workflow (***Figure 4-3***) is introduced, that abridges the gap between the design and the manufacturing workflows as described in section 2.2. The proposed workflow is based on the list of requirements (***Table 4-1***). This list of requirements is successfully translated into the initial design phase to facilitate the subsequent 3D modelling (with and without lattice structure), manufacturing, and assembly phases. In the given workflow, it can be seen that both the design phases are dependent on the list of requirements, while the prototyping & validation phase is dependent on both the list of requirements and design phases.

The design optimization is carried out in two stages: first without the lattice structure, and second with the lattice structure. In the first optimization stage, it is ensured that the optimized design (without lattice) has the capability to stack up three wafer assemblies successfully, withstand a fail-safe cryogenic operation, and the prototyping with AM in accordance with the stipulated requirements. In

the second optimization stage, the infill volume lattice (with an optimal cell structure) is employed in the wafer holding ring, under the consideration of the assembly constraints, to further reduce the structural weight, reduce the mechanical vibrations, and improve the thermal efficiency. In addition, to facilitate the AM of the desired component and minimize the possible thermal distortion, the support structure for the AM is also designed with an optimized lattice structure.

The proposed design is initially validated through numerical simulations (structural, modal, and thermomechanical analysis), and virtual 3D assembly. However, it is physically validated through prototyping and subsequent experimental tests. Due to the significant importance of the wafer holders and the wafer holding ring, 3D scanning of the additively manufactured components is also performed through the reverse engineering technique of photogrammetry, as a quality check of the AM process.

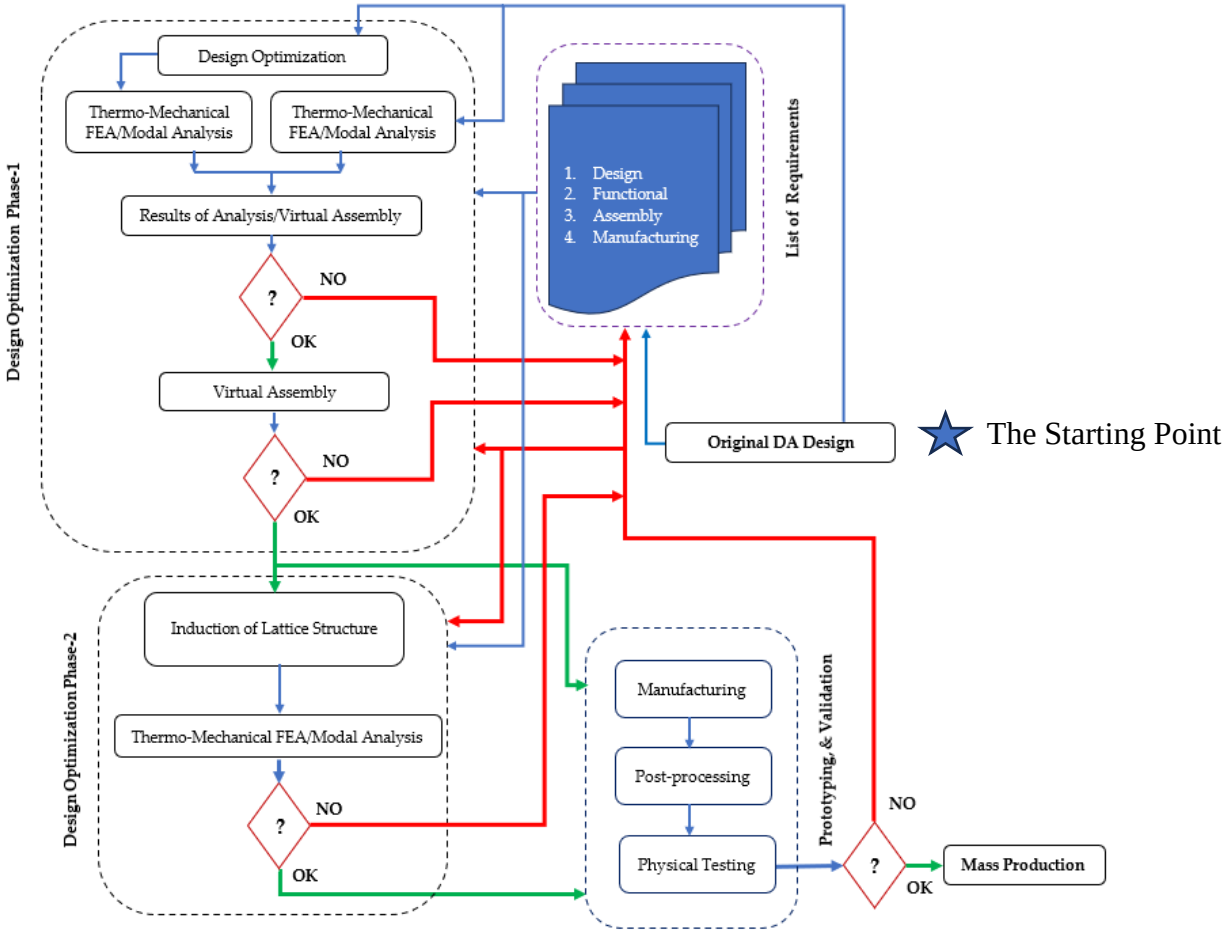

Figure 4-3. *Workflow.*

4.2. Aim and Objectives.

The test case study is extremely challenging due to the fact that it is a multi-physics problem and warrants the achievements of several multi-dimensional requirements simultaneously, such as the structural weight reductions, improving the thermal efficiency, improving the structural stiffness against mechanical vibrations, design for assembly, and design for additive manufacturing.

The basic aim is to achieve the target values of the list of requirements via following objectives:

- To translate the list of requirements into the initial design phase, prototyping, and physical assembly, by adhering to the design-development workflow.
- To develop the appropriate FEA structural, modal, and thermal models for the numerical simulation and validation purposes.
- Selection, design, and implementation of the appropriate lattice structure for the support structure of AM.
- Selection, design, and implementation of the suitable lattice structure for the test case study.
- Selection and implementation of the appropriate reverse engineering technique for the quality inspection of the components prototypes via AM.

4.3. Design and Manufacturing Details of the New Design.

Several software (***Figure 4-4***) is used for the CAD modelling, FEA modeling and simulation (for structural, modal, and thermal analysis), and design of lattice structures for the infill volume and the support structure of AM.

Manufacturing of the new design is executed according to ***Figure 4-5***. However, the post-processing of the AM components is carried out with the help of traditional lath/milling machines.

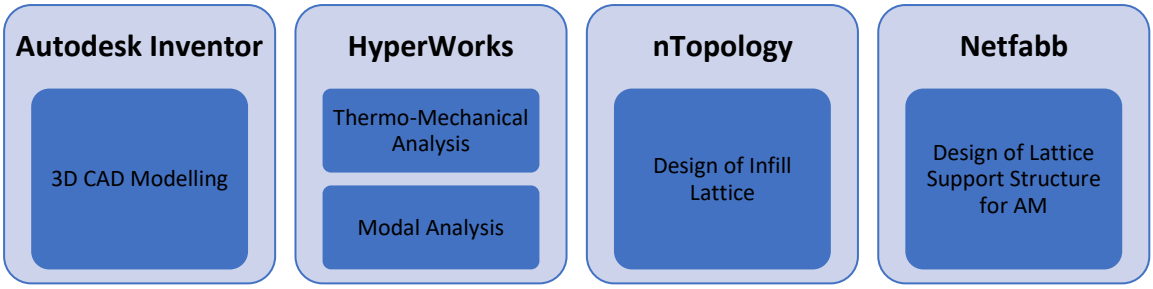

Figure 4-4. *Design Details of the New Design.*

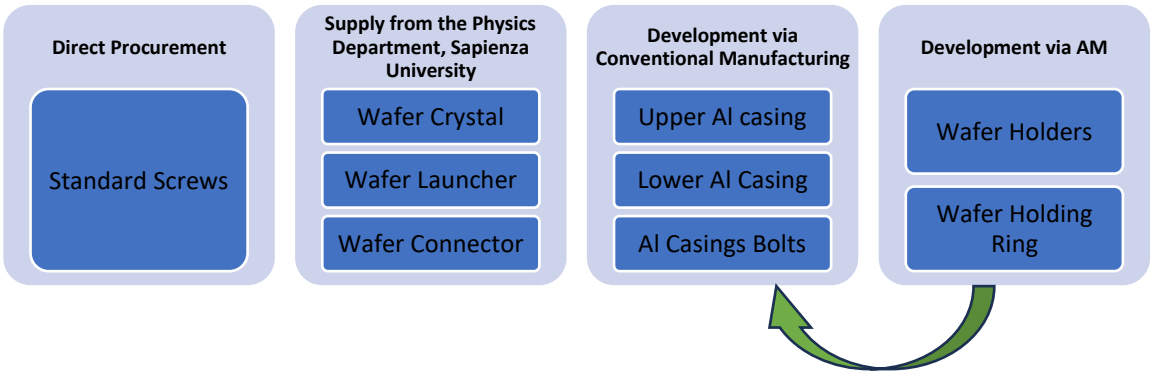

Figure 4-5. *Manufacturing Details of the New Design.*

5. Chapter: Design via Virtual Prototyping.

This chapter describes the 3D modelling of the new design (phase 1; design without lattice) under the prescribed design methodology (section 4.1). It also provides details about the complete virtual assembly. The purpose of the design in phase 1, is to provide a base design for the next subsequent design with lattice structure (phase 2: Chapter 8), after the numerical and physical validation. In phase 1, the new design is finalized after several stages, and each stage is followed by particular feedback during the design, manufacturing, and assembly phases.

The original design of the DA is optimized accordingly based on the list of requirements (***Table 4-1***). The major design modifications are carried out in the wafer holding ring, aluminium casings, and thermalization rods. However, minor changes are performed in the silicon wafer. The design of wafer holders, and the aluminium casings' bolts is completely changed, even the material of the wafer holders is replaced with pure copper to make it lightweight and improve the thermal exchange process.

5.1. Design of the Wafer Holding Ring.

The first optimized wafer holding ring (***Figure 5-1****a*) is provided with several contours to support the new design of the wafer holders and the subsequent wafer assemblies. The height of the wafer holding ring is 6mm and it is designed in such a way to maintain the minimum desired gap/clearance of 1mm between the two consecutive wafer assemblies. The wafer holding ring is also provided with four vertical pins on its top surface to suffice the following functions:

- To lock the next wafer assembly.
- To keep the next wafer assembly vertically aligned, as desired.
- To ensure the rotation of the next wafer assembly by 90^0.

After the prototyping of the first design, some geometrical distortions/deviations were observed during the physical assembly of the DA, which caused poor contact between the wafer and the wafer holding ring. Therefore, the area of the same contact surface was increased by replacing the four wafer's supports with two larger supports. In addition, an extra thickness of 0.2mm was also added to this new contact surface, which is subsequently machined with the help of lath machine to provide the desired flatness as a pot-processing step. In addition, the vertical pins, holes for thermalization rods and thermal strips were also modified to facilitate the AM and assembly.

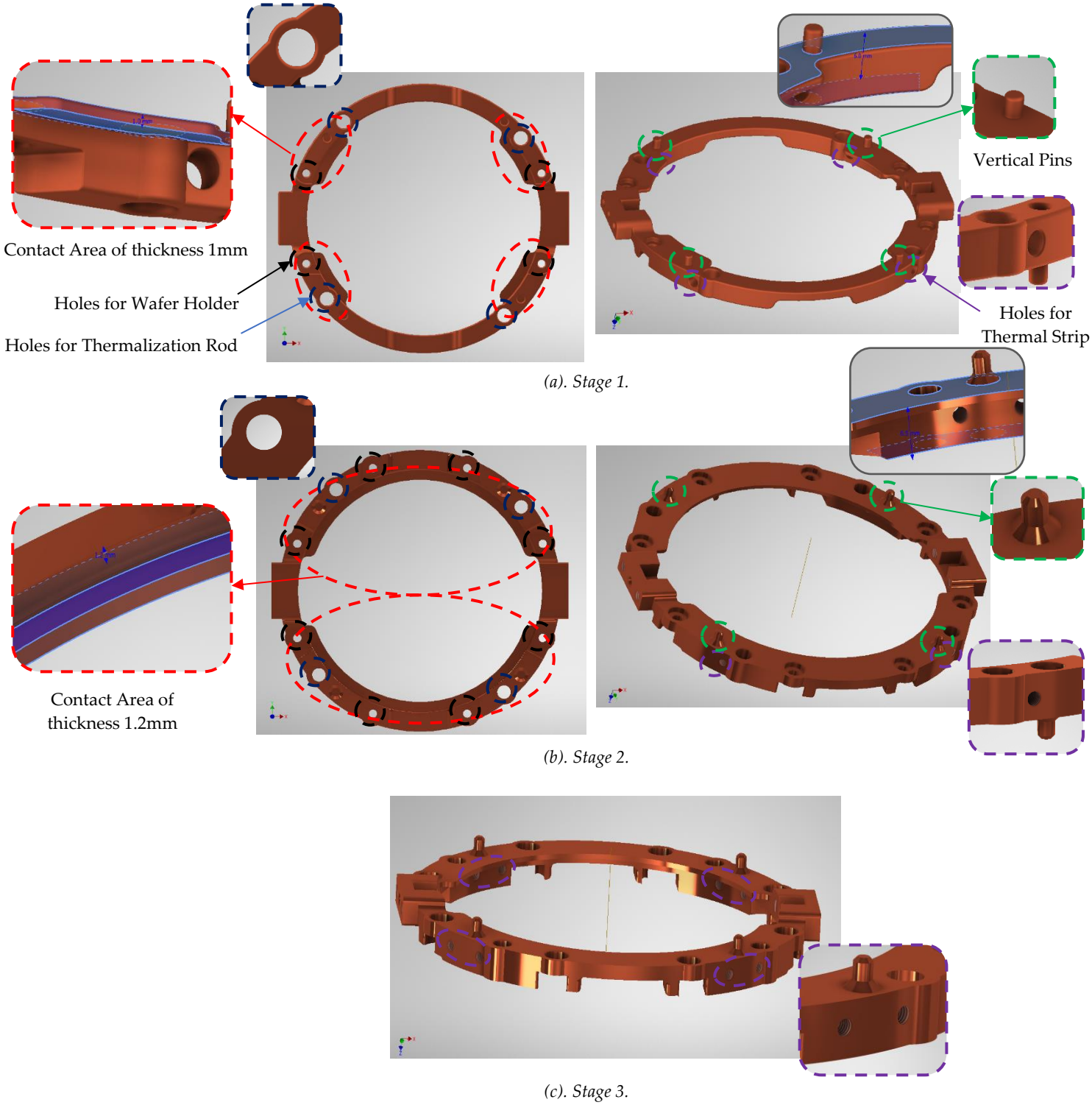

Figure 5-1. *Optimized Design of the Wafer Holding Ring.*

The physics department also proposed to increase the gap/clearance between the two consecutive wafer assemblies from 1mm to 1.5mm. Therefore, the thickness of the top surface of the wafer holding ring is increased by 0.5mm to achieve the desired clearance (***Figure 5-1****b*).

After the second prototyping, the physical assembly stage went well, just the stakeholder of the physics department again proposed to increase the number of holes for the thermal strips from 4 to 8, and to increase the number of wafer holders from 4 to 8. The final modified design after the 3rd iteration can be seen in ***Figure 5-1****c*.

5.2. Design of the Wafer Holders.

The design of the wafer holders is modified in a way to lock the wafer by utilizing the grooves inside the wafer, therefore, the new wafer holders are smartly customized according to the grooves of the wafer crystal. In addition, the Teflon material of the wafer holder is also replaced with pure copper to improve the thermal efficiency of the structure. This new mechanism of locking also provides a better management of the wafer's thermal contraction and subsequent expansion during the cryogenic thermal exchange process. For this new design of the wafer holder, the respective grooves of the wafer crystal are also modified in an efficient way to accommodate the new design of the wafer holder with better physical contact. The new design of the wafer holder is carried out in three iterations. In the first design stage, four wafer holders are utilized to lock the wafer crystal, as shown in ***Figure 5-2****a*. After the first prototyping of the wafer holder with AM, it was observed during the physical assembly process that due to the AM layer roughness the wafer holders are getting stuck inside the wafer's grooves. Therefore, it was proposed to reduce the width of the wafer holder's forks such that to provide a minimum tolerance of 0.2mm between the side walls of the wafer's grooves and the wafer holder's forks, as shown in ***Figure 5-2****b*. Later on, the stakeholder of the physics department also modified the design of the wafer crystal and proposed to modify the wafer holder accordingly and also increase the number of wafer holders from four to eight (***Figure 5-2****c*). In this new design of the wafer crystal, the lengths of the respective grooves for accommodating the wafer holders were also increased to ensure a larger contact area between the wafer crystal and the wafer holder, which will help to lock the wafer crystal efficiently and increase the thermal efficiency of the structure.

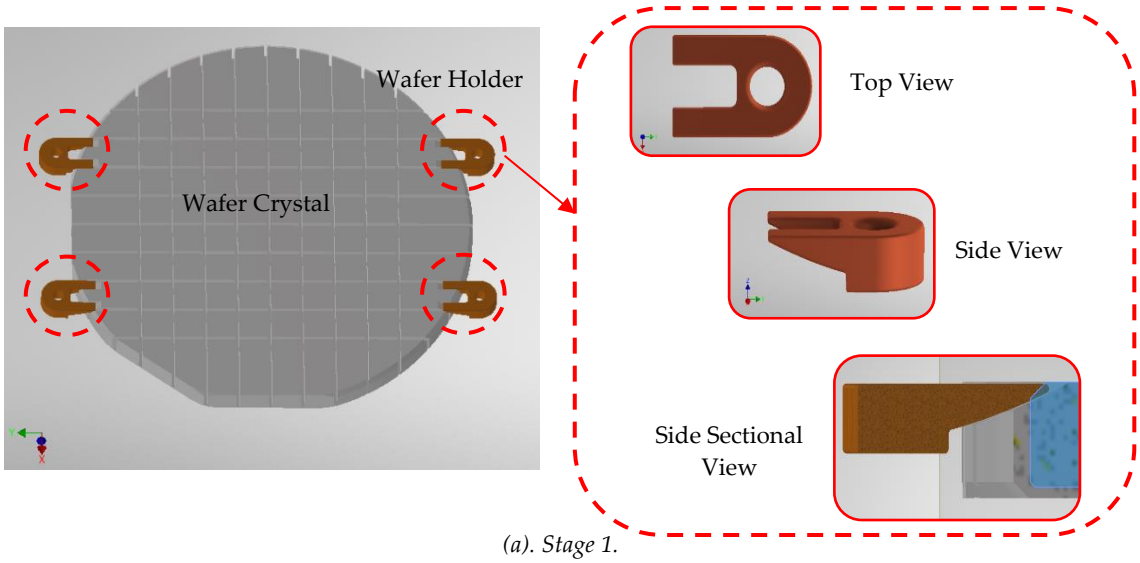

(a). Stage 1.

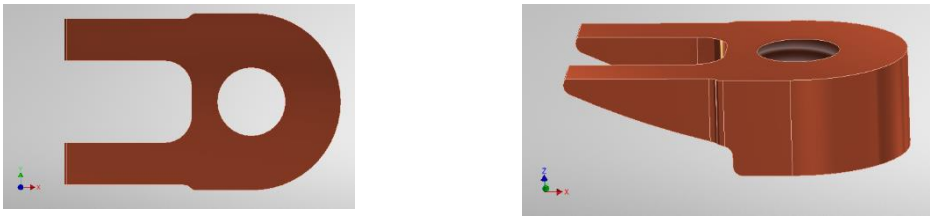

(b). Stage 2.

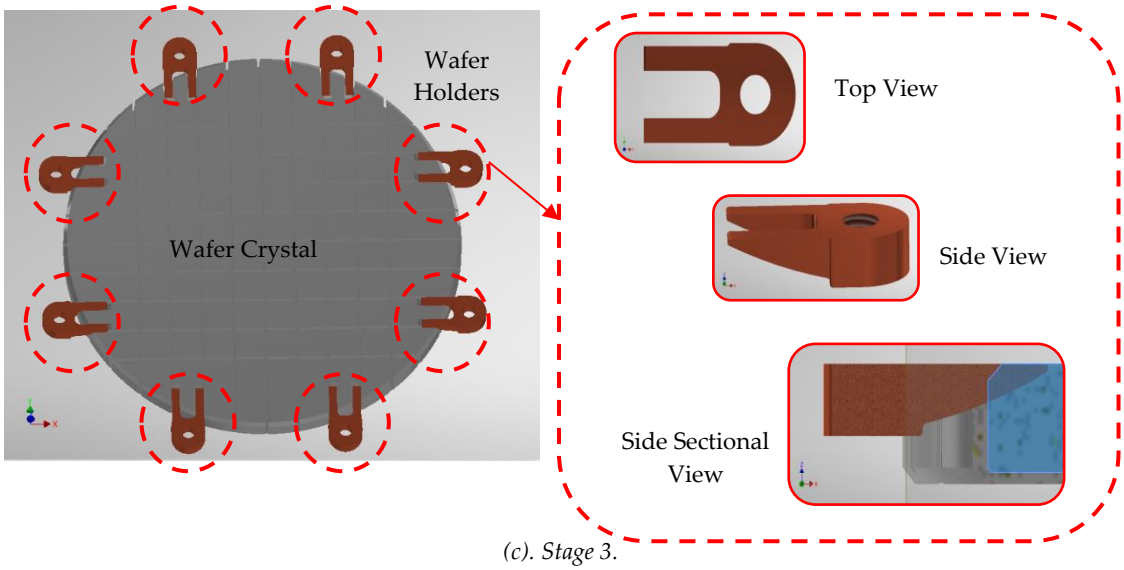

(c). Stage 3.

Figure 5-2. *Optimized Design of the Wafer Holders.*

5.3. Design of the Thermalization Rods.

Design of the thermalization rod is performed into two design stages and all the design parameters are in accordance with the list of requirements. After the first design stage, the physics department proposed to increase the number of thermalization rods from two to four to mitigate the vibration issue and also modify its design in such a way to increase its stiffness and the final assembly should provide a vertical gap of 30mm between the DA assembly and the lower

mounting plate of the cryogenic device. For this purpose, different lengths of the thermalization rod were altered (***Figure 5-3***) to fulfill the requirements.

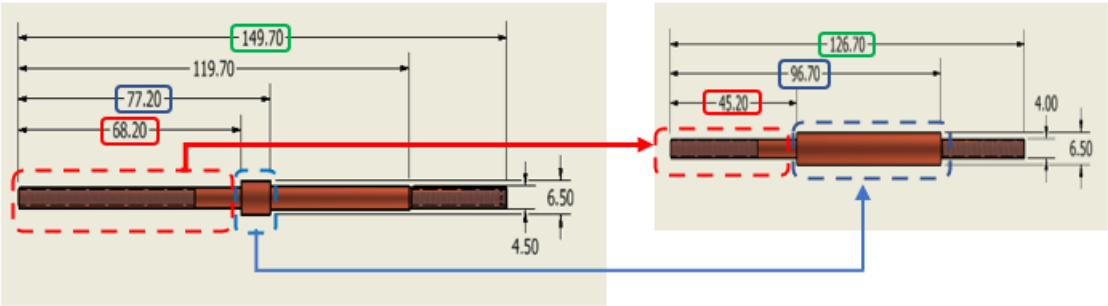

(a). Stage 1. *(b). Stage 2.*

Figure 5-3. *Optimized Design of the Thermalization Rods.*

5.4. Design of the Aluminium Casings.

The design of the lower and upper aluminium (Al) casings, needed for the electromagnetic shielding, is carried out in such a way to accommodate up to three wafer assemblies without intermediate coupling, also allowing the desired gap (0.1mm to 0.2mm) between the upper and lower casings during the DA assembly. In addition, it also provides enough rooming for the interfaces pertaining to wafer electronics, optical fibers, and thermal connectivity. Design of the lower Al casing is carried out into two iterations. The first design stage provides the assembly provision of just two thermalization rods (***Figure 5-4****a,b***). However, after the proposal by the stakeholder for the provision of the four thermalization rods, the design of the lower Al casing is modified in the second design iteration and made it capable to facilitate the assembly of four thermalization rods (***Figure 5-4****c,d***).

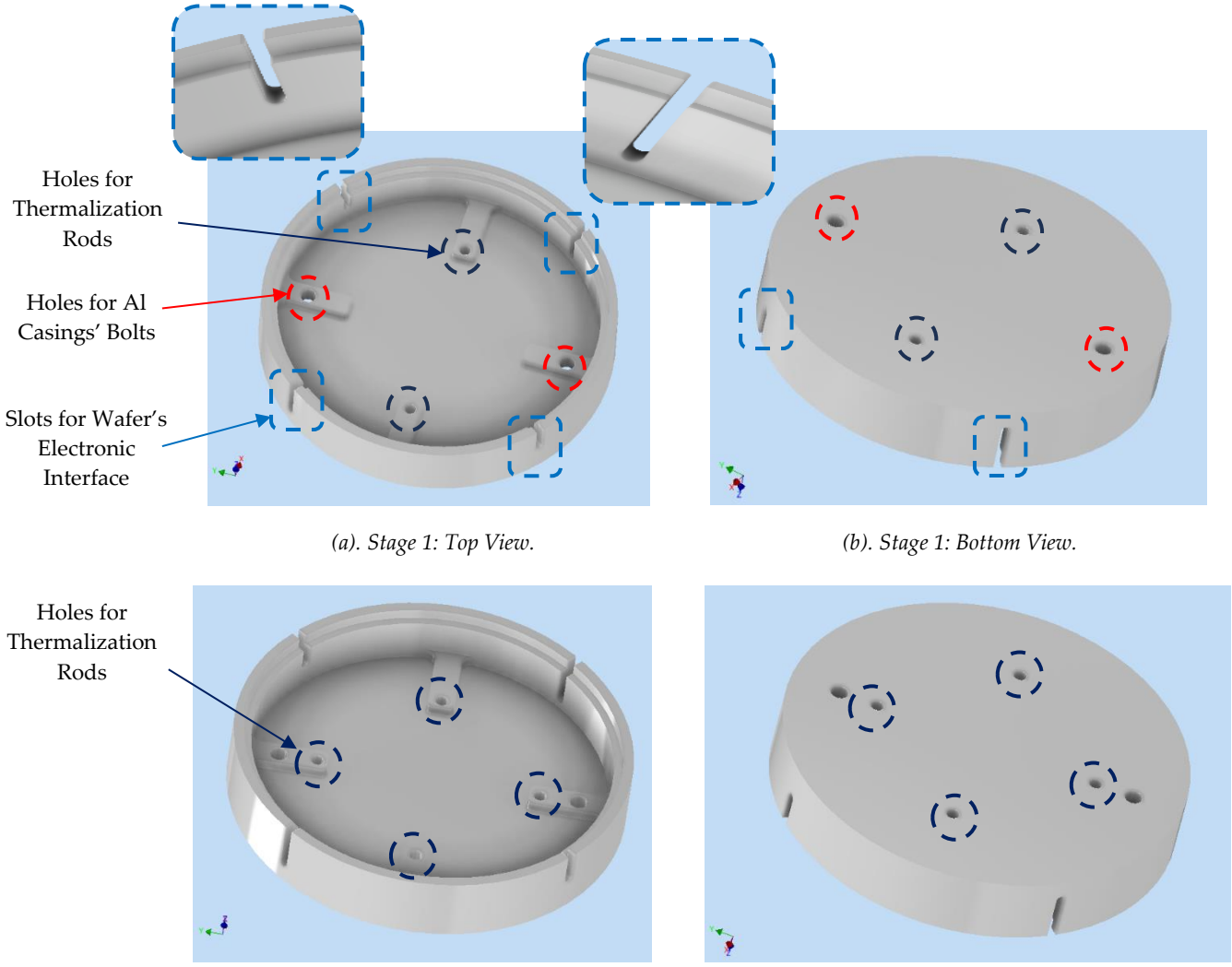

(a). Stage 1: Top View.

(b). Stage 1: Bottom View.

(c). Stage 2: Top View.

(d). Stage 2; Bottom View.

Figure 5-4. *Optimized Design of the Lower Al Casing.*

The upper Al casing is of significant importance, because in addition to the assembly of the wafer's electronic interface and thermalization rods, it is also responsible to provide the assembly provision for the interface of the 8x8 array of optical fibers (***Figure 5-5****a,b*). Furthermore, it also ensures the vertical alignment of the optical fibers with the cells of the wafer crystal (***Figure 5-5****c*). The holes for the optical fibers are designed in the tapered profile in order lock the optical fibers effectively and avoid any possible disturbance due to the mechanical vibrations. Design of the upper Al casing is performed into three iterations. The first design iteration provides the assembly provision of just two thermalization rods. However, after the proposal by the stakeholder for the provision of the four thermalization rods, the design of the upper Al casing is modified in the second design iteration and made it capable to facilitate the assembly of four thermalization rods, and its extruded features are also removed to reduce the machining efforts (***Figure 5-5****d,e*). While in the third design iteration, the additional four slots are provided for the thermal strips suggested by the stakeholder of physics department (***Figure 5-5****f,g*).

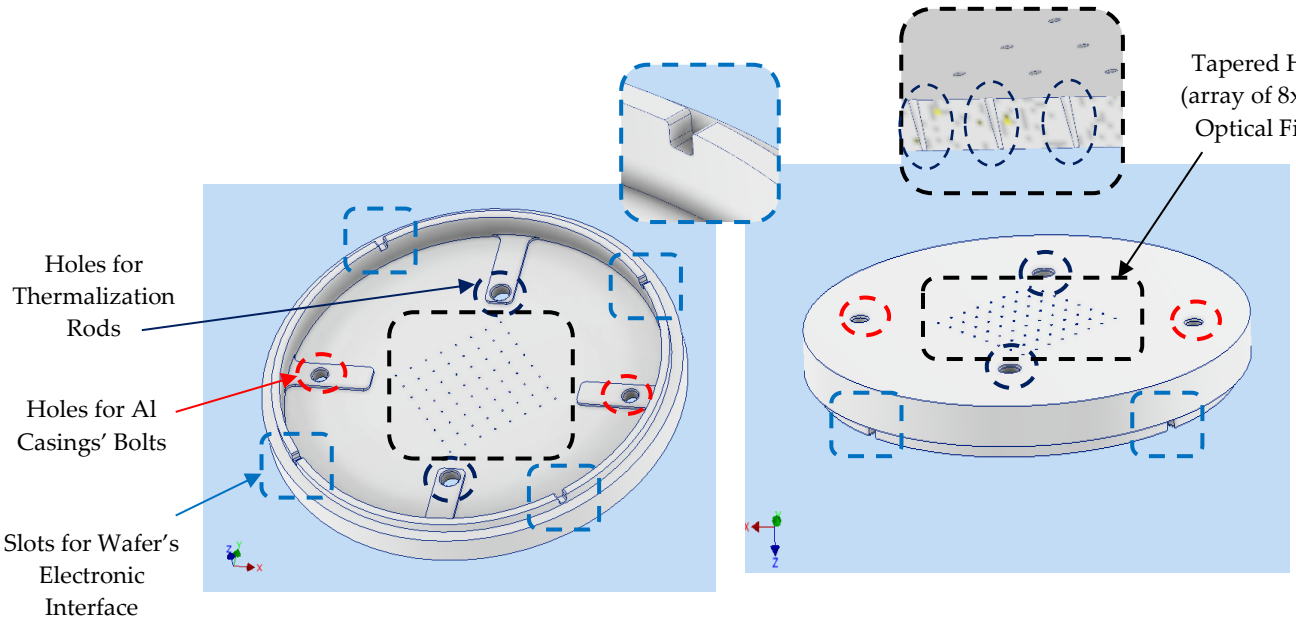

(a). Stage 1: Bottom View. *(b). Stage 1: Top View.*

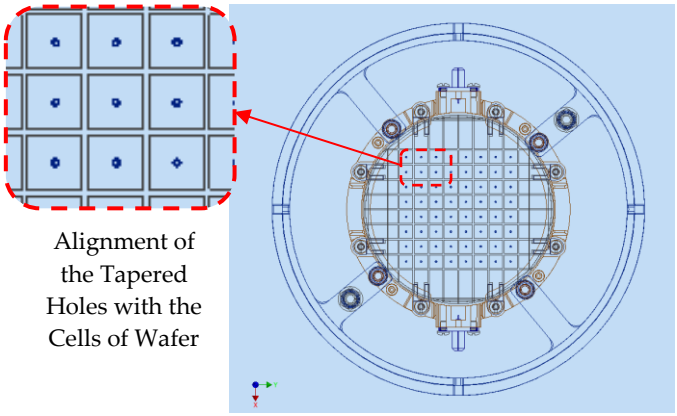

(c). Stage 1.

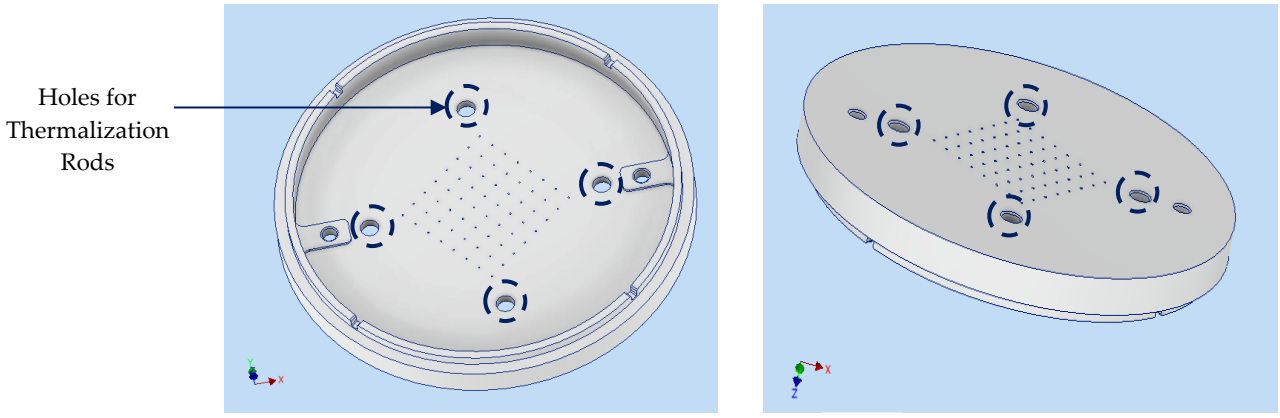

(d). Stage 2: Bottom View. *(e). Stage 2: Top View.*

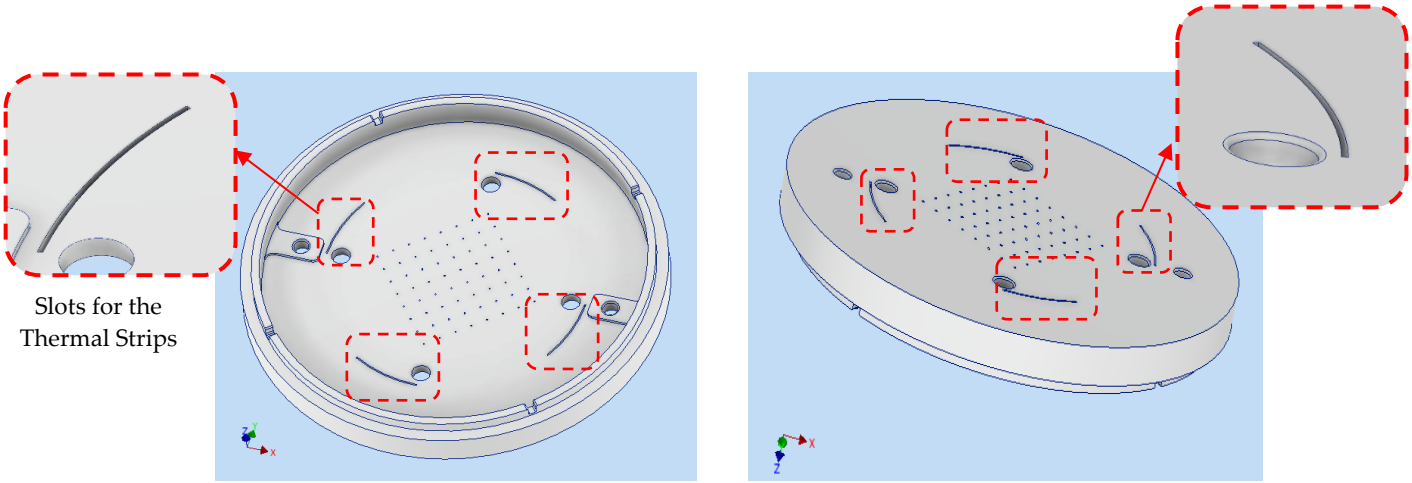

(f). Stage 3: Bottom View.

(g). Stage 3: Top View.

Figure 5-5. *Optimized Design of the Upper Al Casing.*

5.5. *Design of the Aluminium Casings' Bolt.*

The Al casings' bolt is used to assemble the upper and lower Al casings with a fail-safe operation, and it is designed in such a way to allow the desired gap (0.1mm to 0.2mm) between the upper and lower casings. In fact, the commercial hexagonal socket head shoulder screw (ISO 7379 6x40:1) is modified (***Figure 5-6***) to achieve the desired design of the Al casings' bolt. This bolt is a standard item, which minimizes the machining efforts and makes sure the easy market availability. In addition, it is designed with brass material, which is a thermal efficient material for thermal exchange applications.

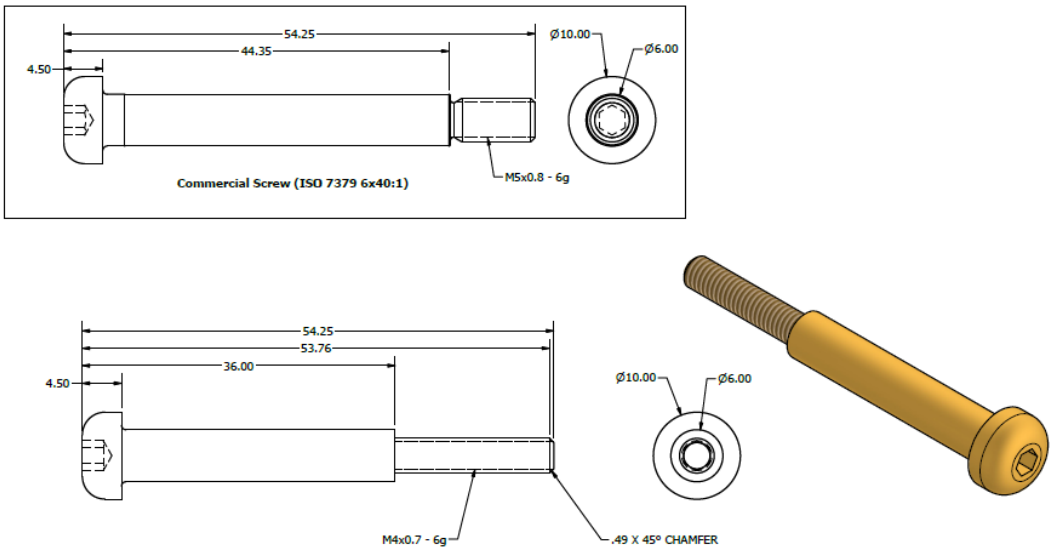

Figure 5-6. *Optimized Design of the Al Casings' Bolt.*

5.6. *Design Modification of the Cryogenic Device Mounting Plates.*

Due to the increase of the thermalization rods from two to four, three mounting plates of the cryogenic device (***Figure 5-7***) are also modified in order to accommodate the modified assembly scheme of the four thermalizations rods. In addition, due to the presence of the existing numerous holes and slots in the mounting plates, the two old holes for the assembly of the two thermalization rods cannot be used anymore with the combination of two new holes for the subsequent two additional thermalization rods, therefore, four new holes are created to fulfill the requirements (***Figure 5-8****a-c*). Cryostat is working with pulse tubes on the top; so, everything is suspended from the top plates in order to remove the heat by conduction with cold parts.

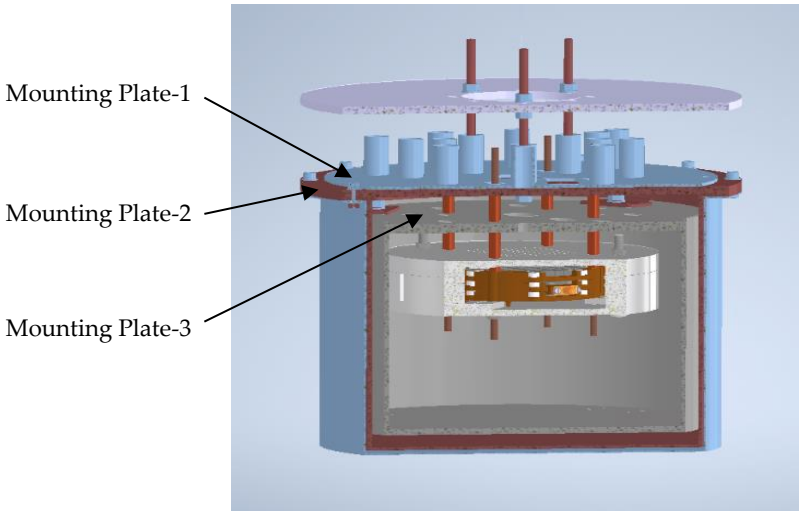

Figure 5-7. *Details of the Cryogenic Device Mounting Plates.*

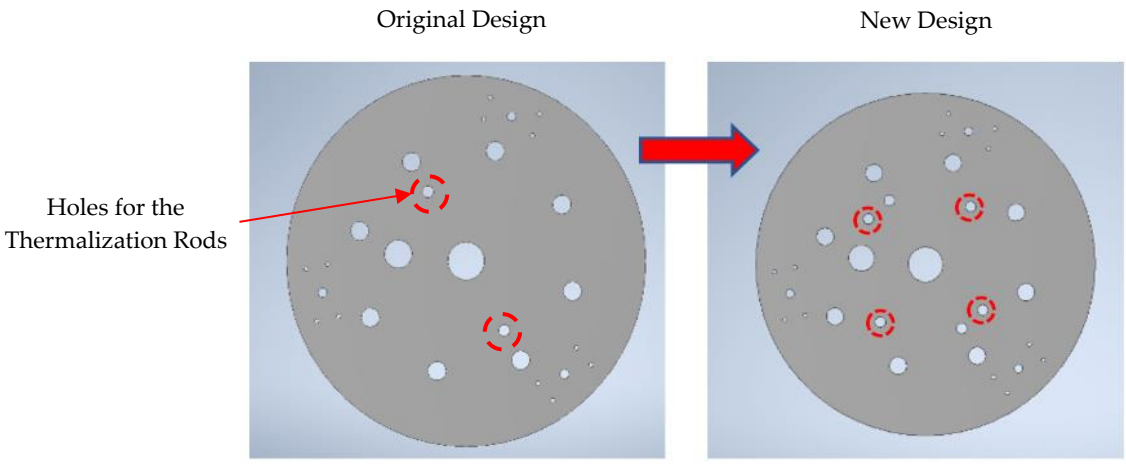

(a). Mounting Plate 1.

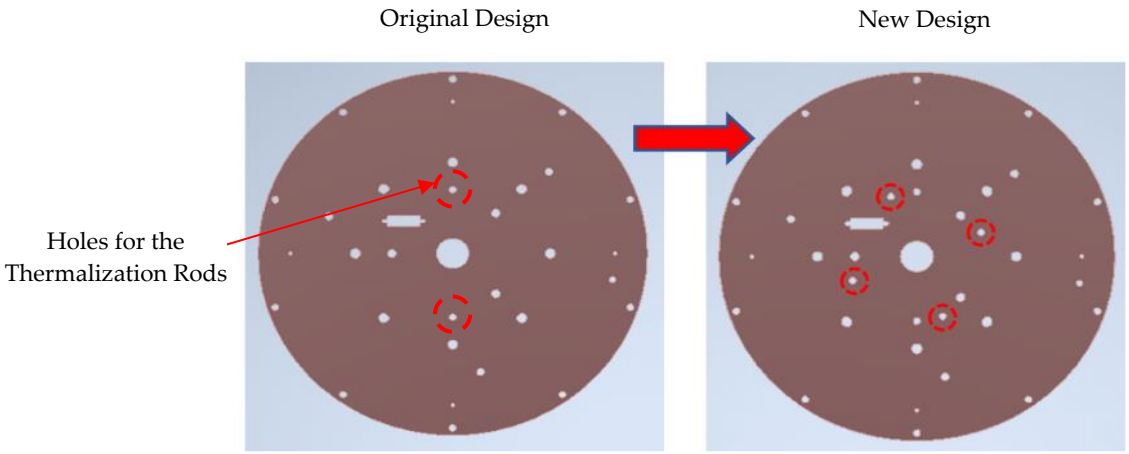

(b). Mounting Plate 2.

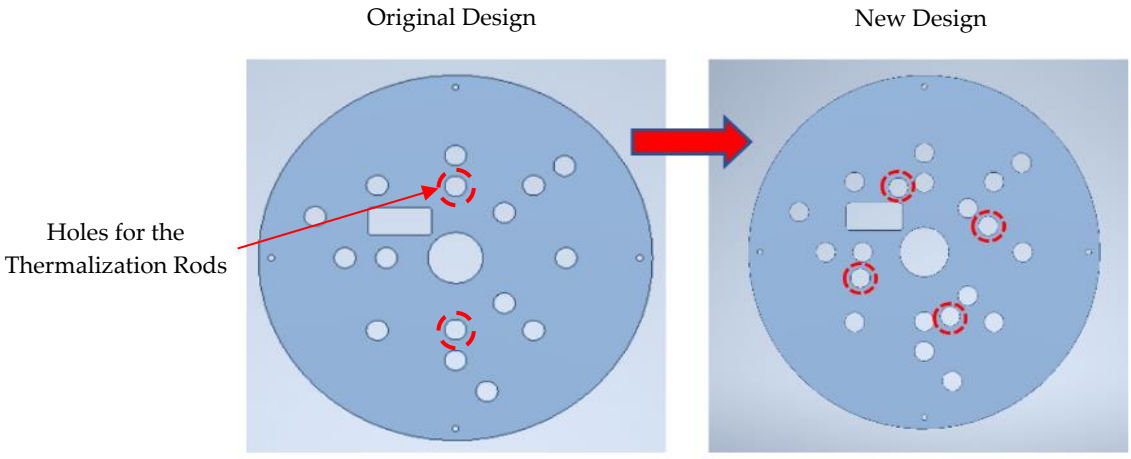

(c). Mounting Plate 3.

Figure 5-8. *Design Modification of the Cryogenic Device Mounting Plates.*

5.7. Virtual Assembly.

The virtual assembly is the first step of the dimensional quality check to conclude that all the components are assembled accordingly within the prescribed tolerances and positions as indicated by the list of requirements. Furthermore, the virtual assembly of this project is carried out into two steps. In the first step it is concluded that all the components are assembled correctly as per the desired tolerances and positions. However, in the second step, the physics department proposed to maintain a vertical gap of 30±0.5mm between the DA assembly and the lower mounting plate of the cryogenic device, and a vertical gap of 5.5±0.5mm between the wafer assembly (wafer's top surface) and the upper Al casing (upper Al casing's lower surface). Therefore, the additional two sets of Teflon spacers are designed to cater for this requirement. Both the sets of the Teflon spacers have the same internal and external diameters but with different heights. The assembly is performed according to the following workflow (***Figure 5-9***).

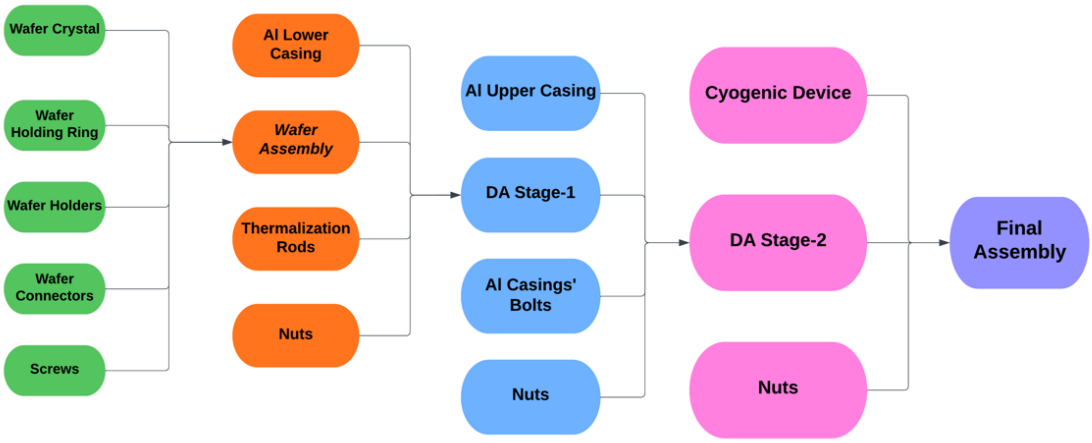

Figure 5-9. *Assembly Workflow.*

5.7.1. Wafer Assembly (WA).

The wafer crystal is assembled inside the wafer holding ring with the help of wafer holders and relevant screws (M2.5x0.45x-6g; AS 1427). In addition, the wafer connectors are assembled to the wafer holding ring with the help of screws (M2.5x0.45x-6g; AS 1427), as shown in (***Figure 5-10***).

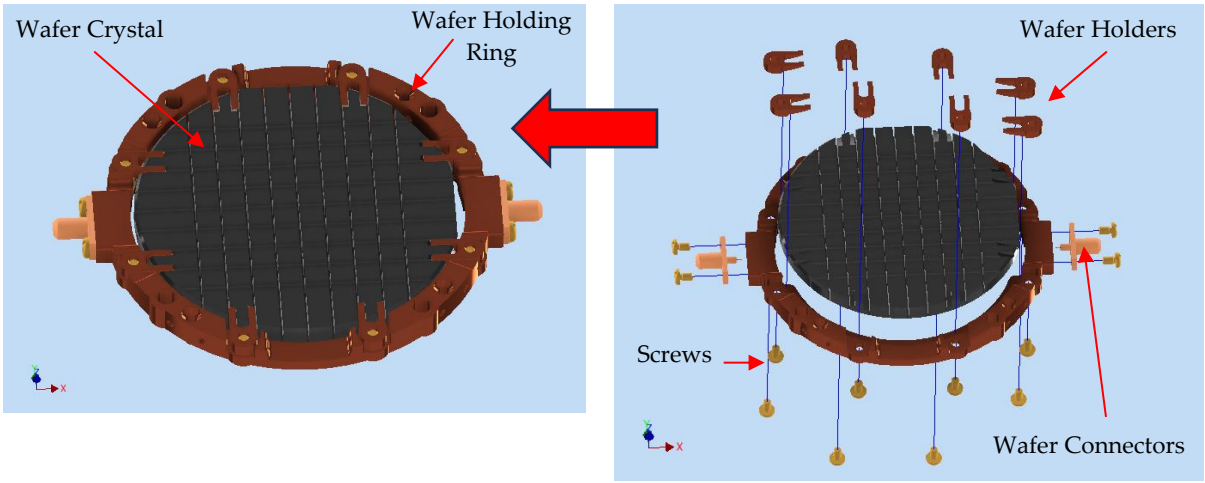

(a). WA. *(b). WA: Exploded View.*

Figure 5-10. *Wafer Assembly.*

5.7.2. DA Stage-1.

In the next step (DA stage-1), a single/or double/or triple wafer assemblies are assembled inside the Al lower casing with the help of thermalization rods and the relevant nuts (M4x0.7-6H; ISO 2432). A combination of double nuts is used to ensure an effective locking of the assembly, as shown in (***Figure 5-11***). In addition, ***Figure 5-11****e* shows that the WA-1 maintains an angle of 90^0 with the subsequent WA-2, and similarly, the WA-2 maintains an angle of 90° with the subsequent WA-3, as desired.

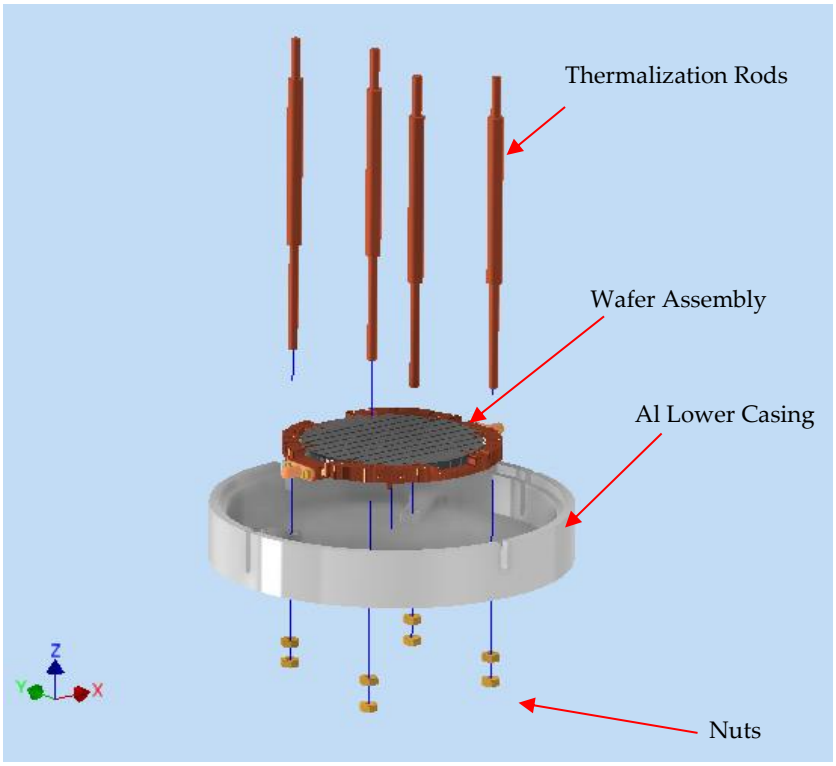

(a). Exploded View.

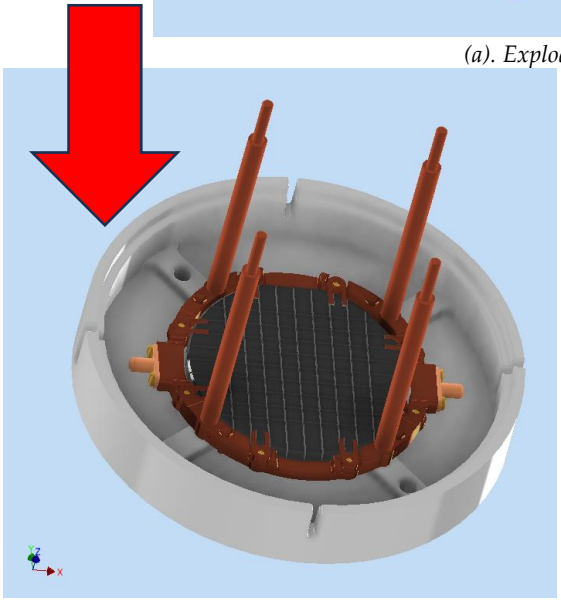

(b). With Single WA.

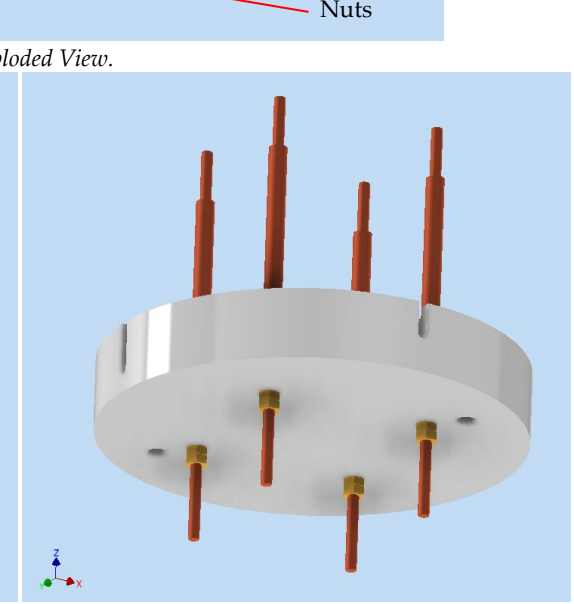

(c). With Single WA.

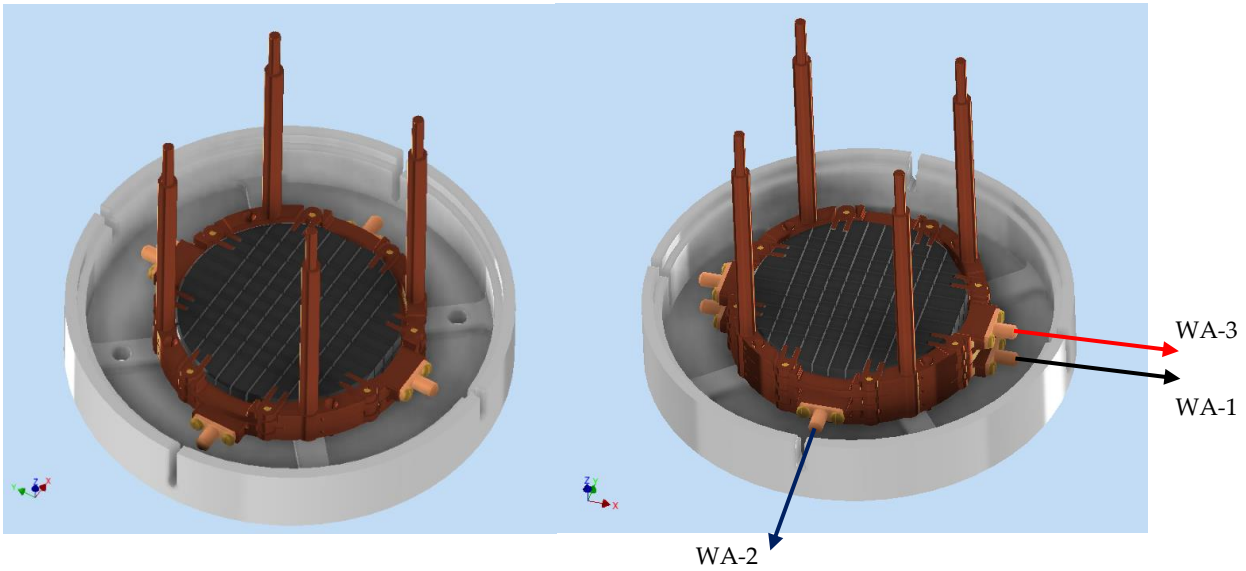

(d). With Two WAs. *(e). With Two WAs.*

Figure 5-11. *DA Stage-1.*

5.7.3. DA Stage-2.

In this step (DA stage-2), the DA stage-1 (with single/or double/or triple wafer assemblies) is assembled with the upper Al casing with the help of Al casings' bolts and the relevant nuts (M4x0.7-6H; ISO 2432). A combination of double nuts is used to ensure an effective locking of the assembly, as shown in (***Figure 5-12***).

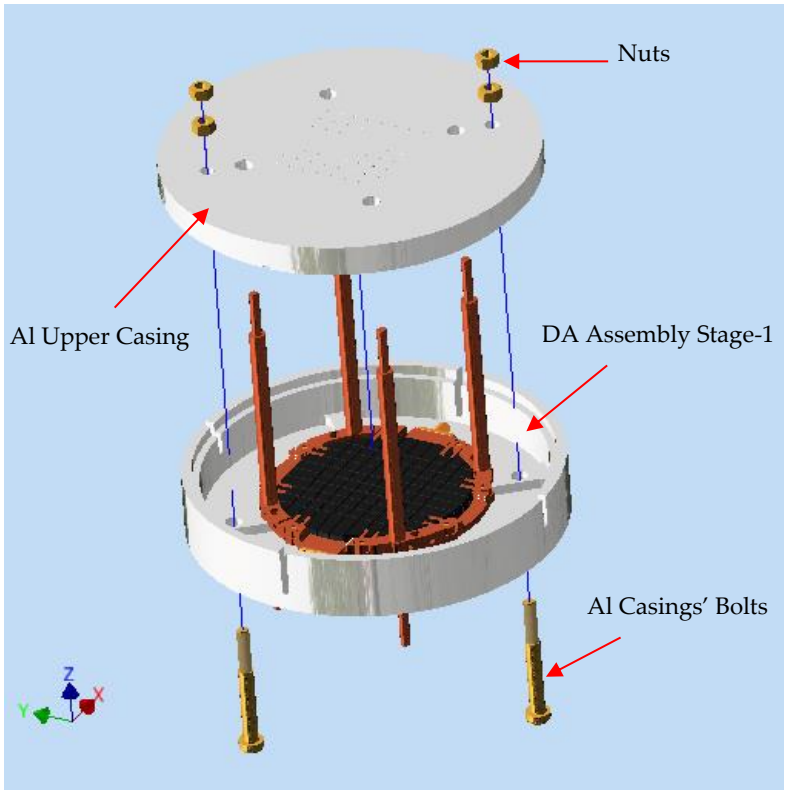

(a). Exploded View.

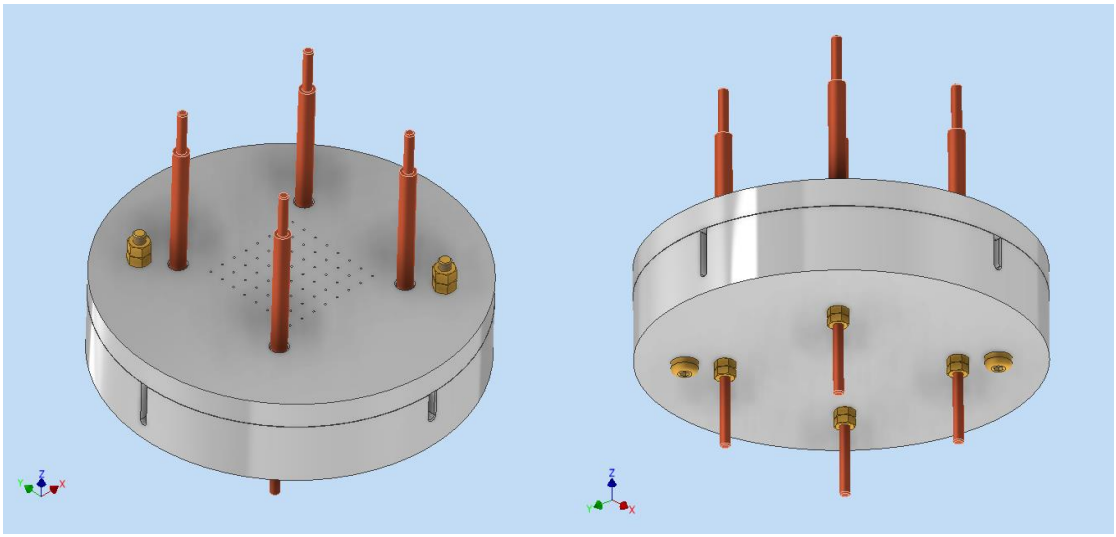

(b). Assembly. *(c). Assembly.*

Figure 5-12. *DA Stage-2.*

5.7.4. Final Assembly.

The DA stage-2 completes the full assembly of the DA and makes it ready for the subsequent assembly to the cryogenic device, which is the final assembly of the project. The full DA (with single/double/triple wafer assemblies) is assembled to the cryogenic device with the help of thermalization rods and the relevant nuts (M4x0.7-6H; ISO 2432). A combination of double nuts is used to ensure an effective locking of the final assembly, as shown in (***Figure 5-13,14***).

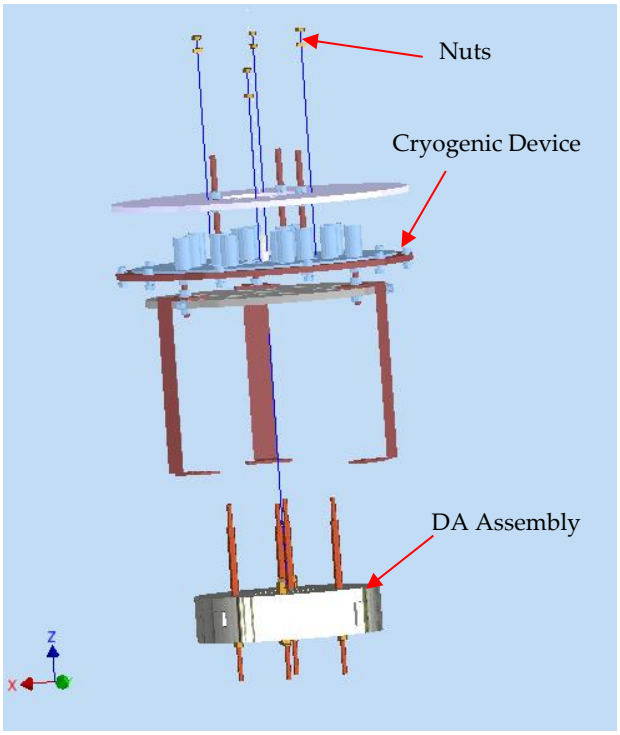

Figure 5-13. *Final Assembly-Exploded View.*

Figure 5-14 shows that the vertical gap between the lower mounting plate of the cryogenic plate and the DA (top surface) is different in all three cases. Similarly, the vertical gap between the Al upper casing (lower surface) and the WA (top surface) is different in all three cases.

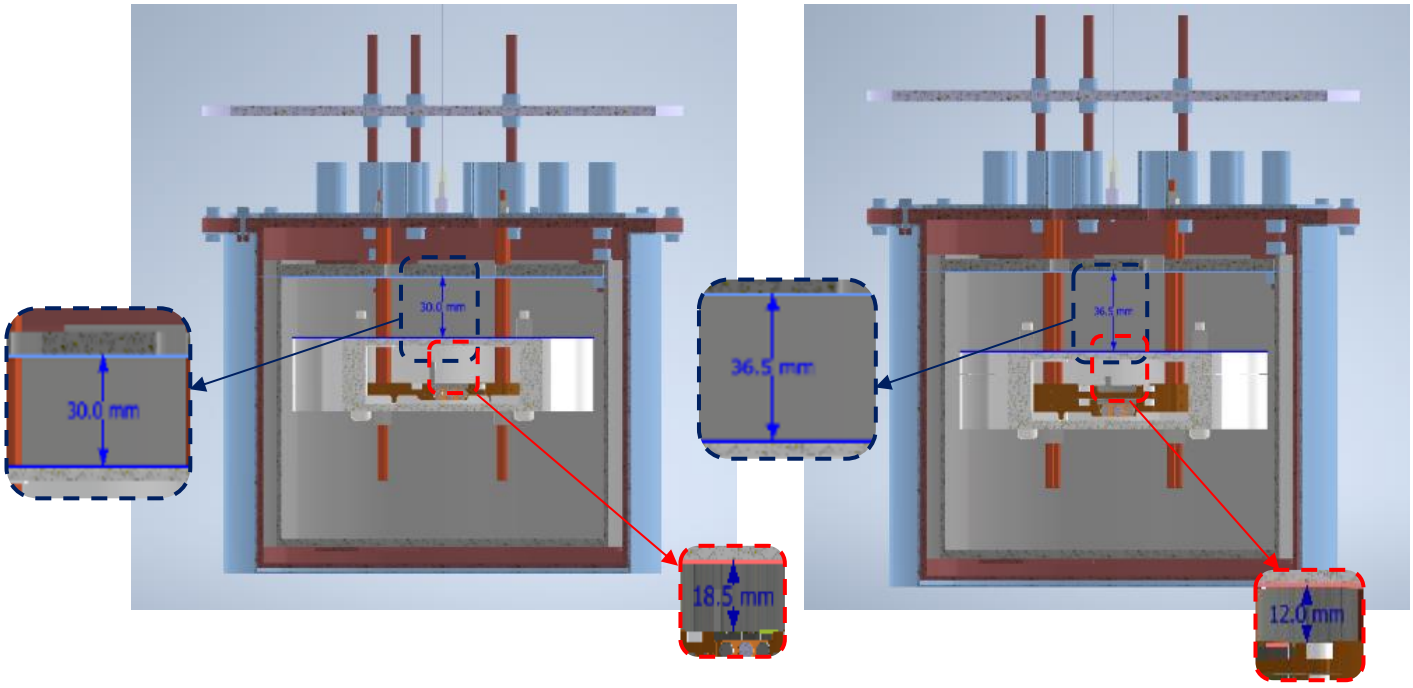

(a). With Single WA. *(b). With Two WAs.*

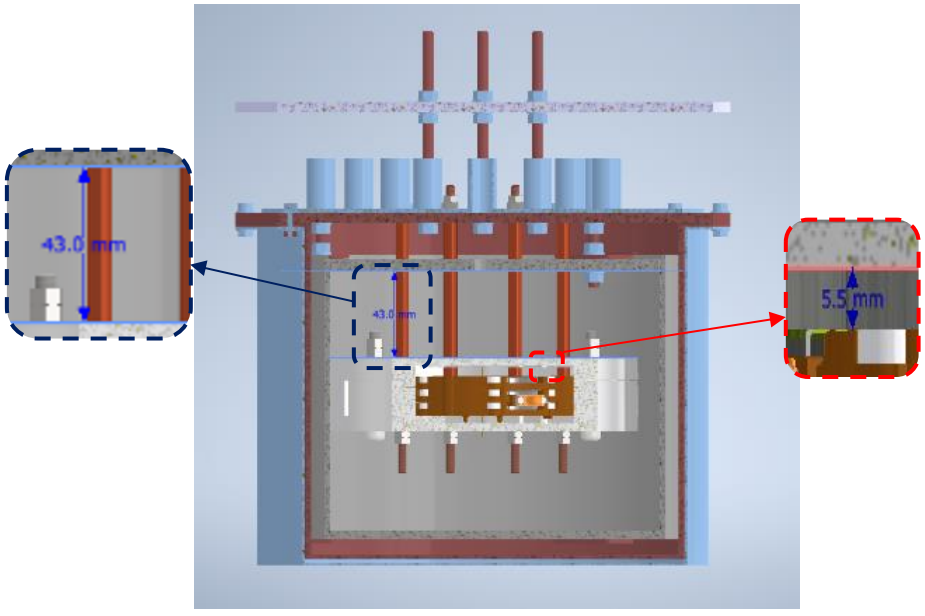

(c). With Three WAs.

Figure 5-14. *Final Assembly: Stage 1.*

In the second step of the assembly, the same assembly steps are followed as applied in the step-1 of the assembly, but just one extra step is added to the DA Stage-1 (in case of single WA and two WAs), i.e., to use the Teflon spacers (***Figure 5-15*****)** in order to obtain the desired vertical gap between the lower mounting plate

of the cryogenic device and the DA, and the vertical gap between the Al upper casing and the wafer crystal. The new scheme of the DA Stage-1 is shown in ***Figure 5-16***, while details of the vertical gaps in all three cases are shown in ***Figure 5-17***.

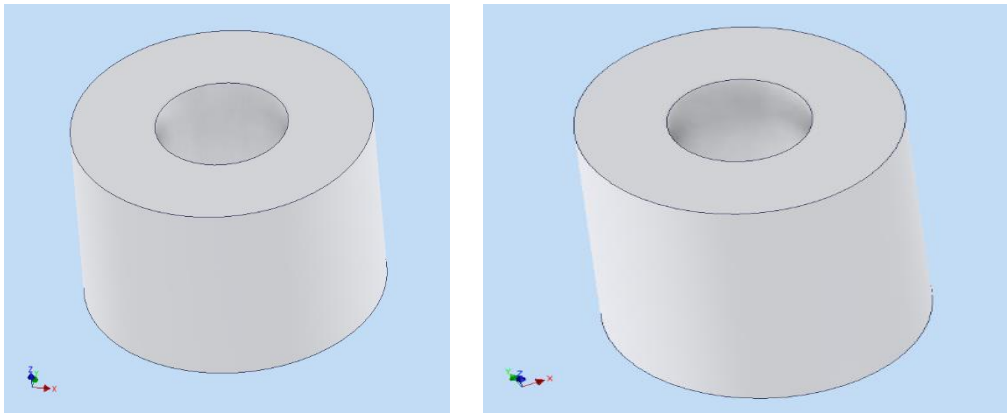

(a). For DA with Two WAs. *(a). For DA with Single WA.*

Figure 5-15. *Teflon Spacers.*

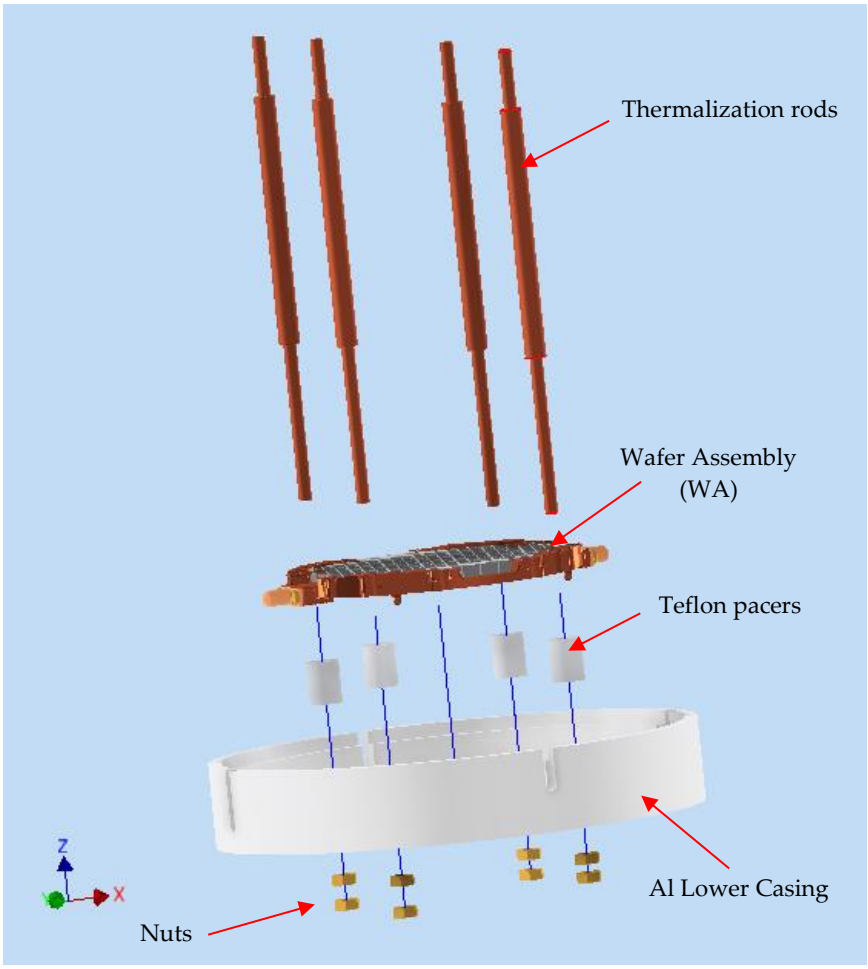

Figure 5-16. *DA Stage-1-Exploded View.*

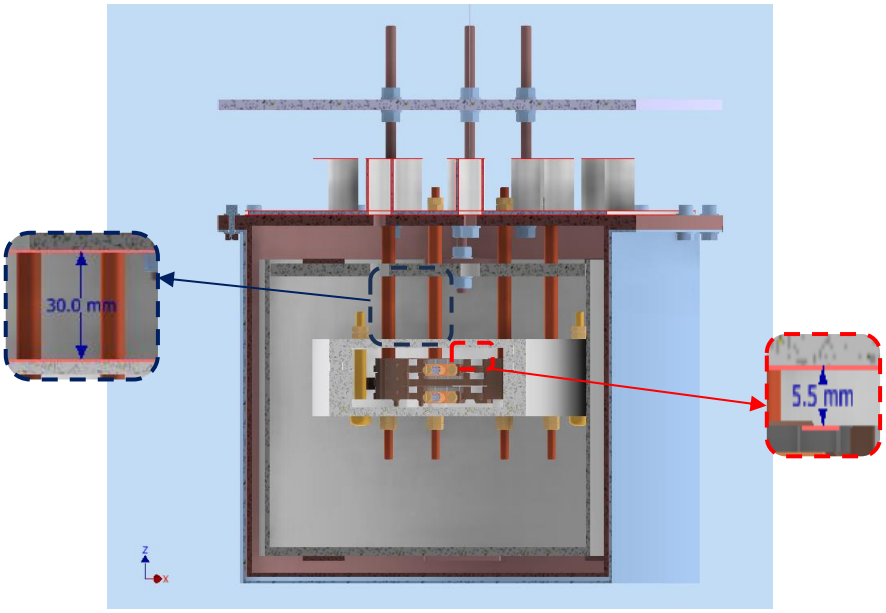

(a). With Three WAs.

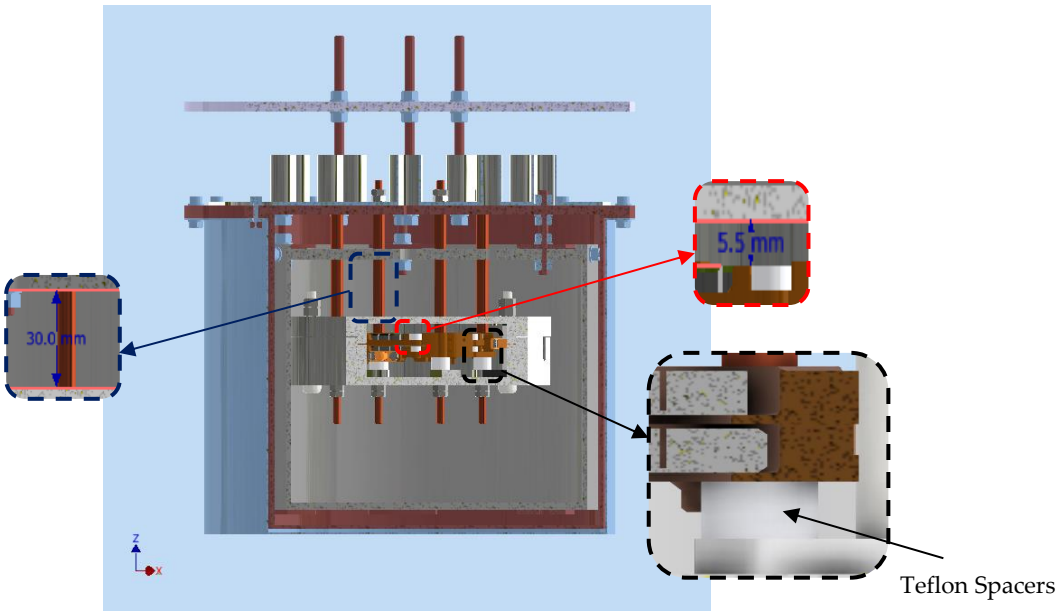

(b). With Two WAs.

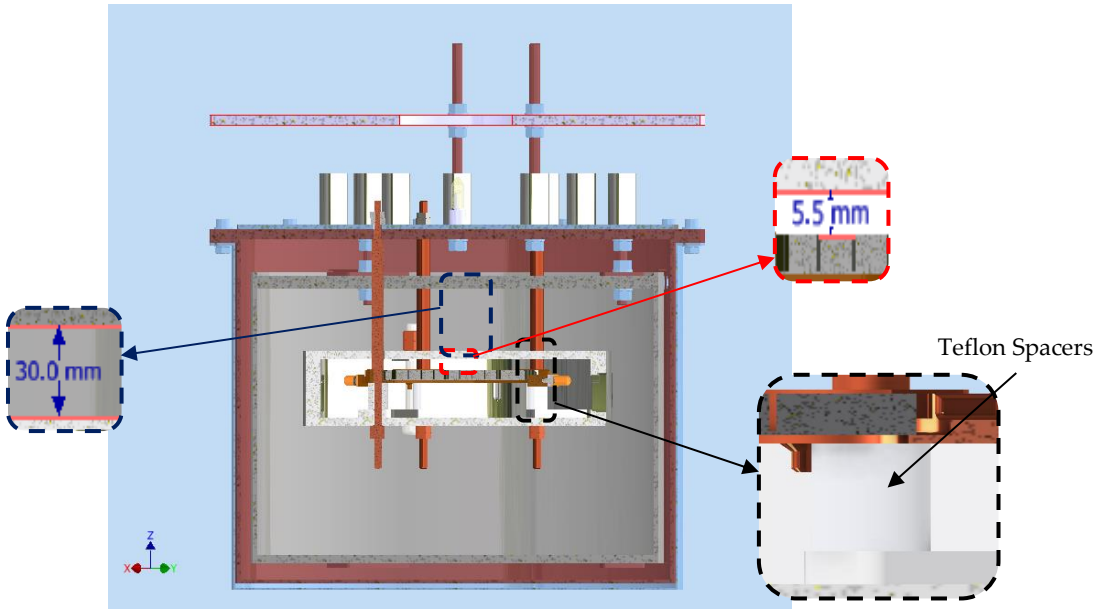

(c). With Single WA.

Figure 5-17. *Final Assembly: Stage 2.*

5.8. Mass Details of the New DA (without Lattice).

The mass details of the new DA are reported in ***Table 5-1***. It shows that the new DA with a single WA has a minimal difference with the original DA, due to the fact that mass of some components are reduced but on the other hand mass of the aluminium casings is increased to house more than one WA. However, in the case of two and three WAs, it makes a substantial difference.

Table 5-1. *Mass Details of the New DA (without Lattice).*

Number	Component	Mass (kg)	Quantity	Total Mass (kg)	Mass of Single WA (kg)
1	Upper Aluminium Casing	0.26	01	0.26	
2	Lower Aluminium Casing	0.366	01	0.366	
3	Thermalization Rod	0.026	04	0.104	
4	Wafer Holder	0.001	08	0.008	0.008
5	Wafer Holding Ring	0.07	01	0.07	0.07
6	Wafer Crystal	0.061	01	0.061	0.061
7	Aluminium Casings' Bolt	0.013	02	0.026	
			Total Mass (kg)	**0.895 kg**	**0.139 kg**
	Total Mass of the New DA with Single WA.			**0.895 kg**	
	Total Mass of the New DA with Two WAs.			**1.034 kg**	
	Total Mass of the New DA with Three WAs.			**1.173 kg**	

6. Chapter: Structural Performance Assessment via FEA.

In this chapter the FE modeling for the analysis and numerical simulations of Structural, modal, thermal (both steady-state and transient), and thermomechanical analysis are performed. Subsequently, these FEA results are utilized for the initial validation of the new design (phase 1). After this step, the successful validated 3D model is moved to the next step i.e., prototyping phase.

6.1. FEA Modelling.

For the entire analysis and numerical simulations, the generic FEA workflow (***Figure 6-1***) of FEA is followed. Hence the original design of the DA is based on a single WA, therefore, the FEA model will be setup only for the new design with a single WA in order to make an appropriate comparison with the original design of the DA and deduce the final conclusions. To simplify the FEA modelling, the wafer connectors, fasteners (such as nuts, bolts, and screws), Teflon spacers, and Al casings are excluded, however, their effect in the form of constraints (wherever is necessary) and collective effect of its structural weight is applied accordingly to increase the accuracy level of the FEA results. It is pertinent to mention that material of brass and aluminium become passive (non-conductive) at cryogenic temperature.

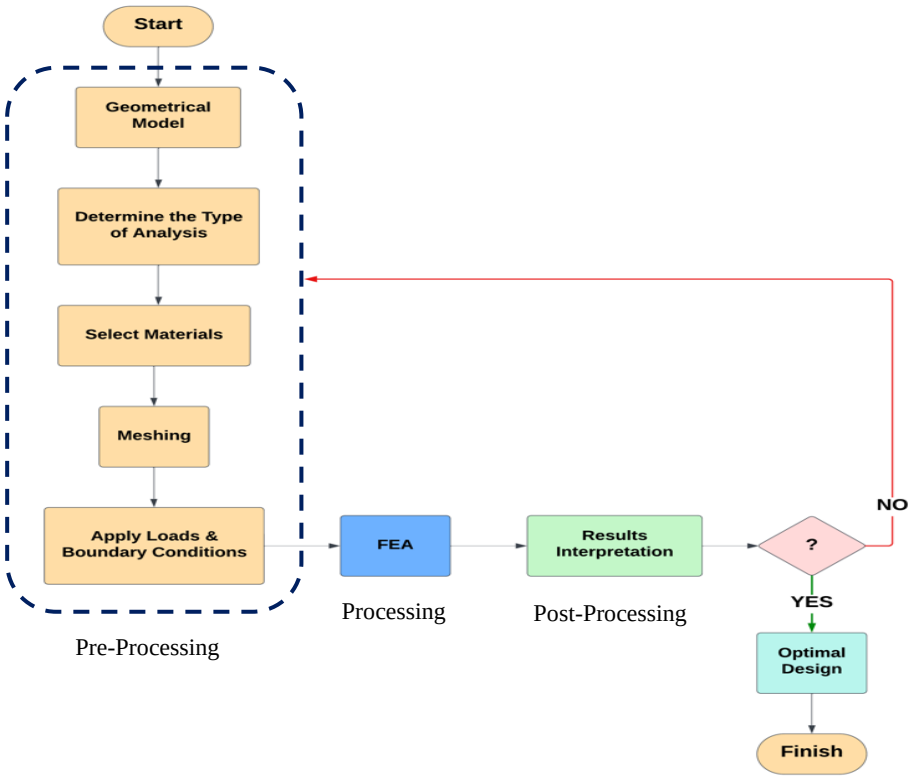

Figure 6-1. *FEA Workflow.*

6.2. *Materials & Properties.*

The following material properties (***Table 6-1***) are used for all the analysis. The materials are assigned accordingly to the CAD models as per ***Table 6-2***. Hence in the original design of the DA, the wafer holders are made with the Teflon, therefore, the Teflon material is used in their analysis. However, pure copper is used for the analysis of the wafer holders in the new design of the DA.

Table 6-1. *Material Properties.*

Properties	Materials				
	Pure Copper	**Silicon Single Crystal**	**Teflon**	**Pure Aluminium**	**Brass**
Density (Kg/m^3)	8940	2329	2170	2700	8490
Youngs Modulus (Pa)	115e^9	129e^9	0.599e^9	68.9 e^9	97 e^9
Poisson Ratio	0.31	0.278	0.46	0.33	0.31
Yield/*Tensile Strength (Pa)	365e^6	*950e^6	131e^6	275e^6	124 e^6
Coefficient of linear Thermal Expansion (K^{-1})	17e^{-6}	2.6e^{-6}	10e^{-6}	-	-
Thermal Conductivity (W/mK)	391	149	0.3	-	-
Heat Capacity (J/KgK)	385	713	1500	-	-

Table 6-2. *DA Assembly Details by Material.*

Number	Component	Material
1	Al Casings	Pure Aluminium
2	Thermalization Rod	Pure Copper
3	Wafer Holders	Pure Copper/Teflon
4	Wafer Holding Ring	Pure Copper
5	Wafer Crystal	Silicon Single Crystal
6	Al Casings' Bolt	Brass

6.3. *Meshing.*

Meshing is carried out to discretize the continuous structure and so to reduce the degree of freedom from infinite to finite. Meshing is the network of elements (with different shapes for 2D and 3D elements) that represents the geometry of the continuous structure. It is important to choose the appropriate shape and size for these elements, that increases the accuracy and reliability of the analysis, as well as reduce the computation time. For numerical simulations, the quality check of the elements is carried out through the numerical solvers to conclude the reliability of the numerical simulations. Generally, the following significant parameters are checked:

- Aspect Ratio: It is ratio between the maximum edge length of the element to its minimum edge length.
- Wrap Angle: It is the deviation of the element or element's face from being planner.

- Skewness: It is deviation of the element from its ideal shape.
- Jacobian: It is the determinant of the Jacobian matrix, that transforms the elements from the global to local coordinates.

The meshing is applied to all the FE components in accordance with ***Table 6-3*** and ***Figure 6-2***. In addition, the mesh quality check criterion and subsequent failure result is shown in **Figure 6-3**, which shows that all the elements are within the mesh quality criterion and none of the elements violate the thresholds.

Table 6-3. *Meshing Details.*

Component	Meshing Details		
	2D element	3D element	Mesh size (mm)
Wafer Holding Ring	Trias	Tetras	0.5
Silicon Wafer Crystal			
Wafer Holders			
Thermalization Rods			

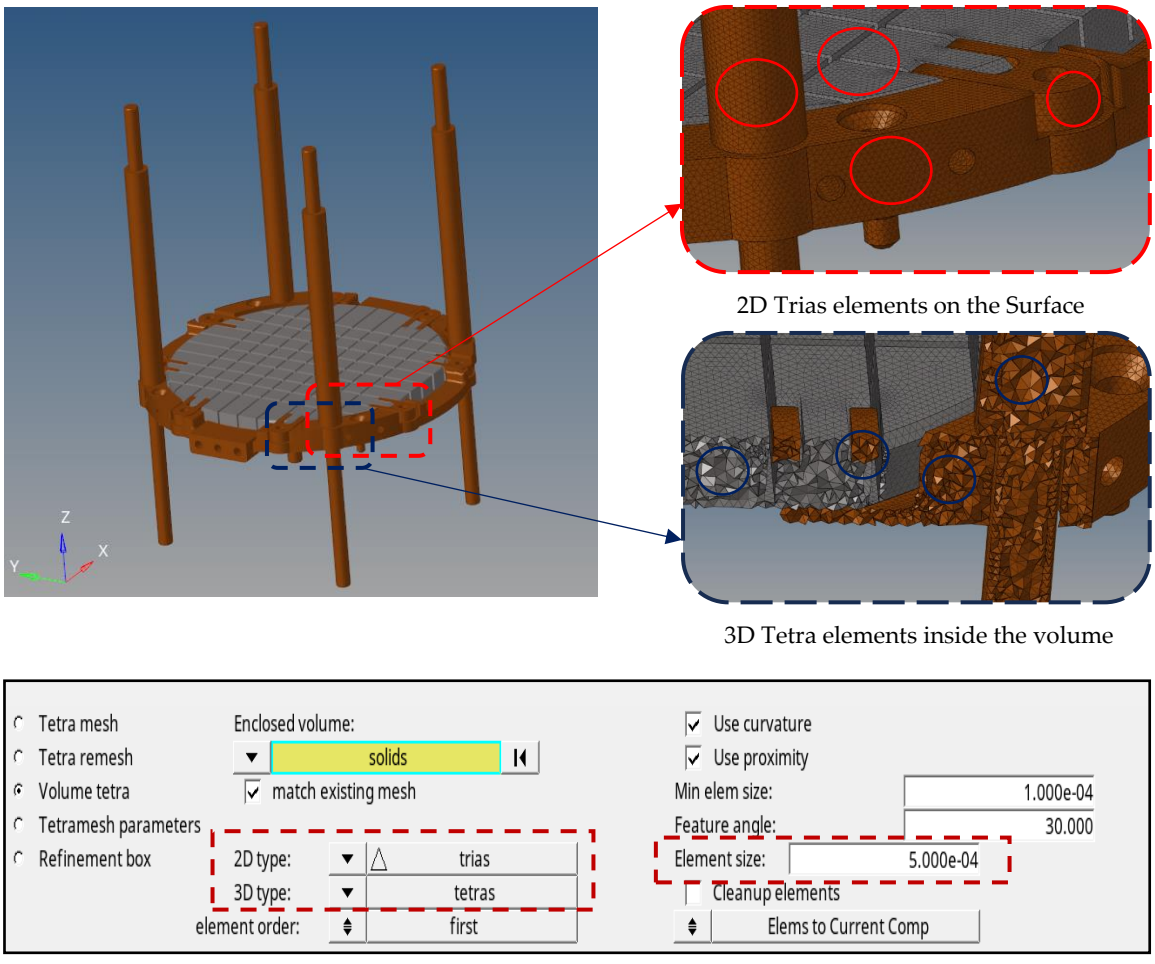

Figure 6-2. *2D and 3D Meshing Details.*

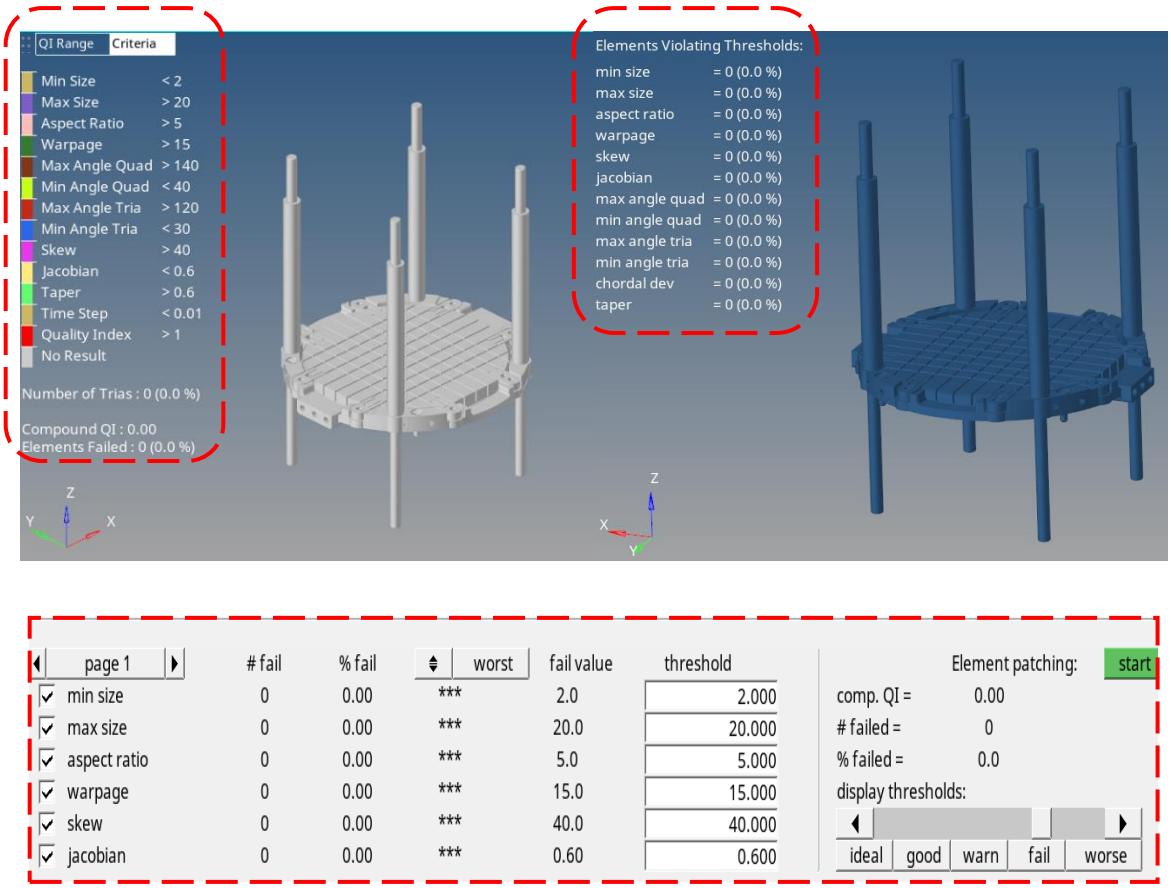

Figure 6-3. *Mesh Quality Criterion and Failure Check.*

6.4. Loads and Boundary Conditions.

The loads and boundary conditions are applied according to ***Table 6-4***. Regarding the structural and modal analysis, the problem is purely static and subjected to structural weight due to gravity. Therefore, linear static analysis is performed based on the structural weight. For the constraints, the upper part of the thermalization rods (which is connected to the cryogenic device with the help of nuts) is constrained with zero DoF (i.e., no translation and no rotation), as shown in ***Figure 6-4***. In addition, the collective effect of structural weight of the excluded components is applied at the lower mounting interface of the thermalization rods as a load vector along the negative z-axis, hence the thermalization rods bear the entire structural weight of the DA at the lower mounting interface. The final results for the structural analysis are concluded based on the maximum Von Mises stress and the maximum displacement, while in the case of modal analysis it is concluded based on natural frequency range.

For the thermal analysis, the whole system is initially considered at room temperature and then a thermal load of zero kelvin (0K) is applied. For the thermomechanical analysis, the steady state thermal analysis is performed, in which the thermal load case is coupled with the load step of the linear static structural analysis for the computation of the thermal stresses. The final results are concluded based on the maximum thermal stress, and respective maximum

displacement. The linear transient heat transfer analysis is also carried out to gauge the thermal efficiency of the new design with respect to time. For this purpose, the thermal load is applied as a temperature-time curve. The whole simulation is carried out for a certain time with specific time steps.

Furthermore, due to the assembly nature of the problem, there are some contacts involved between different components, therefore, the contacts with appropriate contact surfaces and types are defined in ***Table 6-5***, to increase the accuracy level of the analysis.

Table 6-4. *Loads and Boundary Conditions.*

Thermal Loads		Gravity Load	Load Vector	Constraint(s)
Initial Temp (⁰C)	**Applied Temp (⁰C)**			
25	-273	Gravity Load due to the structural weight of DA along the negative z-axis	The collective structural load of the excluded components (i.e. the fasteners and the aluminium casings) is applied at the lower mounting interface of the thermalization rods along the negative z-axis	$F_{x,y,z} = M_{x,y,z} = 0$ (Applied at the top mounting interface of the thermalization rods)

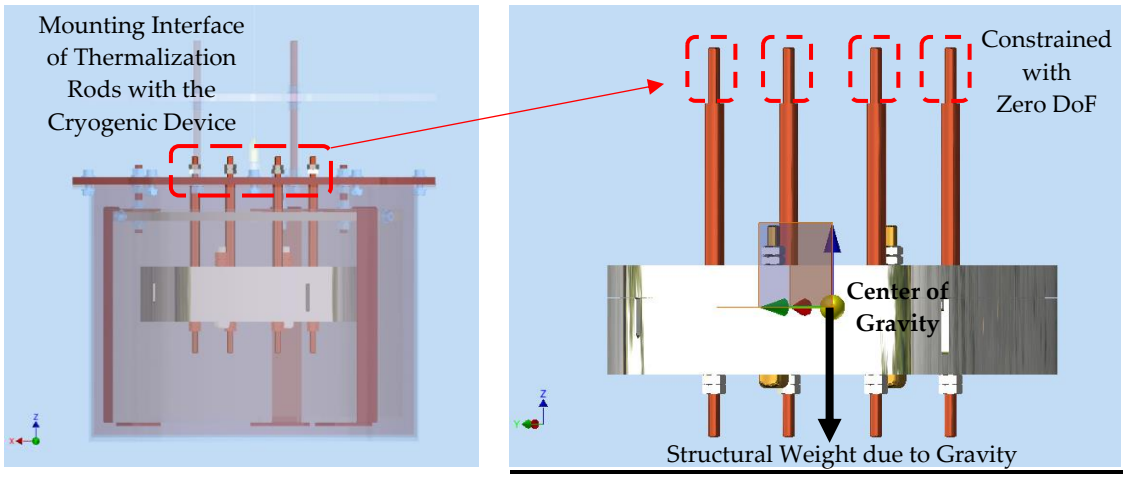

Figure 6-4. *Load and Boundary Condition for Structural and Modal Analysis.*

Table 6-5. *Details of Contact Surfaces.*

Contact Between the Surfaces		Contact Type
Wafer Holding Ring	Thermalization Rods	Freeze
Wafer Holding Ring	Wafer Holders	
Wafer Holding Ring	Silicon Wafer Crystal	Sliding
Silicon Wafer Crystal	Wafer Holders	

6.5. FEA Simulations.

In this section, structural, modal, thermal, and thermomechanical analysis are carried out subsequently for the validation purpose of the new design (without lattice).

6.5.1. Structural Analysis.

In this section, the structural analysis of both the original and new design of the DA is carried out in order to make an appropriate comparison for the numerical validation of the new design. The FEA modelling is carried out according to the preceding sections and a linear static structural analysis is performed. The final results are concluded based on the maximum Von Mises stress and the maximum displacement.

The constraint of zero DoF is applied at the top mounting interface of the thermalization rods (***Figure 6-5****a,b*) using the SPC card, and the GRAV card is activated (***Figure 6-5****c*) in the numerical solver HW to enforce the gravity load due to structural weight of the components being taking part in the analysis. The fixed constrait (with zero DoF) is represented by 123456, where 123 represent the fixed translation along x, y, and z-axis respectively, while the 456 represent the fixed rotation along x, y, and z-axis respectively. However, the collective effect of the structural weight of the excluded components is applied as a load vector at the lower mounting interface of the thermalizations rods (***Figure 6-5****d,e*). The collective structural weight in the case of original DA is 6.5N, while it is 7N in case of the new DA, and it is divided equally by the number of respective thermalization rods. The net effect of both the loads (i.e., gravity and vector load) is collected using the card LOADADD (***Figure 6-5****f*).

The results of the linear static structural analysis are shown in ***Table 6-6*** and ***Figure 6-6***.

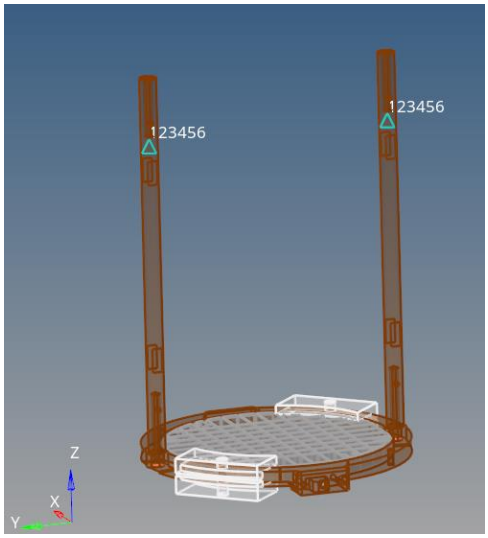

(a). Original DA Design: Constraints (zero DoF).

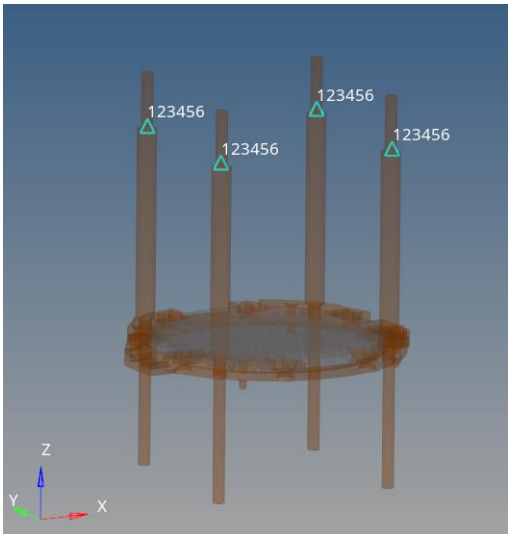

(b). New DA Design: Constraints (zero DoF).

Name	Value
Name:	Gravity Load
ID:	3
Color:	
Include:	[Main Model]
Card Image:	GRAV
User Comments:	Do Not Export
CID:	<Unspecified>
G:	9.8
N1:	0.0
N2:	0.0
N3:	-1.0

(c). Activation of the Grav Card for Gravity Load.

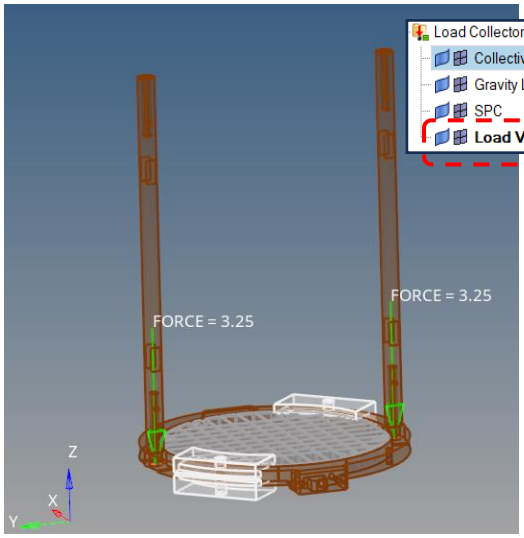

(d). Original DA Design: Load Vector of the excluded components.

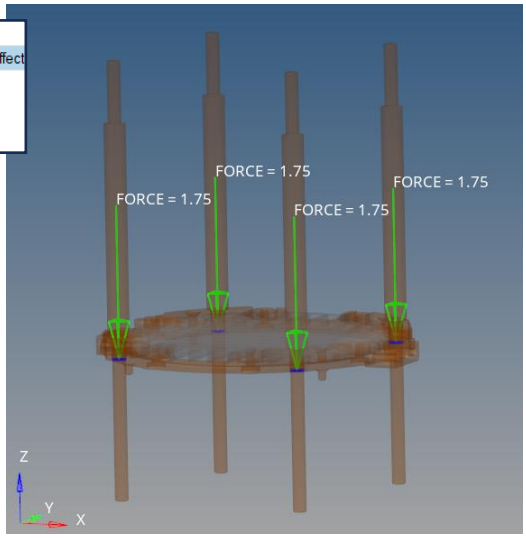

(e). New DA Design: Load Vector of the excluded components.

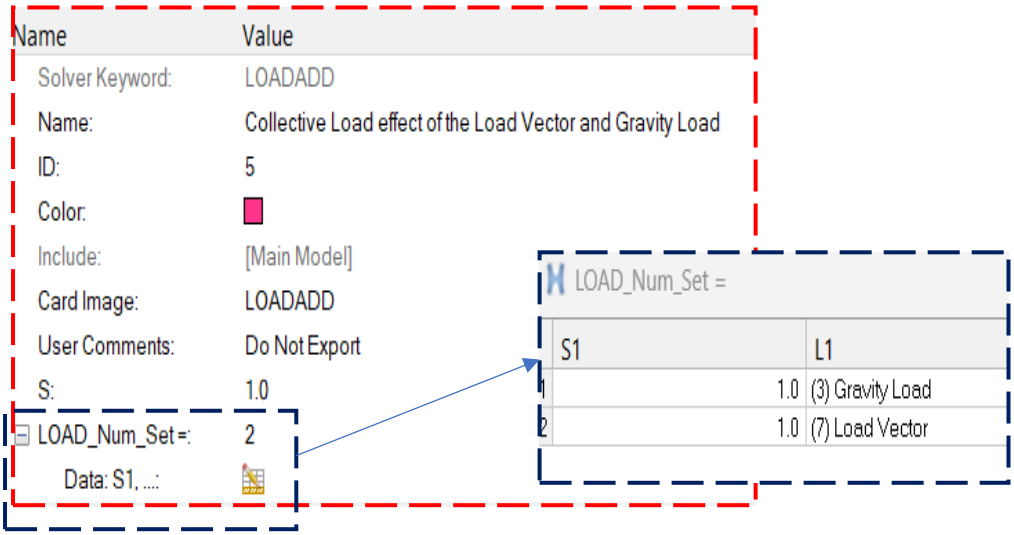

(f). Adding the Net Effect of the Gravity and Vector Load.

Figure 6-5. *Structural Analysis: Applying the Loads and Boundary Conditions*

Table 6-6. *Results of Structural Analysis.*

Component	Max. Displacement (mm)	Max. Von Mises Stress (Pa)	Factor of Safety
Original DA Design	0.0094	$82.8e^{6}$	>1.8
New DA Design	0.015	$6.47e^{6}$	>2

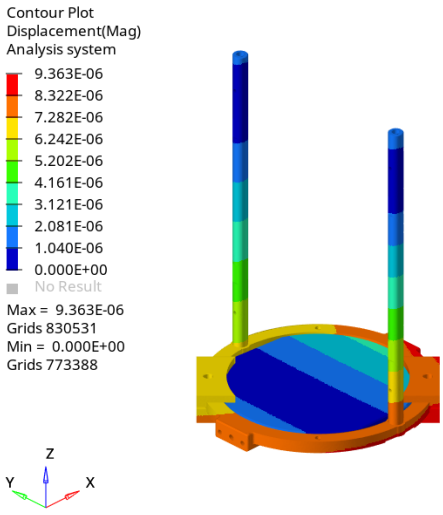

(c). Original DA: Max. Displacement (m).

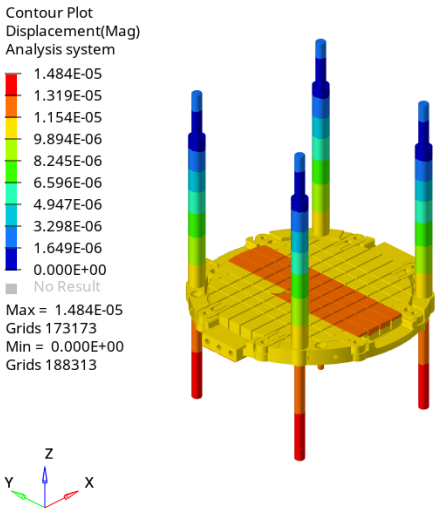

(d). New DA: Max. Displacement (m).

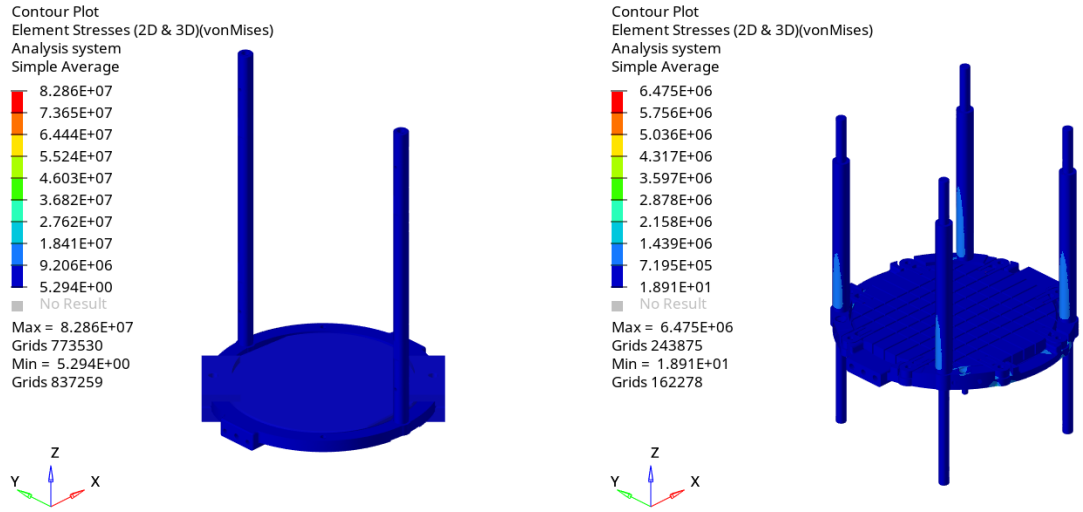

(c). Original DA: Max. Von Mises Stress (Pa). *(d). New DA: Max. Von Mises Stress (Pa).*

Figure 6-6. *FEA Results of the Structural Analysis.*

The FEA results show that the new design improves the stiffness of the structure and reduces the structural stress and respective maximum displacement.

6.5.2. Modal Analysis.

The modal analysis is performed on both the original and new design of the DA to delineate appropriate comparison for the numerical validation of the new design based on the range of natural frequencies with respect to number of modes.

The same constraints are applied as applied in the case of structural analysis. The EIGRL card is activated (***Figure 6-7***) through a load collector to enforce the normal mode analysis with eigen real value. The initial and last frequencies are left blank while the number of modes is set to 10. The results of the frequency range are shown in ***Table 6-7*** and ***Figure 6-8***.

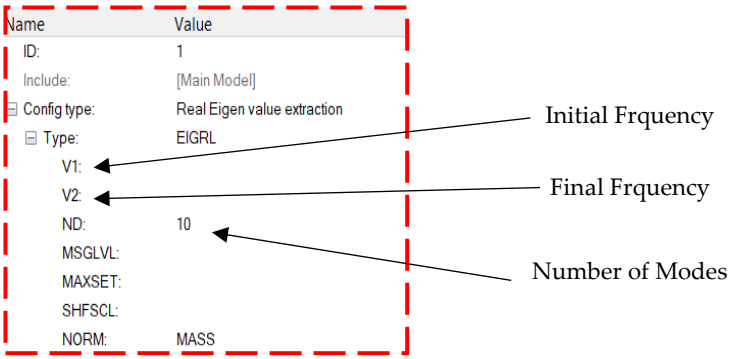

Figure 6-7. *Modal Analysis: Activation of EIGRL Card*

Table 6-7. *FEA Results of the Modal Analysis.*

Natural Frequency (Hz)	Mode Number									
	1	**2**	**3**	**4**	**5**	**6**	**7**	**8**	**9**	**10**
Original DA	62.35	110.4	162	289.8	824	1209	1281.6	1286.5	1342.5	1682.2
New DA	341	341.6	465.5	804.2	805.7	817	818.4	819.5	880.3	880.6

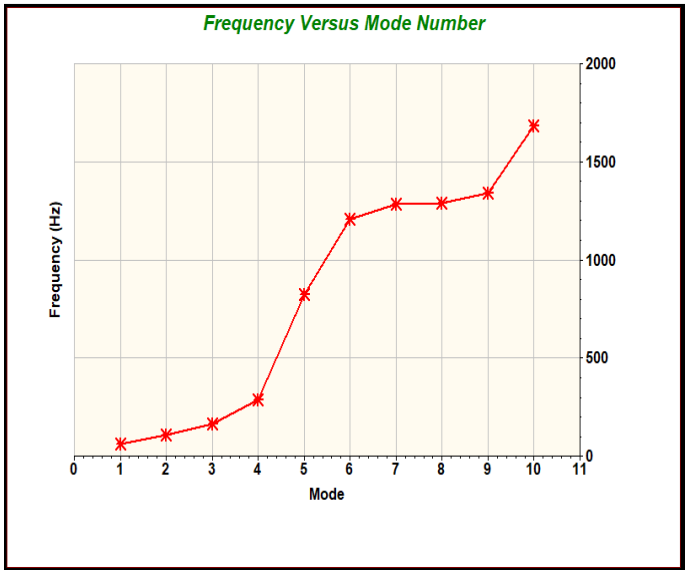

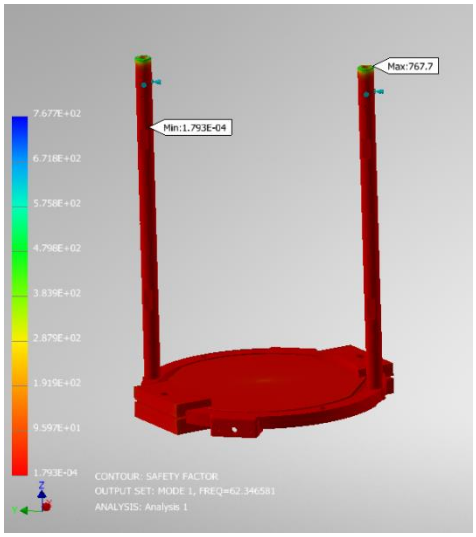

(a). Original DA: Natural Frequency Range (Hz).

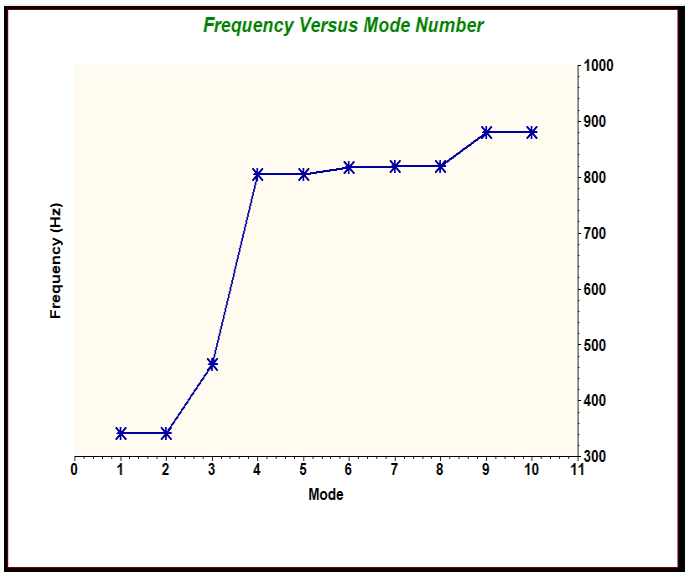

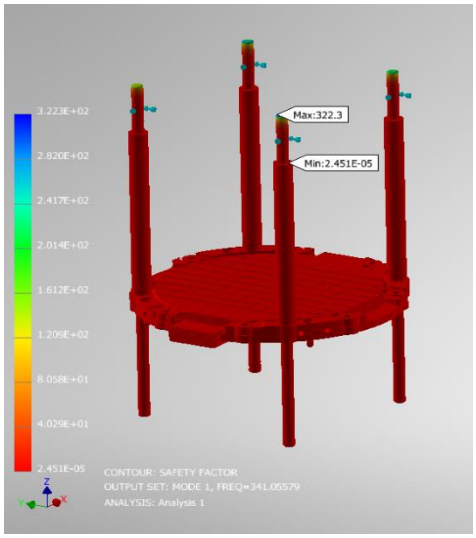

(b). New DA: Natural Frequency Range (Hz).

Figure 6-8. *FEA Results of the Modal Analysis.*

The result of the modal analysis shows that during the first modes (i.e. the first three bending moments and then subsequent torsion), the new design of the DA has improved the natural frequencies significantly, but after, the original DA has the higher natural frequencies. However, we are more interested in the first natural frequency due to the fact that the experimental device is operated at a frequency of 1.3 Hz, so from the operational point of view both the designs are ok, but during the transportation due to the high mechanical vibrations the frequency arrives up to 66Hz, due to which the original design has been reported several times with structural failures/damages. Therefore, the new design achieves the first natural frequency of 341Hz, which provides a much higher factor of safety to the DA during transportation.

6.5.3. Thermomechanical Analysis

For the thermomechanical analysis, the whole system is initially considered to be at room temperature and then a thermal load of zero kelvin (-273^{0}C) is applied under the consideration of the steady state heat transfer, and the thermal load case is coupled with the load step of the linear static structural analysis (***Figure 6-9***) for the computation of the thermal stresses. However, the structural loading and boundary conditions remain the same. The final results are concluded based on the maximum thermal stresses, and respective maximum displacement.

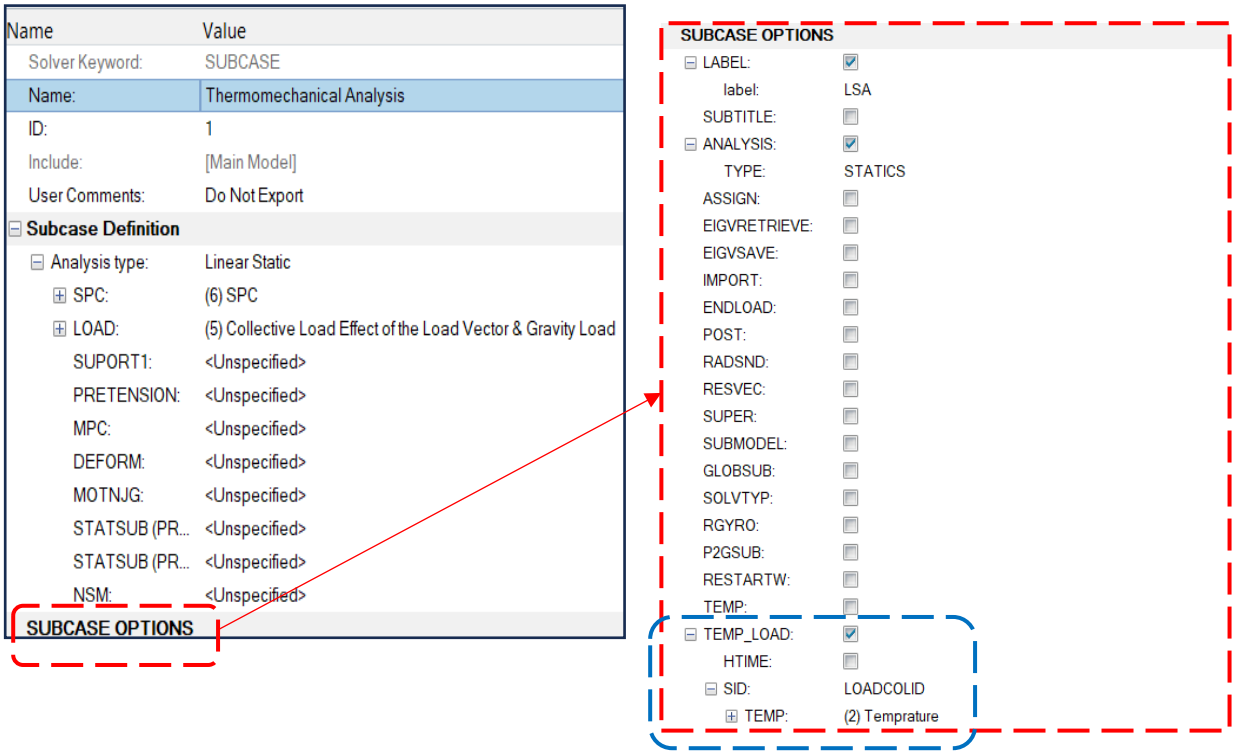

Figure 6-9. *Thermomechanical Analysis: Coupling the Thermal Load Case with Structural Load Step.*

The results of thermomechanical analysis pertaining to the original DA design are shown in ***Table 6-8*** and ***Figure 6-10***, while the results for the new DA design are shown in ***Table 6-9*** and ***Figure 6-11.***

Table 6-8. *Thermomechanical Analysis of the Original DA Design.*

Component	Max. Displacement (mm)			Max. Von Mises Stress (Pa)	Factor of Safety
	x-axis	y-axis	z-axis		
Wafer Holding Ring	8.64	0.2	4	$859e^6$	< 0.5
Silicon Wafer	0.211	0.0244	3.32	$2.16e^6$	> 2
Wafer Holders	8.7	0.19	3.77	$10.8e^6$	> 2
Thermalization Rods	7.9	0.2	0.72	$247e^6$	> 1.4

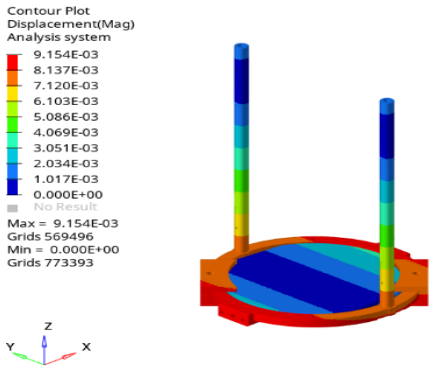

Original DA: Max. Displacement (m)

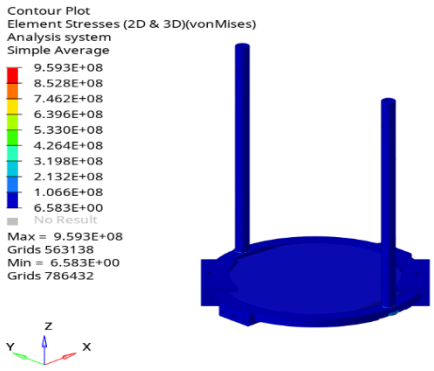

Original DA: Max. Von Mises Stress (Pa)

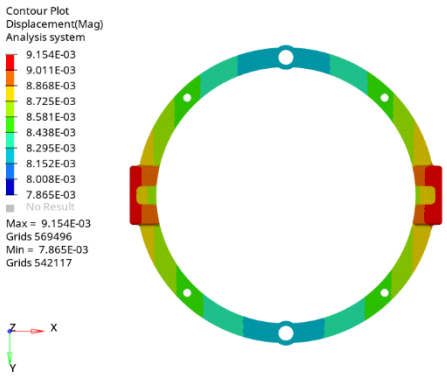

Wafer Holding Ring: Max. Displacement (m)

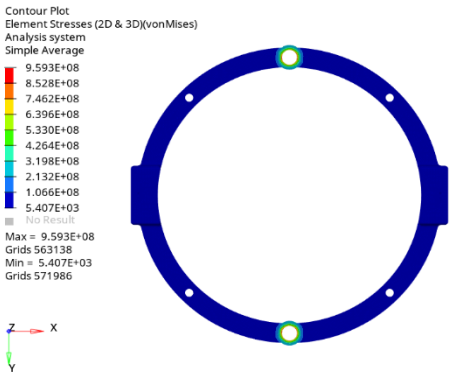

Wafer Holding Ring: Max. Von Mises Stress (Pa)

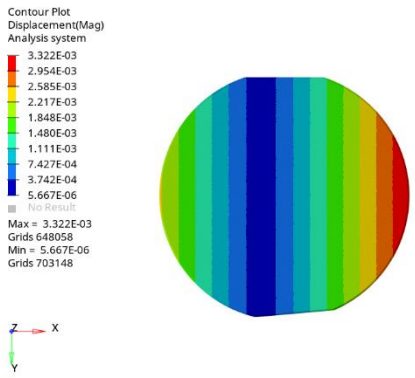

Silicon Wafer: Max. Displacement (m)

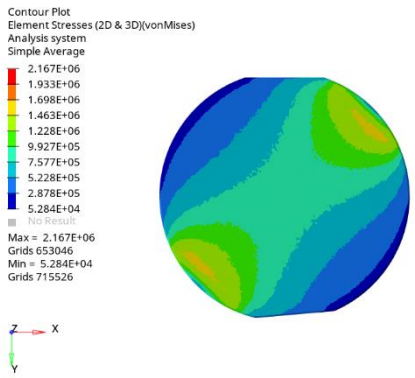

Silicon Wafer: Max. Von Mises Stress (Pa)

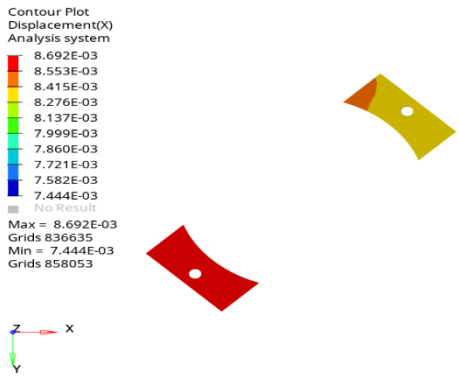

Wafer Holders: Max. Displacement (m)

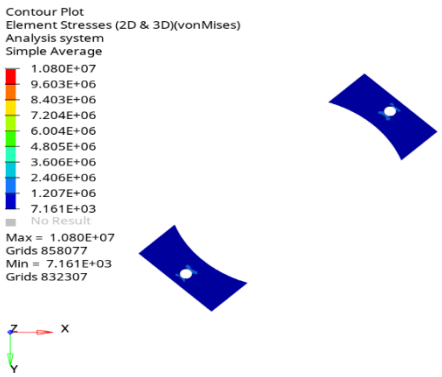

Wafer Holders: Max. Von Mises Stress (Pa)

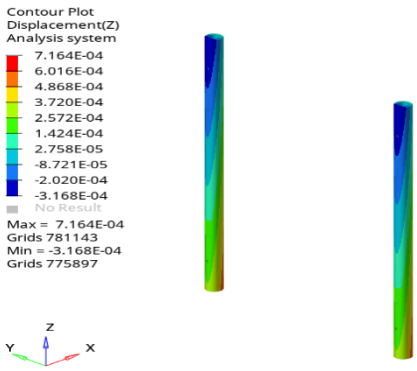

Thermalization Rods: Max. Displacement (m)

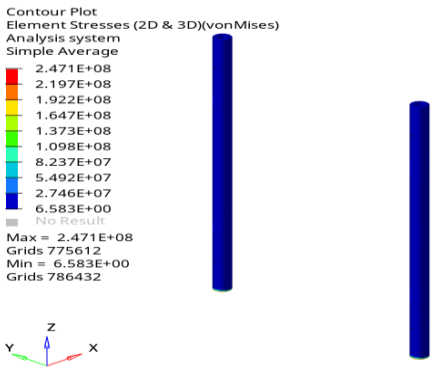

Thermalization Rods: Max. Von Mises Stress (Pa)

Figure 6-10. *FEA Results of the Thermomechanical Analysis: Original DA Design*

Table 6-9. *Thermomechanical Analysis of the New DA Design.*

Component	Max. Displacement (mm)			Max. Von Mises Stress (Pa)	Factor of Safety
	x-axis	y-axis	z-axis		
Wafer Holding Ring	0.227	0.211	0.358	72.45e^6	5
Silicon Wafer	0.0185	0.0244	0.381	501.5e^6	1.89
Wafer Holders	0.198	0.199	0.421	13.99e^6	9.36
Thermalization Rods	0.222	0.218	0.535	38.87e^6	9.39

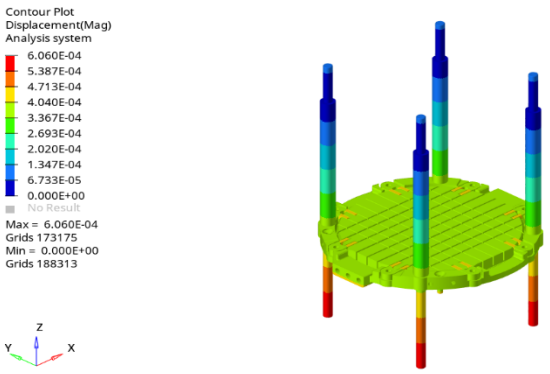

New DA: Max. Displacement (m)

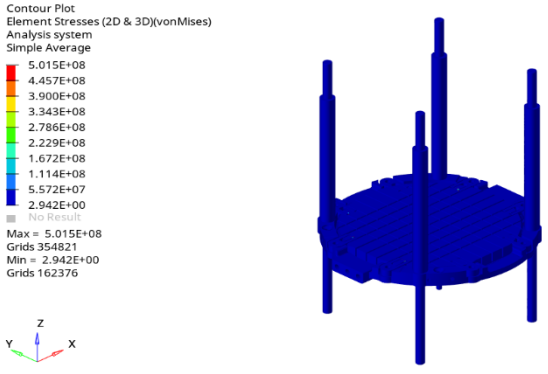

New DA: Max. Von Mises Stress (Pa)

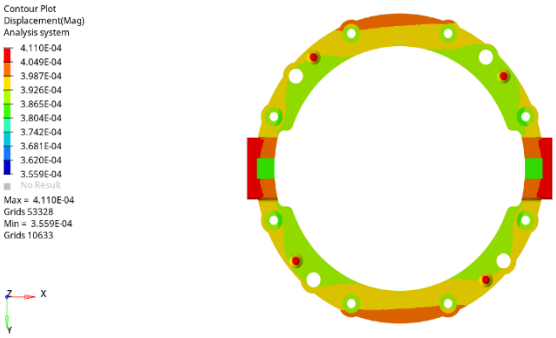

Wafer Holding Ring: Max. Displacement (m)

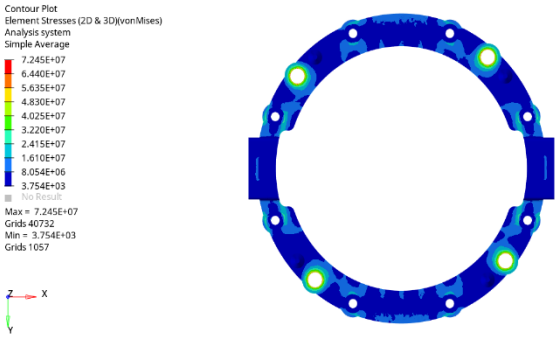

Wafer Holding Ring: Max. Von Mises Stress (Pa)

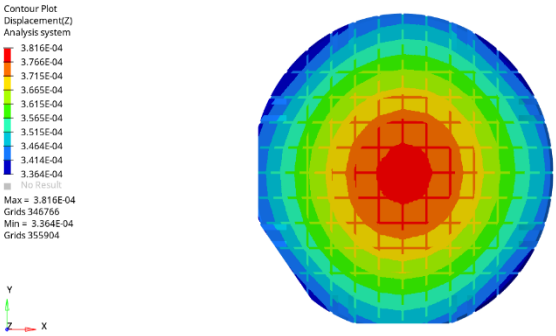

Silicon Wafer: Max. Displacement (m)

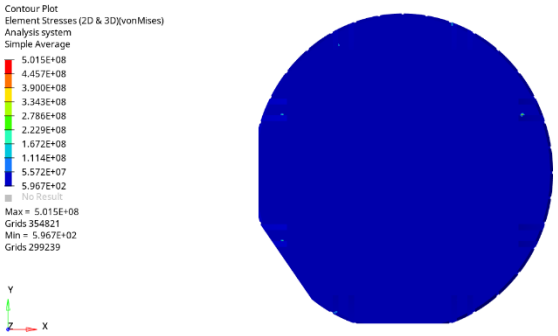

Silicon Wafer: Max. Von Mises Stress (Pa)

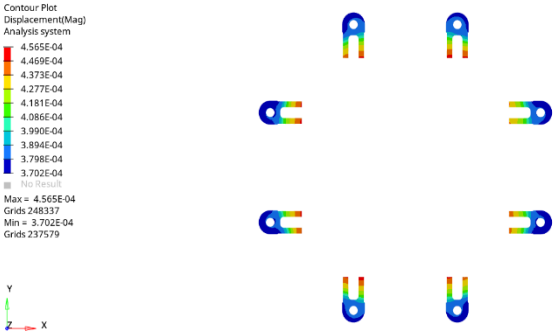

Wafer Holders: Max. Displacement (m)

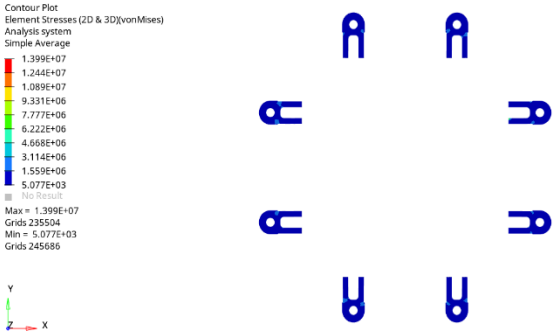

Wafer Holders: Max. Von Mises Stress (Pa)

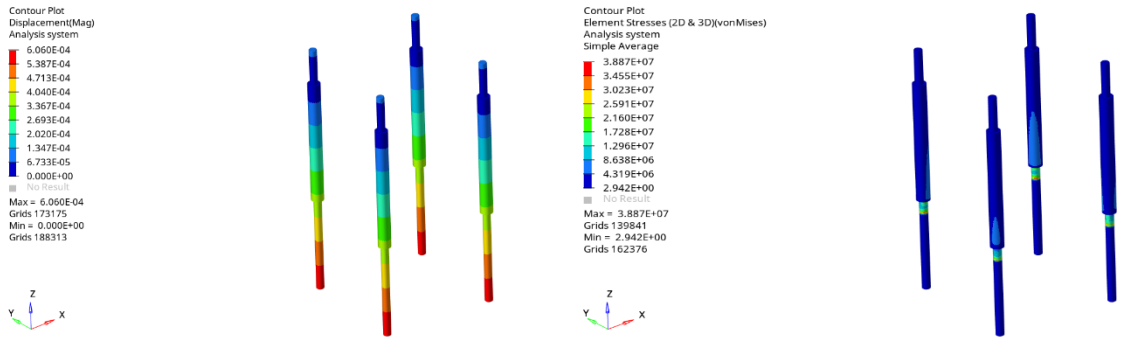

Thermalization Rods: Max. Displacement (m) Thermalization Rods: Max. Von Mises Stress (Pa)

Figure 6-11. *FEA Results of the Thermomechanical Analysis: New DA Design*

Results of thermomechanical analysis indicate that the new design improves the structural integrity of the DA at cryogenic temperature and increases the factor of safety of maximum components remarkably against thermal stresses and respective maximum displacements.

6.5.4. Transient Thermal Analysis

In this section, the linear transient heat transfer analysis is carried out to gauge the thermal efficiency of the new design with respect to time. Hence the transient thermal analysis requires a huge memory and time for the computation, therefore, the FEA model of the transient thermal analysis will be simplified in such a way that only the thermalization rods and the wafer holding ring will take part in the analysis. However, the same conditions will be applied in all cases in order to maintain uniformity and increase the level of accuracy for the precise comparison and conclusions. For the conclusion point of view, the results are captured at several time intervals, and finally the results of the original DA and the new DA are compared for the conclusion.

For the transient thermal analysis, the initial condition of the structure is considered at room temperature (i.e., 25^0C) and defined by the card TEMPD, the thermal load is applied as a temperature-time curve (***Figure 6-12***) and defined by the card TABLED. The whole simulation is carried out for 100 seconds with a time step of 10 and defined by the card TSTEP. The excitation load factor is applied at the nodes where the low temperature is supplied to the DA, and it is defined by the card SPCD. In the temperature-time curve, the DA initially remains at room temperature (i.e., 25^0C) for 50 seconds, then the lower temperature of -273^0C is applied (***Figure 6-13***) and maintained for 950 seconds, and finally the DA is brought back to the room temperature within last 50 seconds.

Finally, the thermal load and the excitation load factor are combined using the card TLOAD1. Subsequently, the load step of the transient heat analysis is created to perform the analysis. The results are given in ***Figure 6-14.***

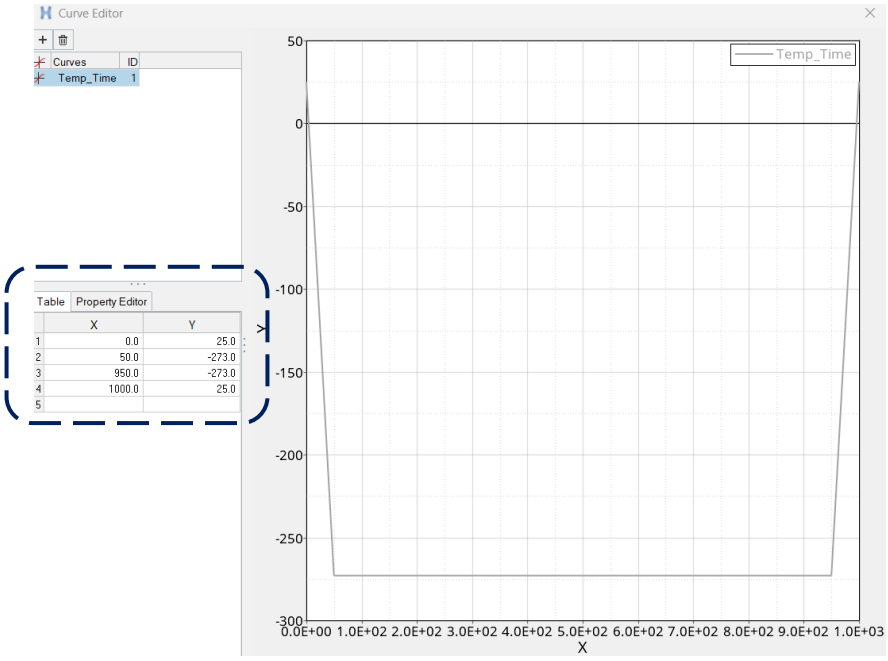

Figure 6-12. *Transient Thermal Analysis: Temp-Time Curve*

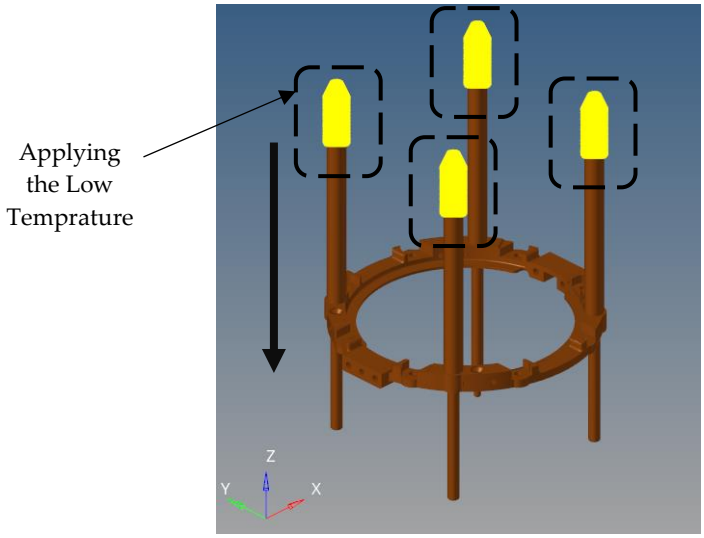

Figure 6-13. *Transient Thermal Analysis Setup.*

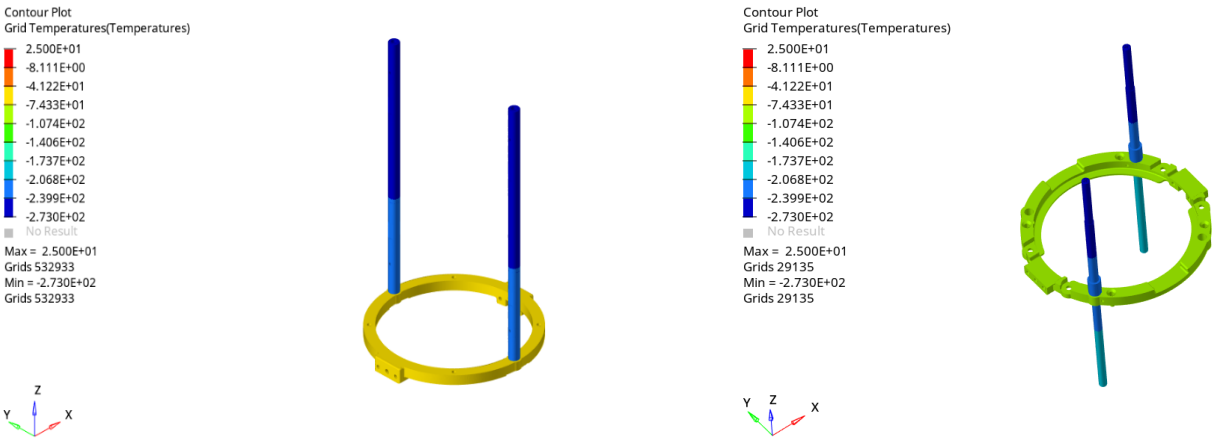

At 200 seconds

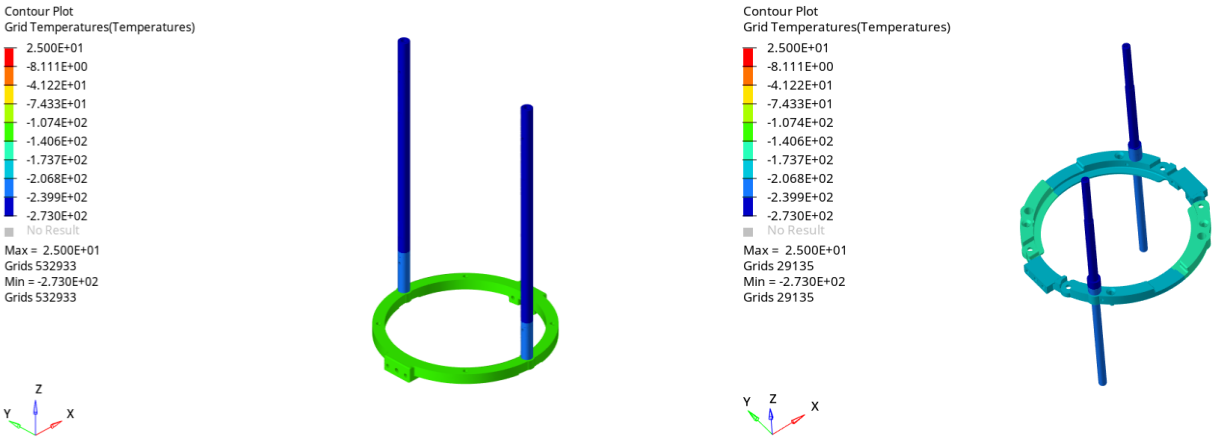

At 400 seconds

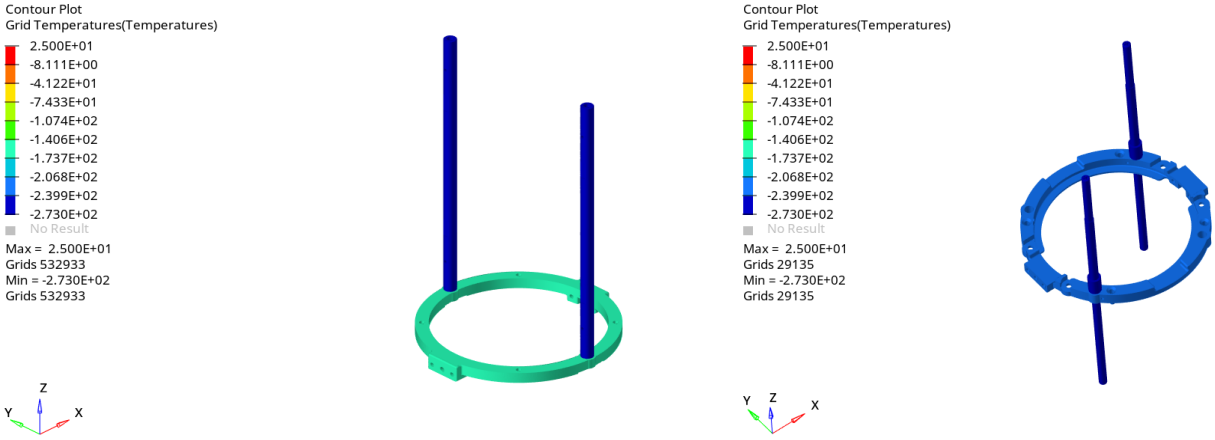

At 600 seconds

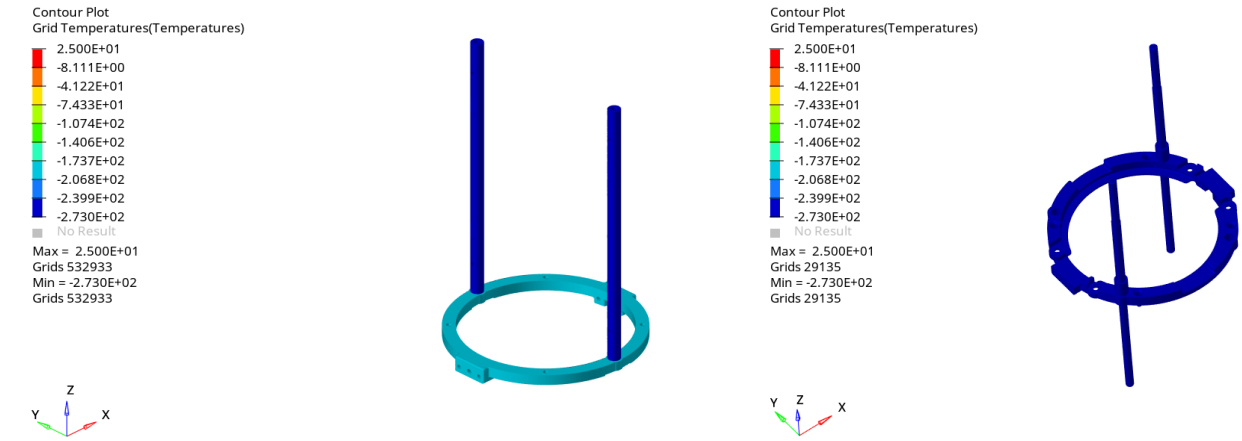

At 800 seconds

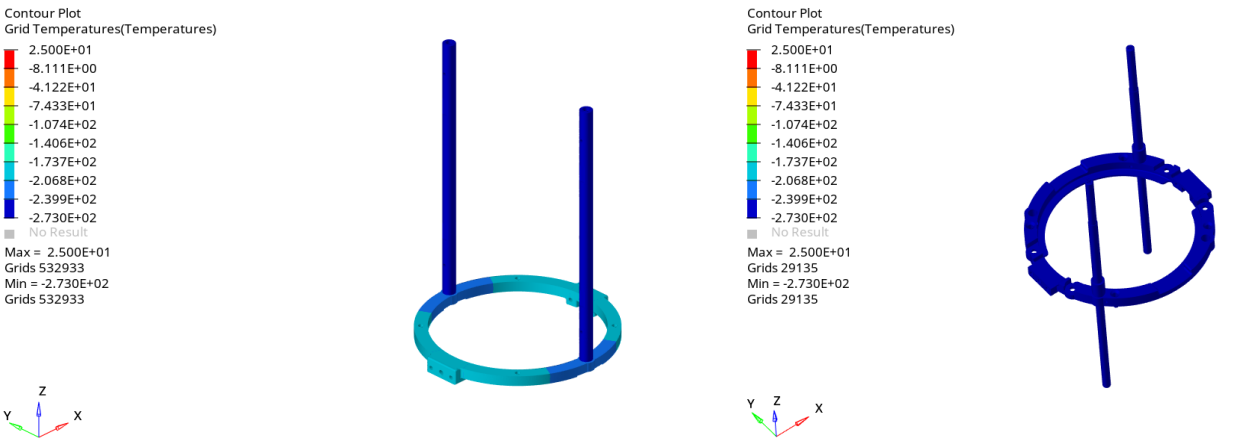

At 900 seconds

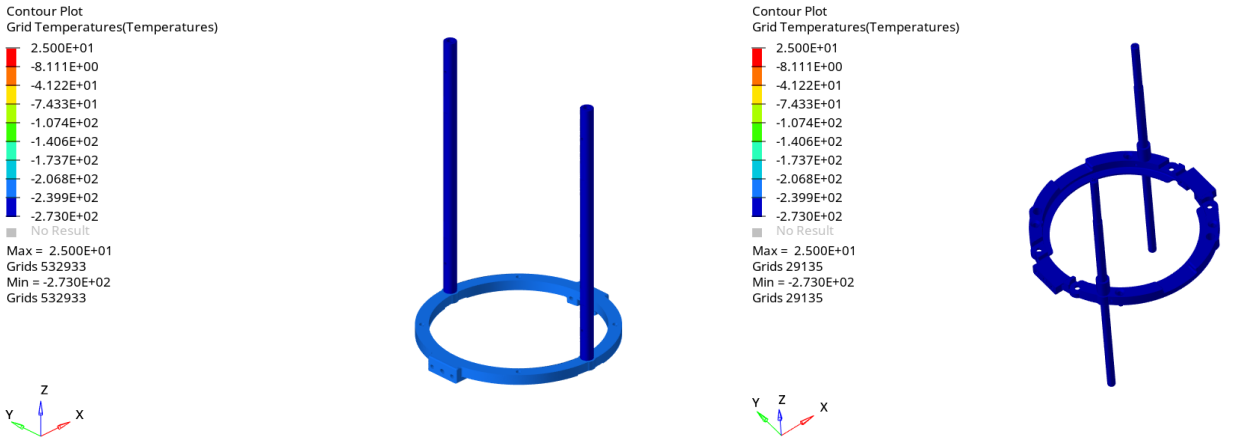

At 950 seconds

Figure 6-14. *Results of Transient Thermal Analysis: Original DA on the left side; New DA on the right side.*

The transient analysis indicates that the new DA design achieves the desired temperature of -273^{0}C at 800 seconds, while the original DA at this stage is approximately -206^{0}C, which shows that the new design is thermal efficient.

7. Chapter: Physical Prototyping, Assembly, and 3D Scanning.

In this chapter the production of wafer holding ring and wafer holder through additive manufacturing (AM) via SLM technique is discussed. It also elaborates the working limitation, process parameters, and design of the support structure pertaining to AM. In addition, it also explains the post-processing through sand blasting after AM. It also highlights the physical assembly, 3D scanning of the AM wafer holding ring as quality check, and status of the physical experimentation.

One of the significant requirements of this research project was to develop the wafer holding ring and wafer holder via AM (Sisma MySint 100), which is installed in INFN LNGS Gran Sasso Lab. The AM is suggested due to the fact that the wafer holding ring and the wafer holders have complex geometry, and the AM has the capability to develop such complex shapes. However, this could also be achieved via conventional manufacturing, but of course with more effort, excessive time, and more material consumption. Hence, the wafer holding ring and the wafer holders are made of copper material, and the LNGS lab has already expertise in developing the cryogenic copper components via AM (SLM), therefore, these components were developed with the already established AM process parameters. However, the AM support structure was designed with an optimized lattice to improve the efficiency of the AM and minimize the possible thermal distortion.

7.1. Prototyping via Additive Manufacturing (SLM).

AM (SLM technique) is used for the prototyping of the wafer holding ring and the wafer holders. The AM machine SISMA MYSINT100 PM/RM (***Figure 7-1***), which is installed in Grass Sasso Lab INFN (available in the framework of the HAMMER collaboration between INFN Roma and INFN LNGS), is used for prototyping. The only limitation that was faced by this machine is related to the nominal size of its working cylinder. The nominal size of the working cylinder is 90mm while the maximum outer geometrical dimension of the wafer holding ring is more than 98mm, therefore, the build orientation of the AM for the prototyping is inclined. According to the literature, the ideal overhang angle for the AM is 45^0, but due to other protrusions on the top surface of the wafer holding ring, the overhung/inclined angle is kept as 30^0, which is the maximum possible angle. In addition, the support structure and the build orientation during the AM are of significant importance and if they are not designed properly then many issues may arise, such as the thermal distortion, usage of excessive material in the support structure, residual stresses, possible development of crakes due to volumetric shrinkage, etc. However, in such cases, these failures also aggravates if the component to be prototyped has delicate geometrical dimensions and features, and in our case is exactly the same, the wafer holding ring is very small in overall dimensions and with many contours and delicate features. To cope these

issues, Netfabb (the commercial solver) is used to define an optimal build direction and the suitable design of the support structure for the AM. Netfabb is FEM based solver which defines the best build direction and the support structure based on the stress field. Finally, a uniform honeycomb lattice structure (cell size: 1.5x1.5mm, wall thickness:0.5mm) is employed as a support structure for AM (***Figure 7-2)***. Serval rounds of the AM were conducted. These rounds were based on feedback of manufacturing issues, assembly issues, and product improvement. The final successful prototype has gone through the assembly test and fulfilled all the requirements, while now it is under the final physical experimental testing.

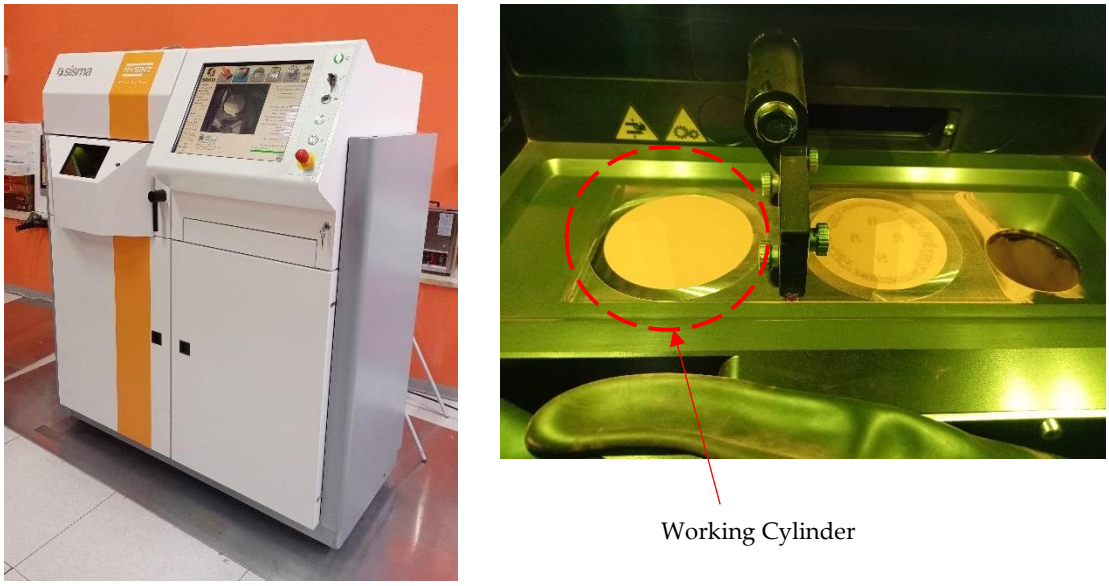

Figure 7-1. *AM (SLM) Mahine: SISMA MYSINT100 PM/RM.*

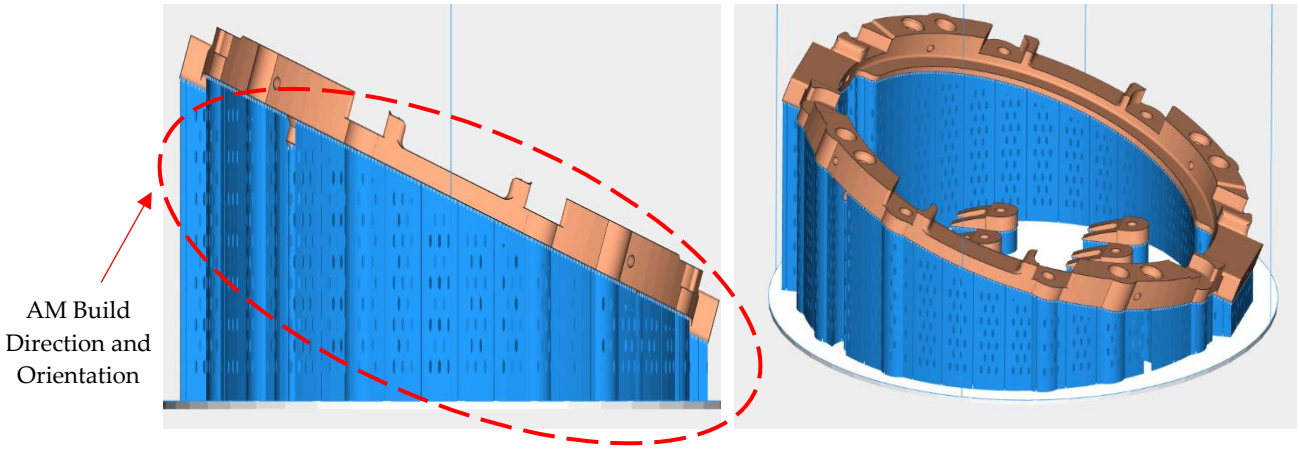

(a). Build Direction.

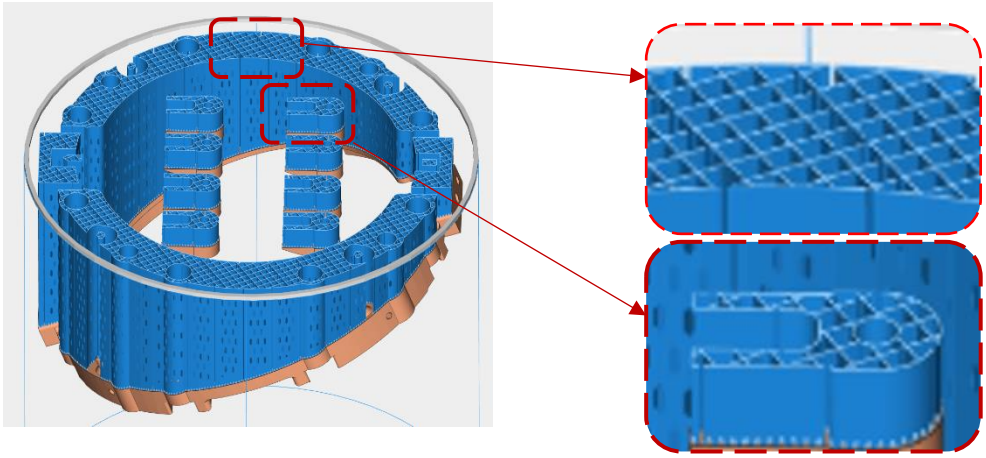

(b). Design of the Support Structure.

Figure 7-2. *AM (via SLM).*

The following process parameters (***Table 7-1***) for AM are used, which are the routine parameters being in practice by the Gran Sasso Lab of INFN for the production of copper structures for the cryogenic applications.

Table 7-1. *AM (SLM) Process Parameters.*

Material	**AM Parameters**							
	Laser Power	Laser Scanning Speed	Hatch Distance	Layer Thickness	Gas	Gas Speed	Oxygen Level	Spot Laser
Pure Copper	150W	300mm/s	40 um	40 um	Nitrogen	3m/s	0.1%	30 um (fixed by machine supplier)

The postprocessing of the AM components is an important process to facilitate the complete removal of the support structure and provide good surface finish. The postprocessing of the AM components is done with sand blading operation. The sand blasting machine NORBLAST (***Figure 7-3***), located in Gras Sasso Lab, is used for this purpose. Micro glass beads of size 200/300µm are used for the sand blasting operation. Similarly, this is a routine process of the Gran Sasso lab, therefore, the routine operating pressure for the sand blast was used.

Figure 7-3. *Postprocessing through Sand Blasting Machine.*

During the first prototyping (***Figure 7-4***), some cracks were observed in the wafer holding ring, and it was concluded that some geometrical features, particularly the thin walls and delicate dimensions caused this problem. Therefore, it was decided to use the pre-drilled holes (pertaining to threaded holes) and remove the small fillets up to 0.2mm, in order to facilitate the AM and minimize the manufacturing issues, as shown in ***Figure 7-5***.

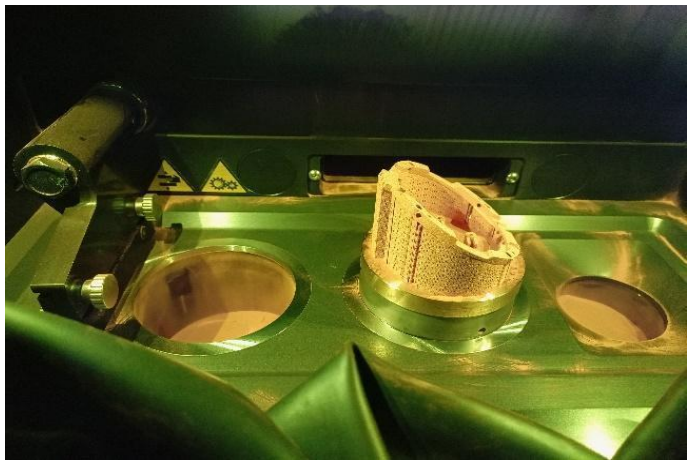

(a). During AM (SLM).

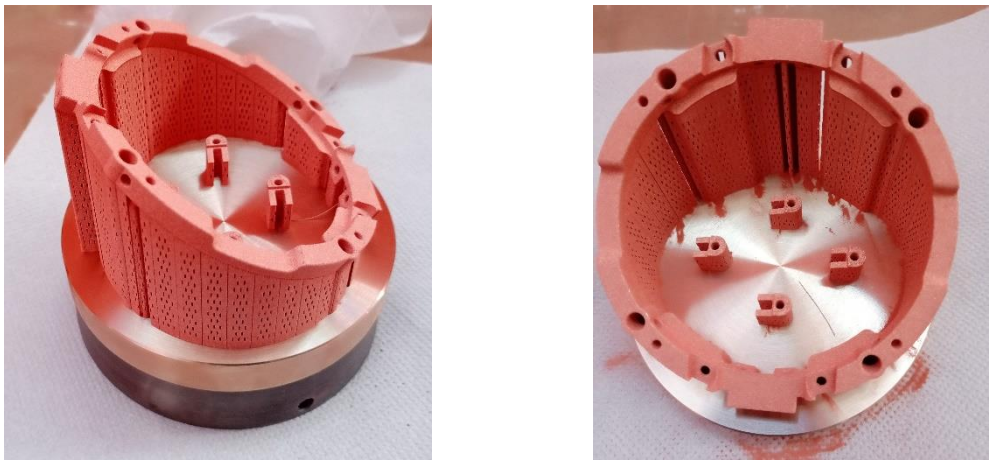

(b). Before Postprocessing.

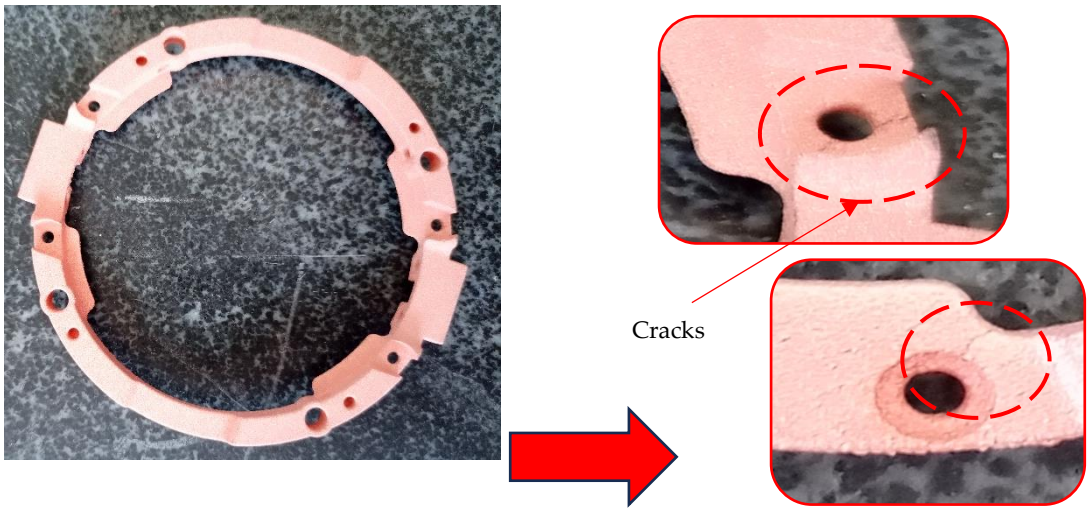

(c). After Postprocessing.

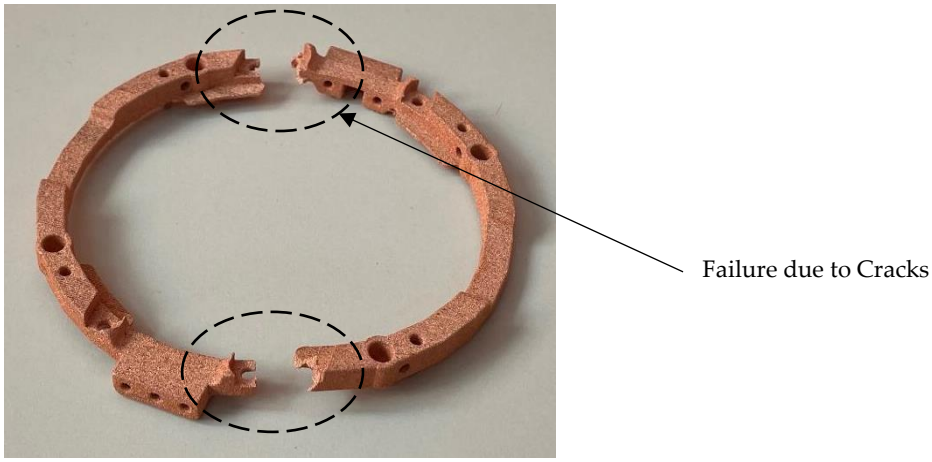

(c). Failure of First Prototyping.

Figure 7-4. *First Prototyping Via AM (SLM).*

(a). Second Prototyping.

(b). Third Prototyping.

Figure 7-5. *Subsequent Prototyping via AM (SLM).*

7.2. Prototyping via Conventional Manufacturing.

The other components of the DA are manufactured successfully via conventional manufacturing (***Figure 7-6***). These components were manufactured by a private company under the coordination and supervision of myself and INFN Roma technical team. They were inspected accordingly and found fit regarding the geometrical, assembly, and functional requirements.

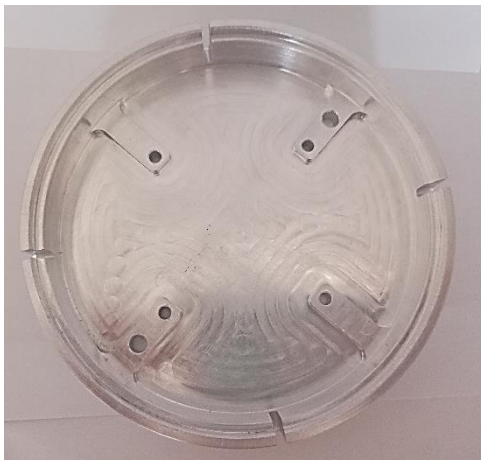

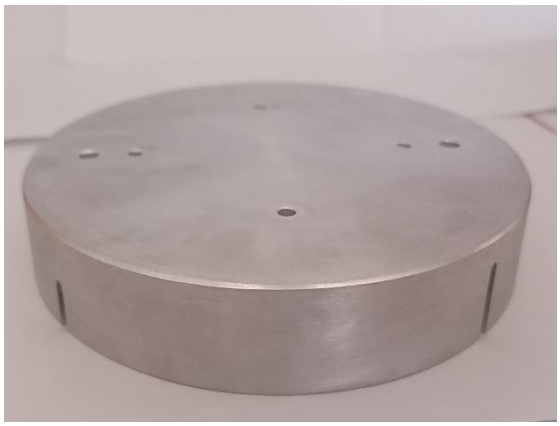

(a). Al Lower Casing.

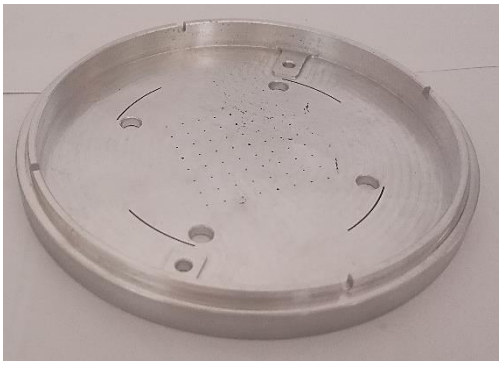

(b). Al Upper Casing.

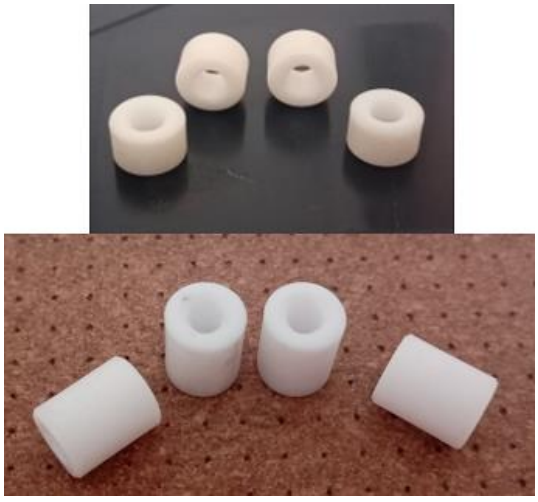

(c). Al Casings' Bolts.

(d). Teflon Spacers.

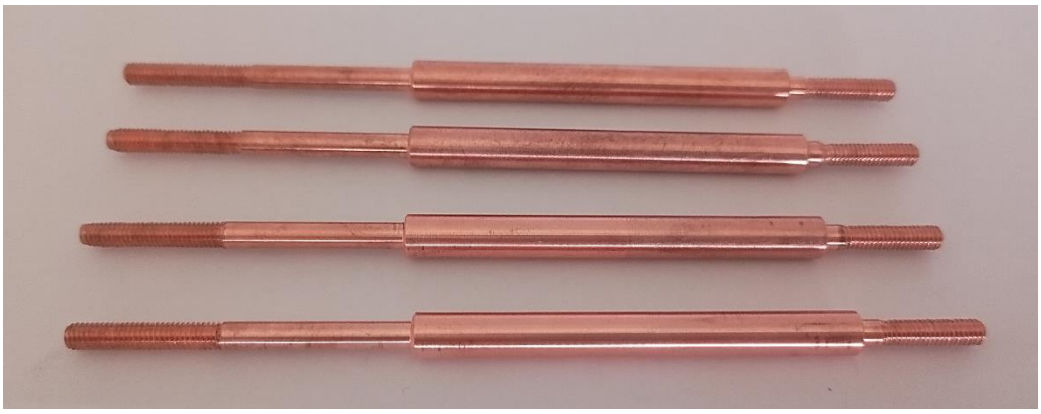

(e). Thermalization Rods.

Figure 7-6. *Prototyping via Conventional Manufacturing.*

7.3. Physical Assembly.

After the AM prototyping, the components are assembled to ensure the fulfillment of the assembly requirements. The physical assembly is carried out in two stages. In the first stage of assembly (***Figure 7-7***), some issues were observed regarding the assembly and some functional requirements, which were addressed successfully and prototyped subsequently. After the second stage of assembly (***Figure 7-8***), the physical assembly was performed successfully without any issue. In addition, the list of requirements is also modified with some additional requirements, as shown in ***Table 7-2***.

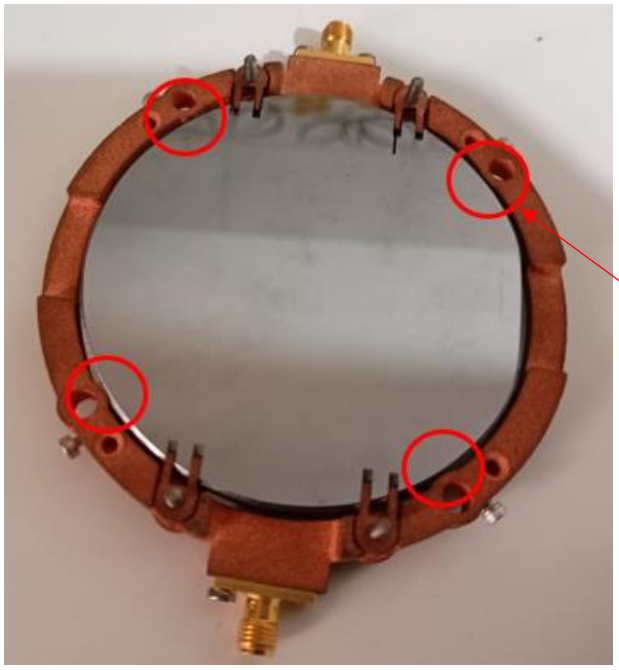

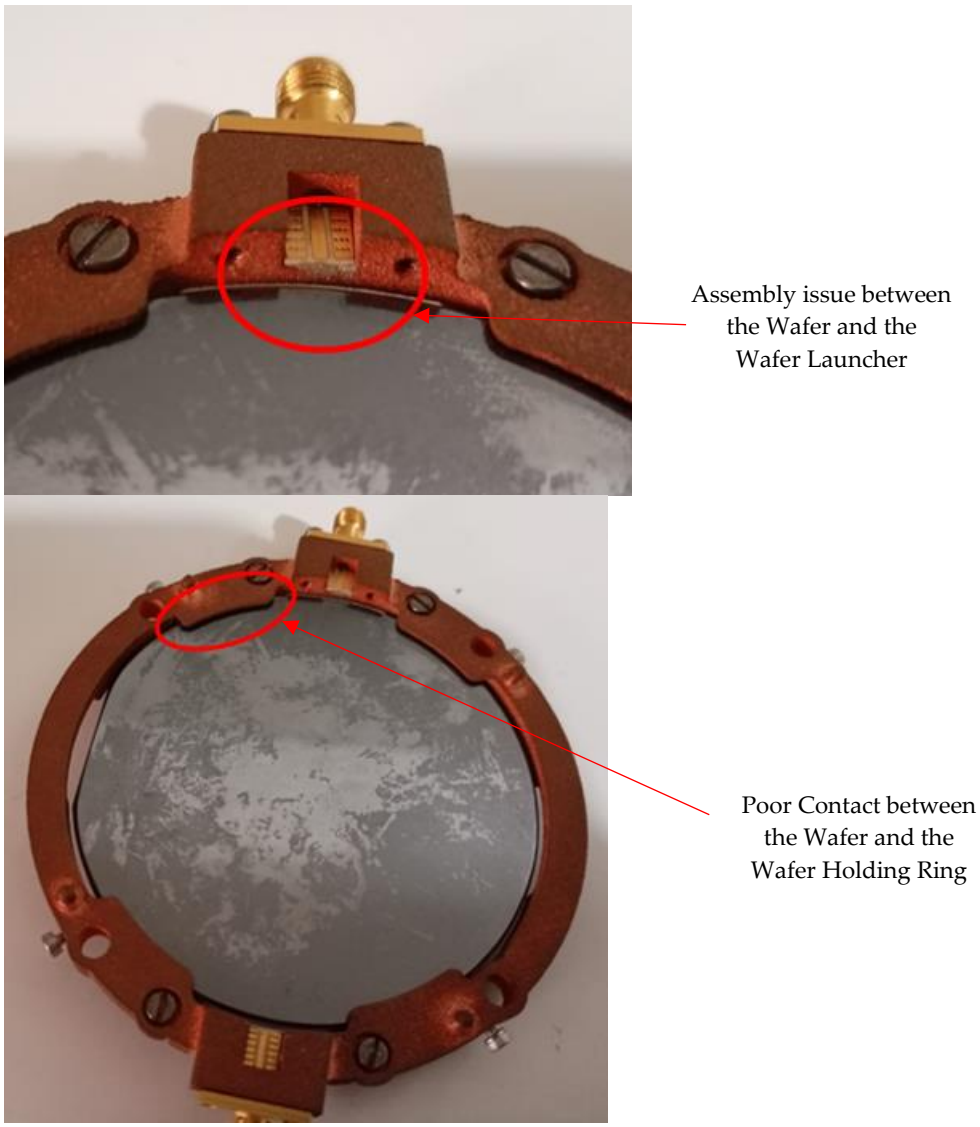

Figure 7-7. *First Stage of Physical Assembly.*

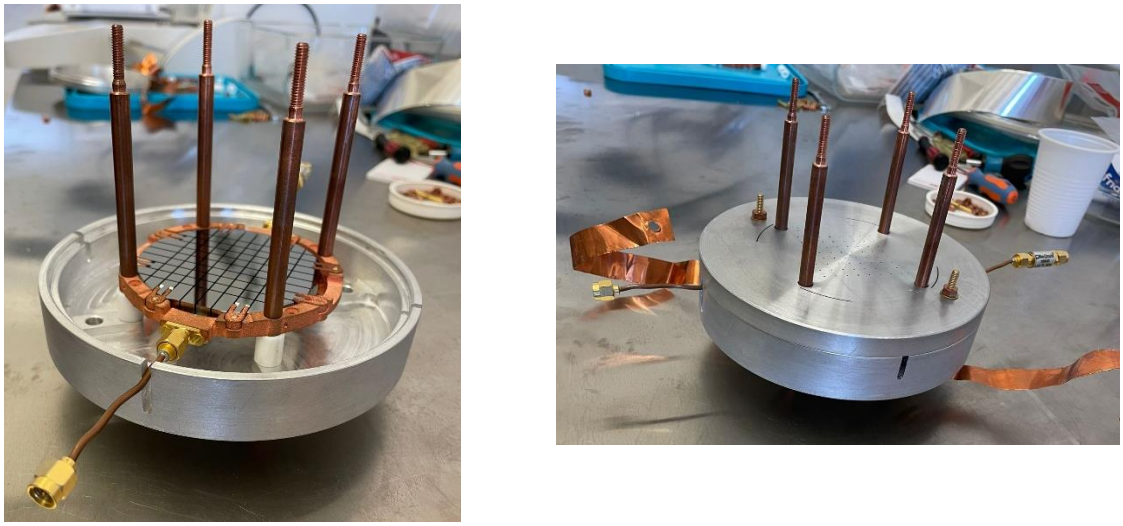

Figure 7-8. *Second Stage of Physical Assembly.*

Table 7-2. *Additional Requirements.*

Number	Requirements	Target Value
1	The new wafer holders should hold the wafer crystal utilizing its grooves with a **minimum tolerance/gap** on each side to facilitate the assembly and to allow a little rotation during the thermal contraction to avoid excessive thermal stresses.	≥ 0.2 mm
2	The top surfaces of both the wafer crystal and wafer launcher should be aligned within the **minimum tolerance**.	≤ 0.3 mm
3	Pin of the wafer connector should be in the **maximum longitudinal contact** with the wafer launcher	≥ 1.2 mm
4	The depth of the wafer launcher pocket should be **within the desired height** to facilitate the tip of the soldering machine.	≤ 3.3 mm
5	The AM can be carried out with the **pre-drilled holes** pertaining to threaded holes, and small geometrical fillets can be removed (wherever is required to facilitate the AM.	-
6	The **height of the wafer holing ring** should be adjusted in such a way to create a gap of 1.5mm between the two consecutive WA.	6.5mm
7	To ensure a flat contact between the wafer and the wafer holding ring, **thickness of the surface**, pertaining to wafer holding ring, which holds the wafer, should be increased by appropriate value, which will be machined later as a postprocessing step.	0.2mm

7.4. 3D Scanning of the Wafer Holding Ring.

After the first prototyping, 3D scanning of the wafer holding ring is carried out as a quality check of the AM process. The 3D model of the prototype is made with 3D scanning (reverse engineering techniques). The acquisition is made by a structured-light-based device, which consists of 253740 points, and tessellated to achieve a manifold stl model. The alignment with the reference CAD model shows a mean deviation 0.00±0.14 mm. ***Figure 7-9****a,b* shows the deviation analysis from the CAD model. Some negative geometrical deviations of about -0.4 to -0.2 mm are present, which highlights the distortion. In ***Figure 7-9****c* a check of cylindricity is made looking for an approximating cylinder passing through the holes. The approximating cylinder has an axis with an angle of 89,956 degrees from the base horizontal plane of the CAD model. This may be seen as a confirmation of a slight deviation, as already shown by the deviation analysis of ***Figure 7-9****a,b*. The 3D scanning concludes some geometrical deviations, details are given in the proceeding lines. However, these deviations are also observed during the physical assembly (as shown in ***Figure 7-10)***.

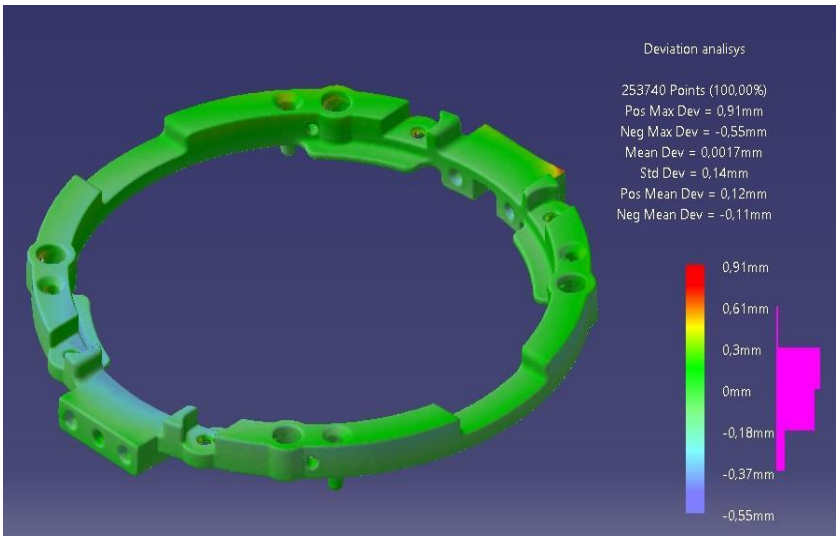

(a)

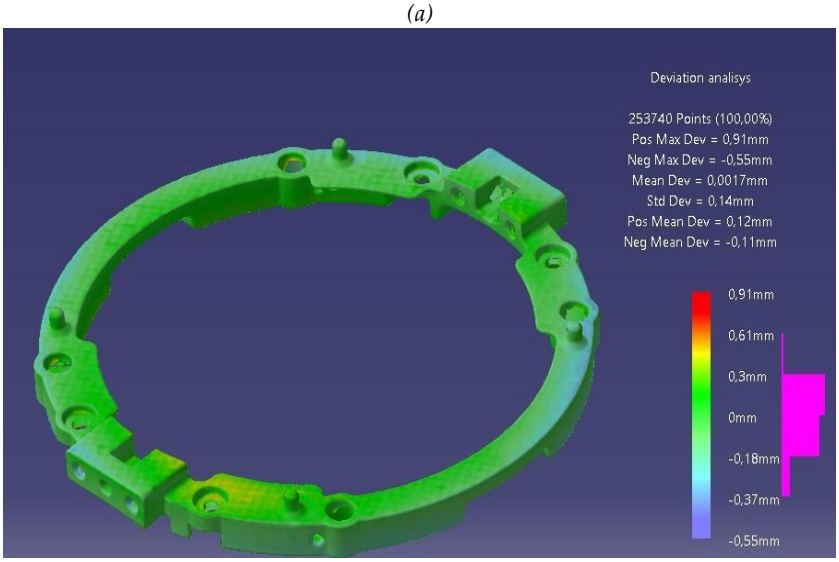

(b)

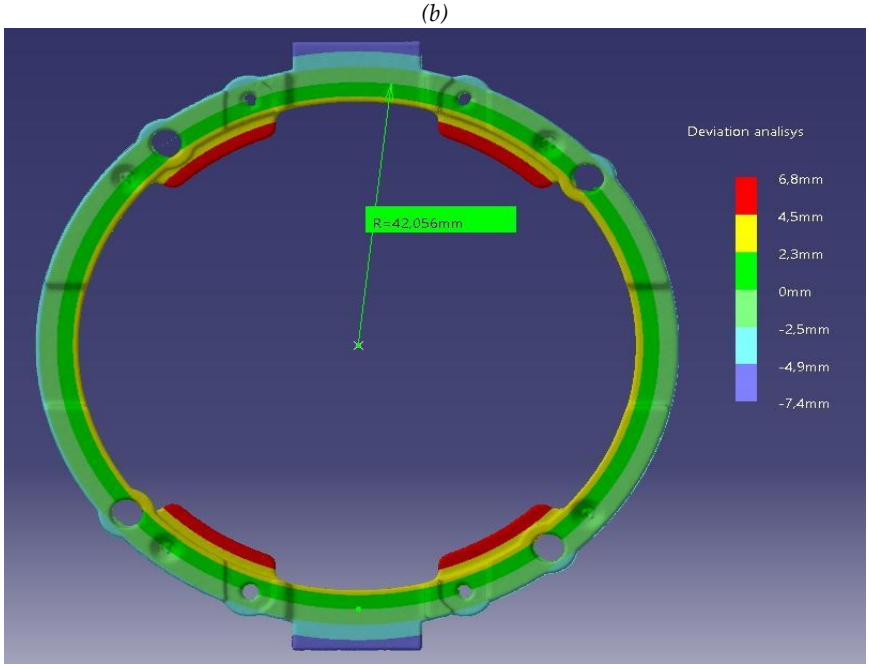

(c)

Figure 7-9. *Deviation Analysis from CAD Model.*

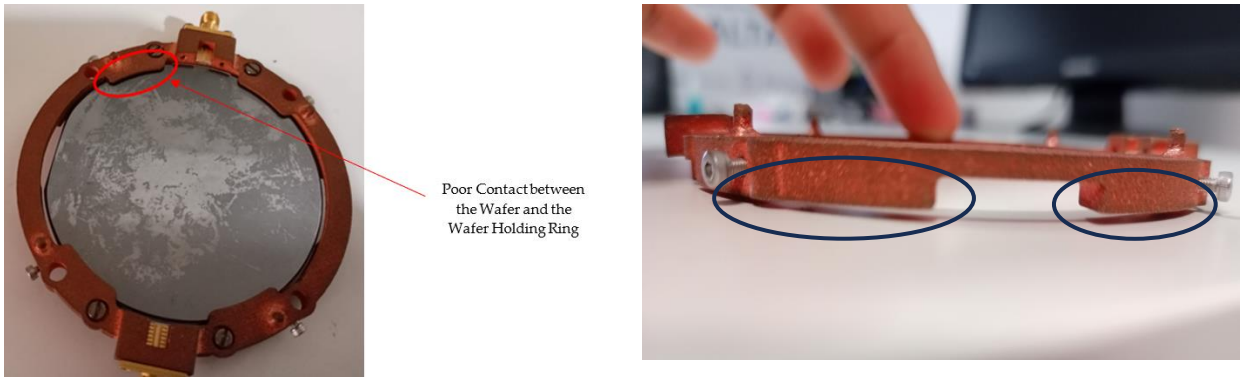

Figure 7-10. *Distortion Issues in the Physical Assembly.*

7.5. Physical Experimentation

The DA with a single wafer assembly has been successfully tested inside the experimental setup of cryostat by the physics department (Sapienza University of Rome) in January 2024. However, the DA with two and three wafer assemblies are in the pipeline for the subsequent and sequential physical testing, which is expected to be completed by the end of June 2024.

8. Chapter: Optimization Study via Lattice.

This chapter describes the design of the new design with lattice (design phase 2) under the prescribed design methodology in section 4.1. After the profound literature review, the TPMS lattice is selected for our test case study. The TPMS Gyroid is employed with a limited design space inside the wafer holding ring and subsequently investigated as a best application for the high-performance structures.

8.1. Design of the Lattice Structure.

In phase 1 of the design, we observed that it fulfilled all the requirements successfully related to design, functions, assembly, and even manufacturing. The design phase 1 was also validated numerically and then subsequently with the physical prototyping and assembly.

This is design phase 2, in which the TPMS lattice structure is designed and induced inside the wafer holding ring. This improvement is particularly interesting beyond the mechanical reason and also because it is lowering the mass to be cooled down thus increasing in that way the efficiency of the cryostat However, the assembly constraints don't provide enough room for the design space to facilitate the design of the lattice structure, therefore an appropriate design space is generated by modifying the design of the wafer holding ring, i.e. reducing the number of wafer holders from 8 to four (***Figure 8-1***). This modification also helps to reduce the number of assembly components.

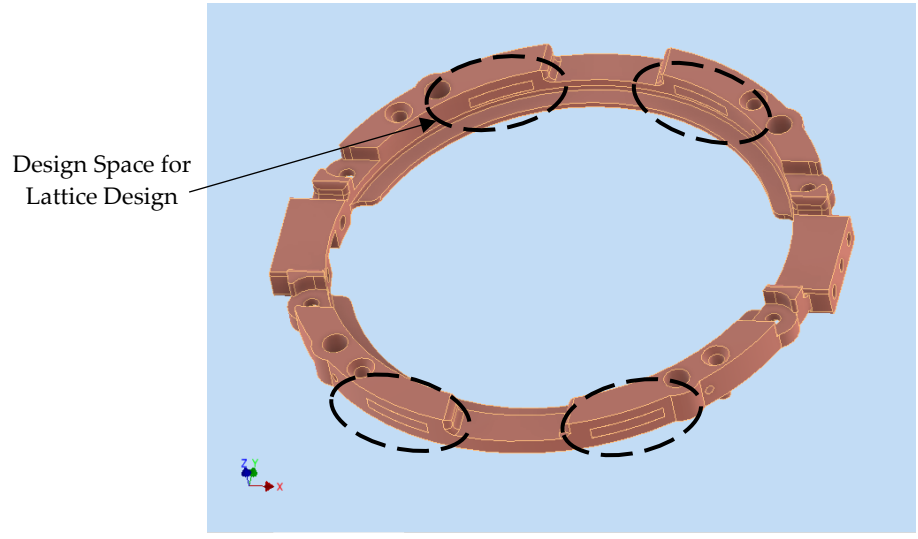

Figure 8-1. *Design Space for the Lattice Design.*

According to the literature review, the Triply Periodic Minimal Surface (TPMS) are being widely investigated. They are bio-inspired cells with boundary surfaces with zero-mean curvature at every point. TPMS are relevant as functionally graded structures, since their geometric characteristics allow them to reach different surface-related properties (e.g., manufacturability, fluid

permeability, electrical and thermal conductivity). In addition, TPMS is also ideal for the design of lightweight structures, structures with capability of energy absorption, efficient thermal structures, etc. Hence our case study pertains to these areas, therefore, TPMS gyroid (***Figure 8-2***) is employed and deeply investigated in accordance with the multi-physics issues to conclude that how it could contribute effectively to the design of a high-performance structure. The TPMS lattice structure is designed with the help of nTopology software, which is based on implicit modeling and uses a mathematical equation to generate the lattice structures. According to the workflow of the nTopology, the unit cell is defined with desired parameters and then mapped inside the design space, as shown in ***Figure 8-3.***

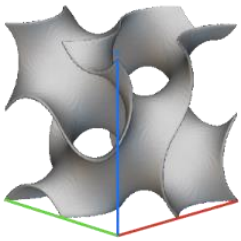

Figure 8-2. *TPMS Gyroid Lattice.*

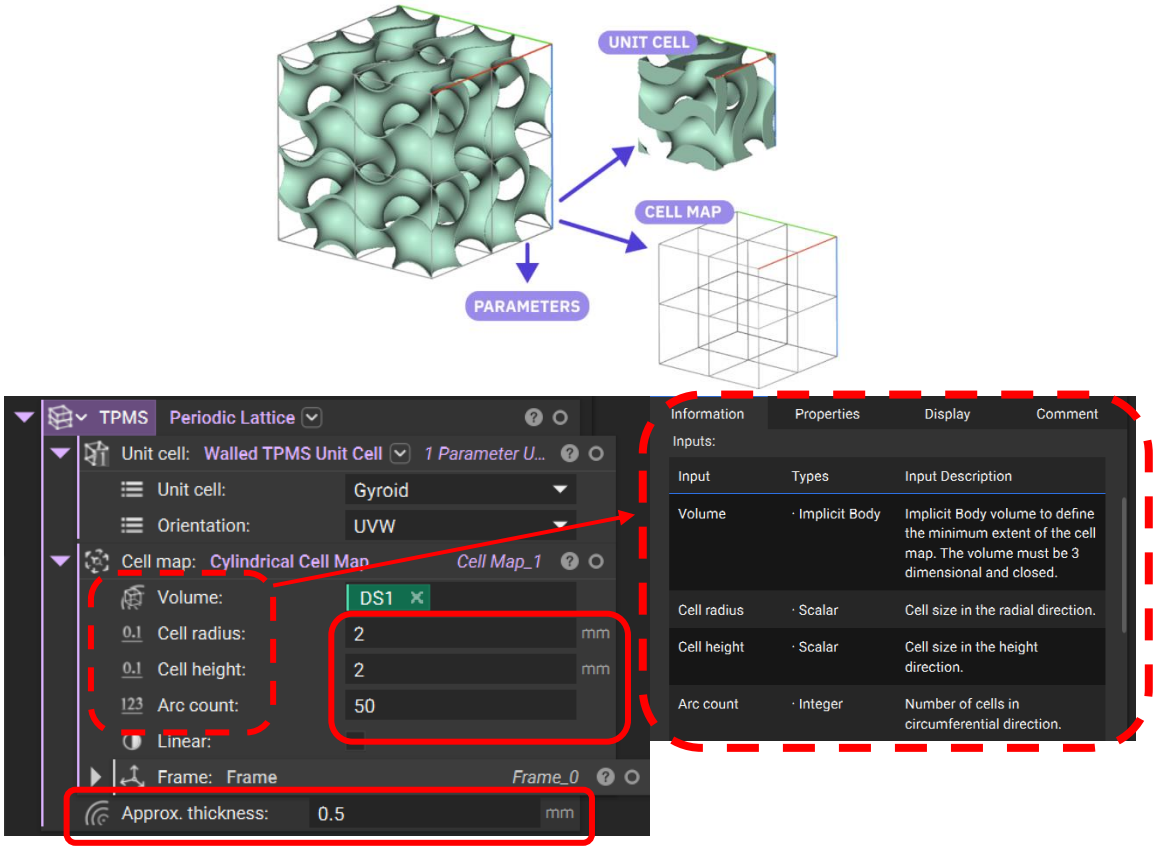

Figure 8-3. *Modeling of the TPMS Gyroid Lattice.*

The cell size of the TPMS gyroid is kept 2mm along the radial direction and 2mm along the height, with the wall thickness of 0.5mm (as shown in ***Figure 8-3).*** However, the cylindrical mapping is selected for the replication. Finally, by the Boolean operation we get the out final design, as shown in ***Figure 8-4.***

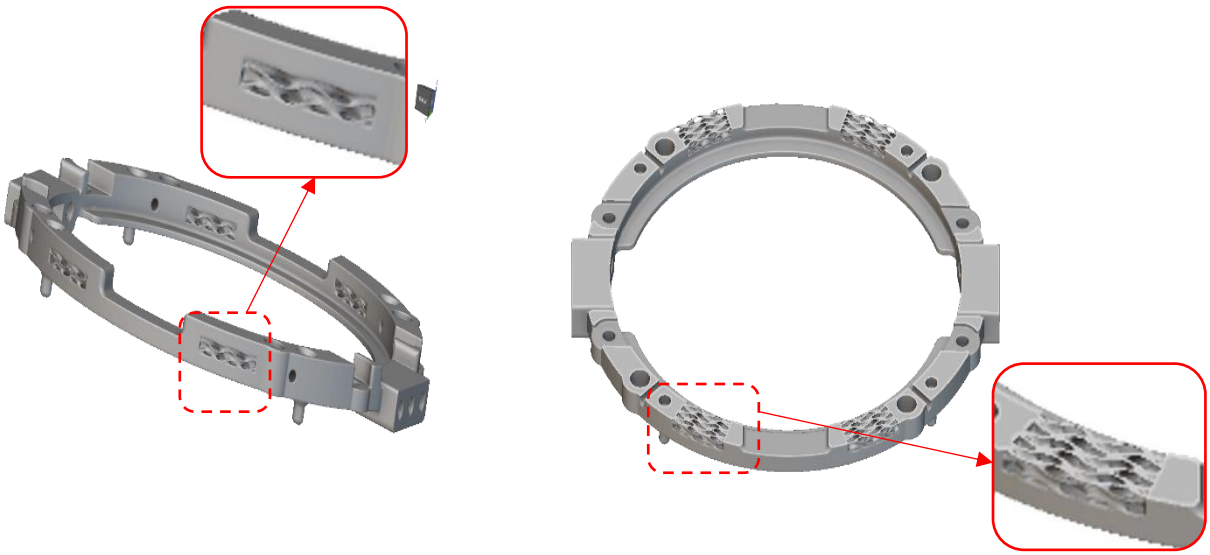

(a). 3D Model. *(b). Sectional View.*

Figure 8-4. *New Design with TPMS Lattice.*

8.2. FEA Simulations.

Hence the FEA simulation of the structures with lattice requires a huge virtual memory and computation time, therefore, we simplify our FEA model, and only the wafer holding ring and the thermalization rods are considered for the analysis (Figure 8-5). However, the effect of the structural weight of the excluded components is included in the simulations, in the same way as applied in the previous FEA simulations. The analysis of this structure will be carried out in the same order, starting from structural, to modal, to thermomechanical, and finally the transient thermal analysis. The loads and boundary condition are applied accordingly, as shown in Figure 8-5. The vector load of 4x1.91N is the cumulative effect of all the excluded components.

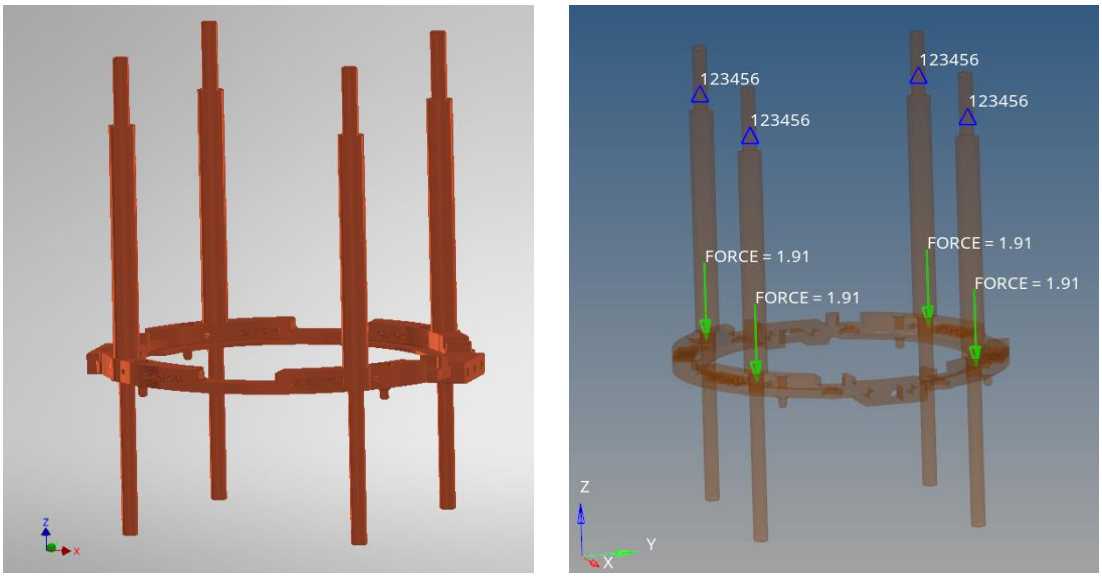

Figure 8-5. *FEA Model: New Design with Lattice.*

8.2.1. Structural Analysis

In this section, the structural analysis of the new design with TPMS lattice is carried out in accordance with the previous structural analysis (**section 6.5.1**). The final results are concluded based on the maximum Von Mises stress and the maximum displacement. The results of the linear static structural analysis are shown in ***Table 8-1*** and ***Figure 8-6***.

Table 8-1. *Results of Structural Analysis: New Design with Lattice.*

Component	Max. Displacement (mm)	Max. Von Mises Stress (Pa)	Factor of Safety
New DA Design (with Lattice)	0.00029	$1.68e^{6}$	>2

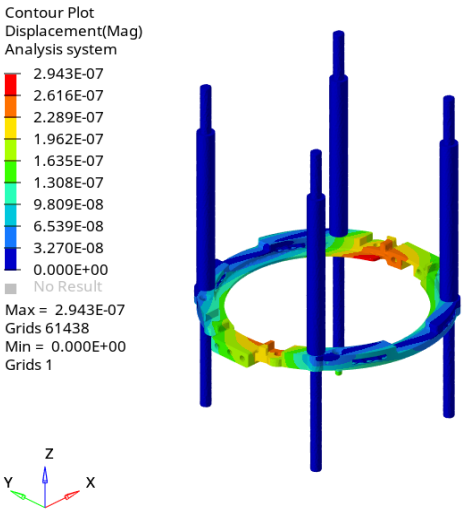

(c). Max. Displacement (m).

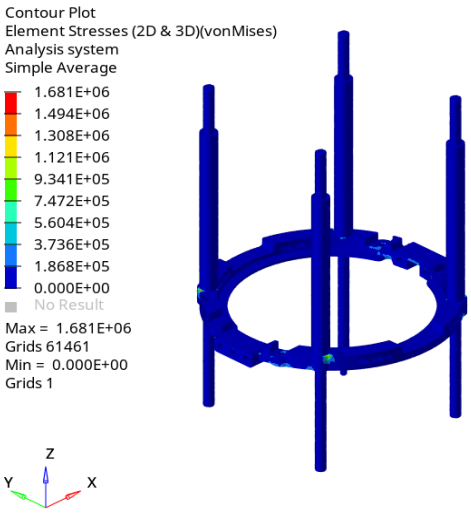

(d). Max. Von Mises Stress (Pa).

Figure 8-6. *FEA Results of the Structural Analysis: New Design with Lattice.*

The FEA results show that the TPMS lattice increases the stiffness of the structure and reduces the structural stresses as compared to the previous two cases.

8.2.2. Modal Analysis of the Lattice Structure

The modal analysis is of the new design with TPMS lattice is performed according to the conditions of section **section 6.5.2**. The results of the frequency range are shown in ***Table 8-2*** and ***Figure 8-7***. The results show that TPMS lattice improves the natural frequency range as compared to the previous two cases and thus improves the overall structural integrity in terms of the stiffness.

Table 8-2. *Results of Modal Analysis: New Design with Lattice.*

Natural Frequency (Hz)	Mode Number									
	1	**2**	**3**	**4**	**5**	**6**	**7**	**8**	**9**	**10**
New DA with Lattice	376.6	412.8	495	771.9	800.6	822.4	824.3	828	955.5	956.5

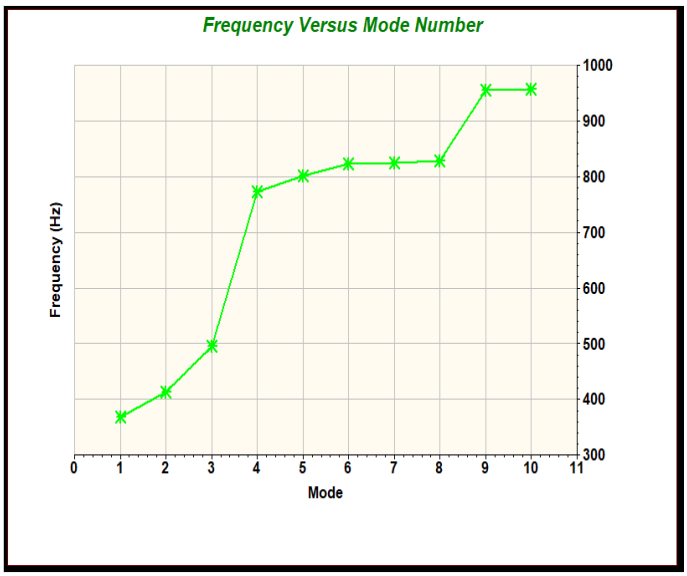

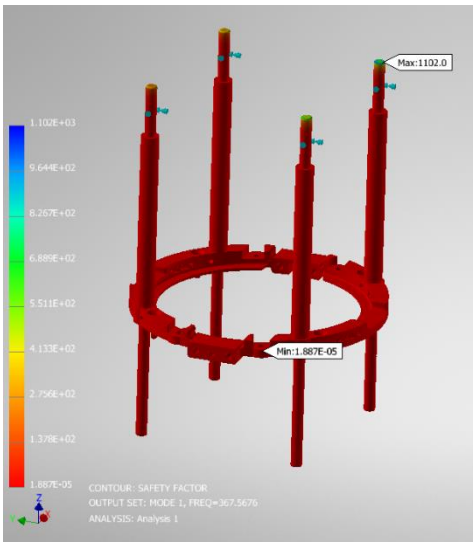

Natural Frequency Range (Hz).

Figure 8-7. *FEA Results of the Modal Analysis: New Design with Lattice.*

8.2.3. Thermomechanical Analysis of the Lattice Structure

Thermomechanical analysis is also performed according to the steps that were followed in **section 6.5.3**. The results are shown in ***Table 8-3*** and ***Figure 8-8***. Even the thermomechanical results conclude that the employment of TMPS lattice improve the structural integrity against the thermal stresses, and due to its flexibility, it absorbs the maximum strain energy during the contraction at cryogenic temperature and minimizes the overall stresses in the structure.

Table 8-3. *Thermomechanical Analysis.*

Component	Max. Displacement (mm)			Max. Von Mises Stress (Pa)	Factor of Safety
	x-axis	y-axis	z-axis		
Wafer Holding Ring	0.22	0.2	0.55	387e^{6}	> 2

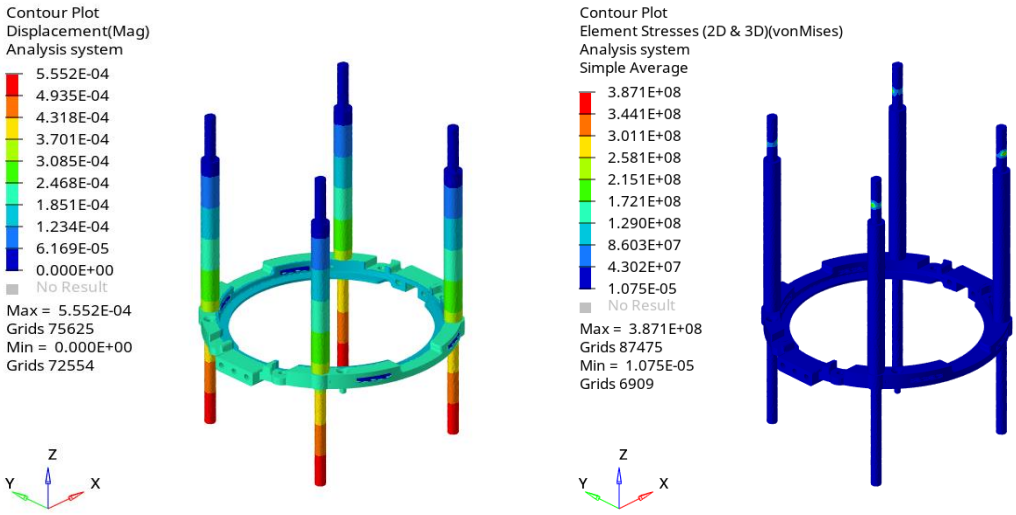

Max. Displacement (m) *Max. Von Mises Stress (Pa)*

Figure 8-8. *FEA Results of the Thermomechanical Analysis: New Design with Lattice.*

8.2.4. Transient Analysis of the Lattice Structure

The transient analysis is carried out on the same parameters as the conducted in **section 6.5.4**. The results are shown in ***Figure 8-9***. Like the previous analysis, several results are collected at the same intervals. The results show that the structure achieves the desired temperature of -273^{0}C at 850 seconds.

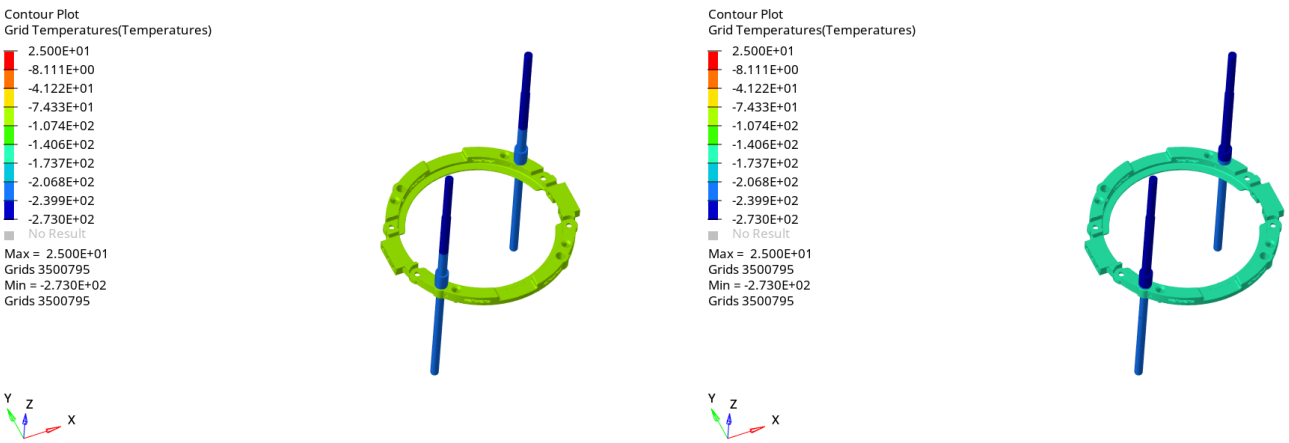

At 200 seconds At 400 seconds

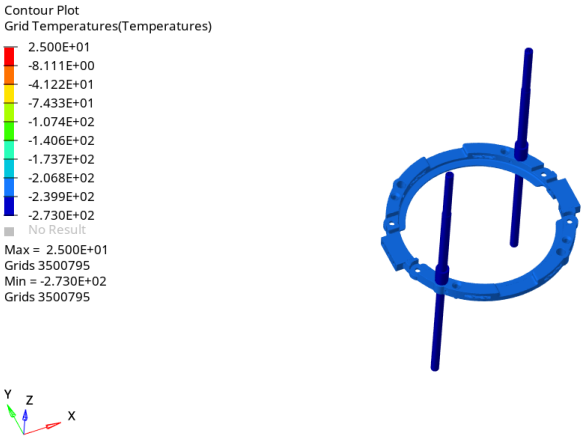

At 600 seconds

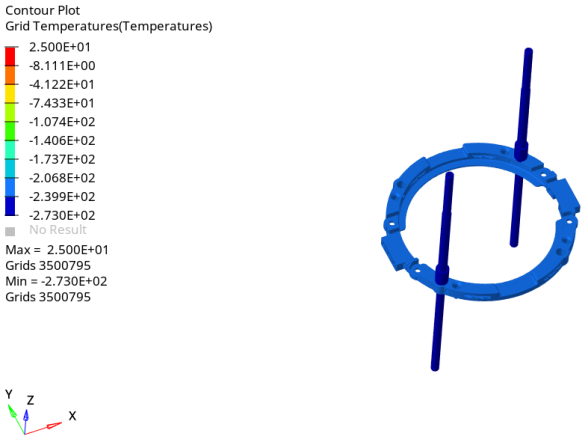

At 800 seconds

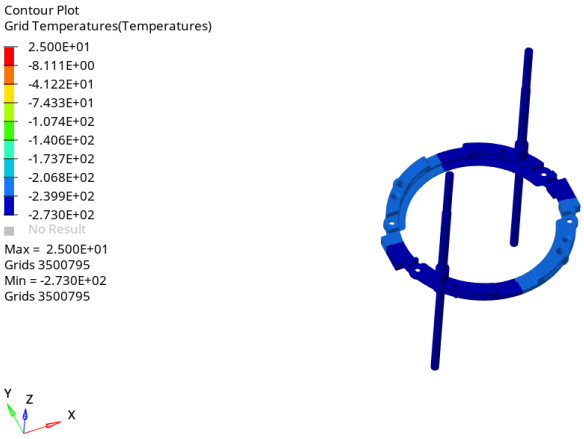

At 820 seconds

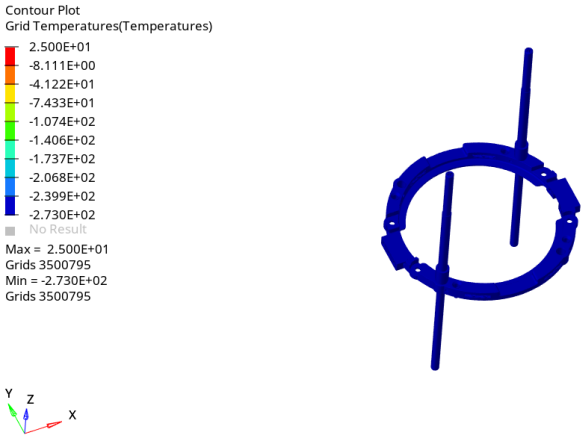

At 850 seconds

Figure 8-9. *Results of Transient Thermal Analysis.*

9. Chapter: Results & Discussion, Conclusions & Future Work.

In this chapter, the all the FEA results are summarized and discussed to conclude the structural performance. Subsequently, the conclusion and the future work are presented at the end of this chapter.

9.1. Results and Discussion.

In this section, the FEA results of the structural, modal, and thermal analysis of all the three designs are summarized for the comparison and final conclusions. The comparison in this section is mainly based on the maximum Von Mises stress. However, the natural frequencies, mass comparison, and thermal performances are also discussed to gauge the overall efficacy of all the three designs.

9.1.1. Comparison of the Structural Analysis.

Table ***9-1*** **and** ***Figure 9-1,*** summarize the maximum Von Mises stress results of all the three designs pertaining to structural analysis, and it is concluded that all the designs are within the safe zone but among them, the new DA design with the TPMS lattice has the lowest stress value, which means that it has improved the structural stiffness effectively.

Table 9-1. *Structural Analysis: Comparison of the Results.*

Design Details	Max. Von Mises Stress (MPa)	Factor of Safety
Original DA	82.8	> 1.8
New DA (without Lattice)	6.47	> 2
New DA (with Lattice)	1.68	> 2

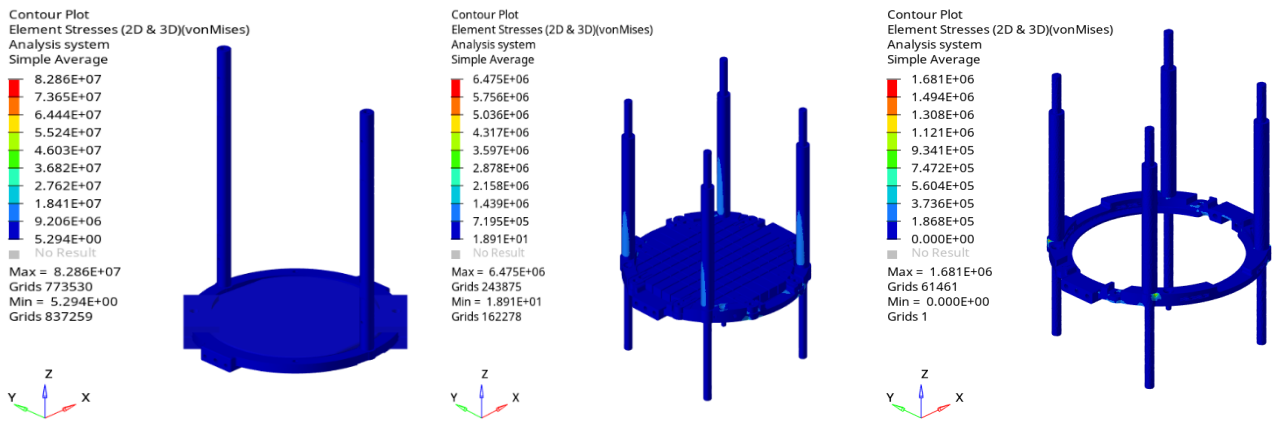

(a). The Original Design. *(B). New Design without Lattice* *(C). New Design with Lattice*

Figure 9-1. *Structural Analysis: Comparison of the Results.*

9.1.2. *Comparison of the Modal Analysis.*

Table 9-2 and ***Figure 9-2*** summarize the range of the first 10 natural frequencies related to the modal analysis. The low natural frequency means that the structure is susceptible to vibrational failure. It can be seen from the table that both the new designs increase the natural frequencies, which means that the new designs are safer than the original one against the mechanical vibrations. But among them, the new DA design without lattice provides higher natural frequencies. The result of the modal analysis shows that during the first 4 modes (i.e. the first three bending moments and then subsequent torsion), the new designs of the DA has improved the natural frequencies significantly, but after, the original DA has the higher natural frequencies. However, we are more interested in the first natural frequency due to the fact that the experimental device is operated at a frequency of 1.3 Hz, so from the operational point of view all the designs are ok, but during the transportation due to the high mechanical vibrations the frequency arrives up to 66Hz, due to which the original design has been reported several times with structural failures/damages, hence its first natural frequency is less than 66Hz. However, the first frequencies of the new designs are much higher than 66Hz, therefore, the new designs provides a much higher factor of safety to the DA during transportation.

Table 9-2. *Modal Analysis: Comparison of the Results.*

	Design	**Mode Number**									
		1	**2**	**3**	**4**	**5**	**6**	**7**	**8**	**9**	**10**
Natural Frequency (Hz)	Original DA	62.35	110.4	162	289.8	824	1209	1281.6	1286.5	1342.5	1682.2
	New DA without Lattice	341	341.6	465.5	804.2	805.7	817	818.4	819.5	880.3	880.6
	New DA with Lattice	376.6	412.8	495	771.9	800.6	822.4	824.3	828	955.5	956.5

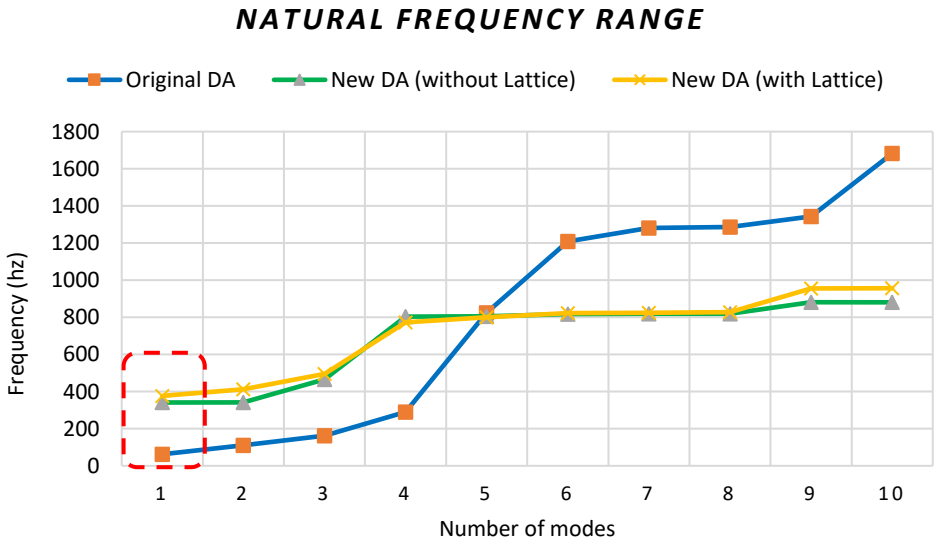

Figure 9-2. *Modal Analysis: Comparison of the Results.*

9.1.3. *Comparison of the Thermomechanical Analysis.*

Table 9-3 and ***Figure 9-3*** makes a comparison among the designs against the thermomechanical analysis. It can be clearly seen that the new DA design with TPMS exhibits outstanding results in the cryogenic thermal environment in terms of the lowest thermal stress value. It concludes that TPMS could be effectively utilized in the application of cryogenic structures. However, the original design has a very high thermal stress and therefore prone to structural failure, and from ***Table 6-8*** it is evident that it will have a structural collapse at in the wafer holding ring.

Table 9-3. *Thermomechanical Analysis: Comparison of the Results.*

Design Details	Max. Von Mises Stress (MPa)	Factor of Safety
Original DA	959	< 0.5
New DA (without Lattice)	501	> 2
New DA (with Lattice)	387	> 2

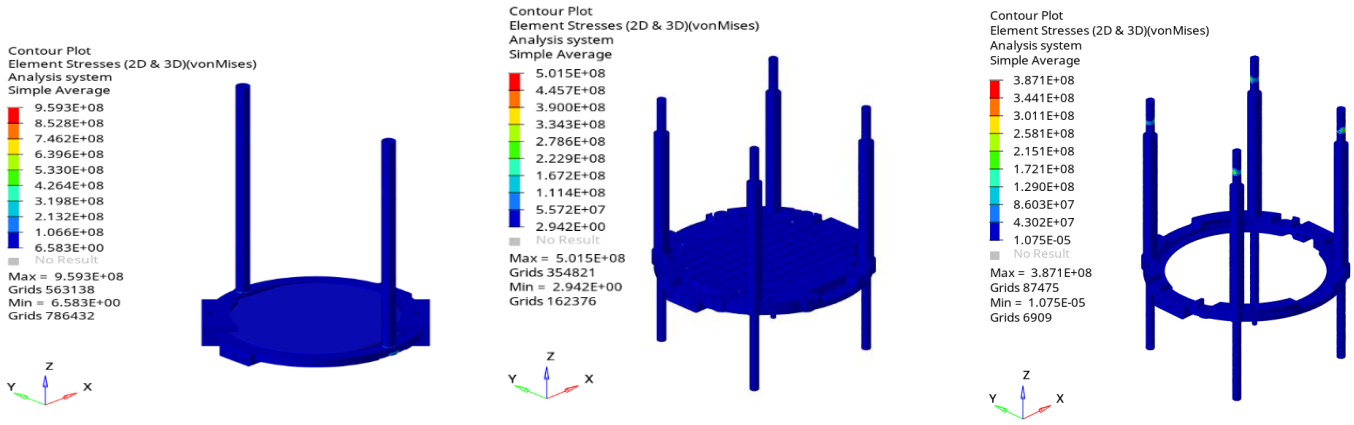

(a). The Original Design. *(B). New Design without Lattice* *(C). New Design with Lattice*

Figure 9-3. *Thermomechanical Analysis: Comparison of the Results.*

9.1.4. *Comparison of the Transient Thermal Analysis.*

Figure 9-4 provides very interesting results related to the transient thermal analysis. All the temperature records pertaining to all three designs are taken at the time interval of 800 seconds. The given figures show the thermal efficiency of the relevant design. Among them, the new DA design without lattice exhibits outstanding thermal performance and it achieves the desired temperature of -273^{0}C at the given time interval. However, at the same interval, the approximate temperature of the original Da design is -206^{0}C, while the new Da design with lattice is approximately -240^{0}C, which is somehow mid of the other two temperatures. It concludes that the new DA design without lattice is the most efficient thermal design. However, in the very limited design space, the TPMS

lattice has still performed very well and finally achieves the desired temperature of -273 at 850 sec.

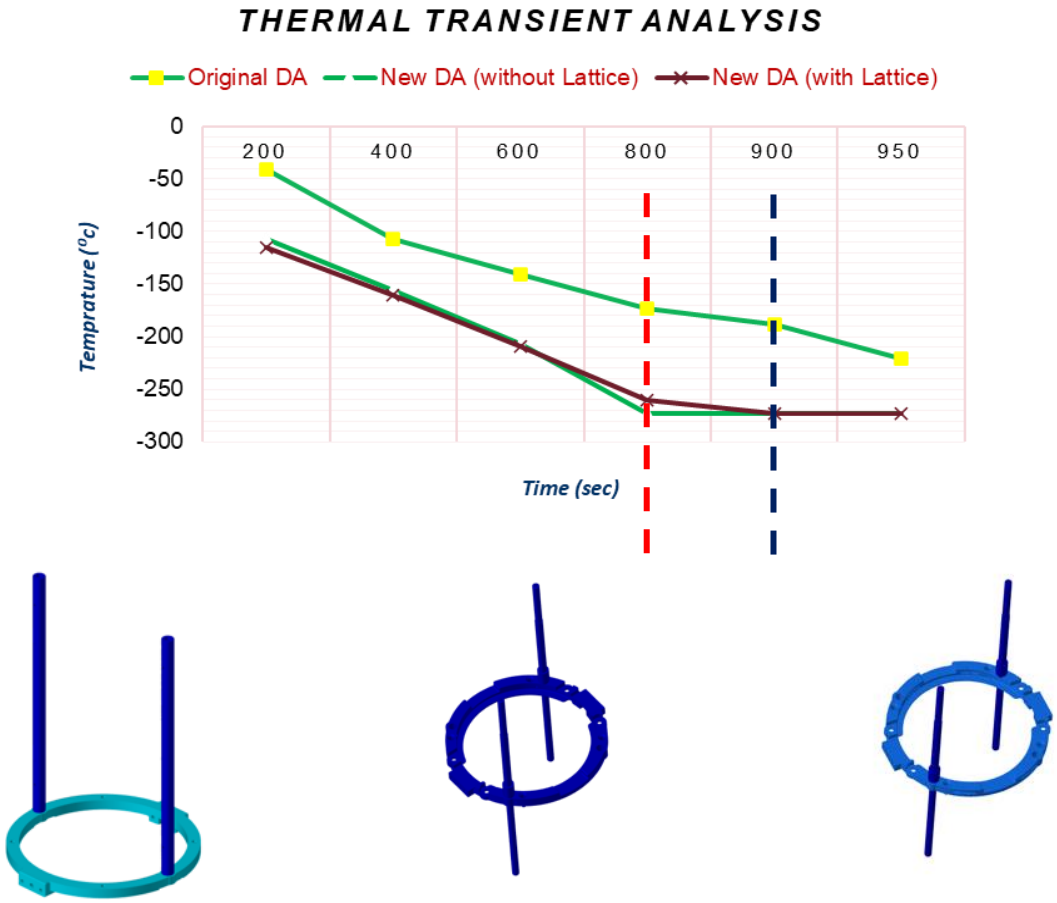

(a). The Original Design. *(B). New Design without Lattice* *(C). New Design with Lattice*

Figure 9-4. *Thermal Transient Analysis: Comparison of the Results @ 850 Sec.*

9.1.5. Comparison of Total Mass.

Table 9-4 and ***Figure 9-5*** represent a comparison among the masses of the three designs. Technically, the difference in the DA with single WA is minimal but for more than one WA, both the new designs are efficient, for example for the DA with three WAs, the design without lattice reduced the overall mass by 54.56% and the design with lattice has reduced the total mass by 55.31%. Which concludes that if we increase the design space for the induction of lattice structure then we can further reduce the overall mass of the DA.

Table 9-4. *Comparison of Total Mass.*

Design	Mass (kg) of Sub-Assemblies			Total Mass (kg) of DA with Single WA	Total Mass (kg) of DA with Three WAs	Mass Reduction in %
	Aluminium Casing Assembly	Wafer Assembly	Thermalization Rods			
Original Design	0.626	0.159	0.58	0.842	2.41	-
New Design without Lattice	0.652	0.139	0.26	0.817	1.095	**-54.56**
New Design Lattice	0.652	0.133	0.26	0.811	1.077	**-55.31**

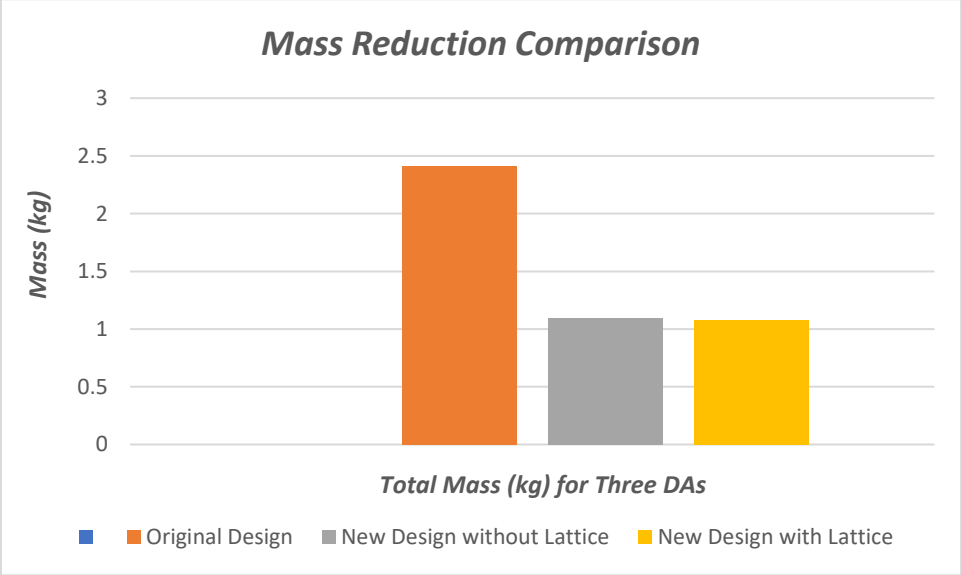

Figure 9-5. *Comparison of Total Mass.*

9.2. Conclusions

The proposed design is initially validated through numerical simulations (structural, modal, and thermomechanical analysis), and virtual 3D CAD assembly. However, it is also physically validated through prototyping and subsequent experimental tests. In addition, 3D scanning of the additively manufactured components is also performed through the reverse engineering technique of photogrammetry, as a quality check of the AM process, and it is concluded that it could be effectively used to analyze the geometrical features of the components being produced via AM.

In conclusions:

- The proposed design successfully supports up to three detector assemblies. It also reduced the structural weight, mechanical vibrations, and improved thermal efficiency, as warranted by the design requirements.

- The new designs were found up to the mark and they fulfilled all the requirements. However, due to the structural and assembly constraints, the design space provided for the design of TPMS lattice was very small, but still in this limited design space the TPMS lattice exhibited tremendous performance to improve the overall structural integrity; it helped to reduce the structural weight, reduce the assembly components, increase the structural stiffness against the mechanical vibrations, and improve the structural thermal efficiency at cryogenic temperature. Therefore, it is concluded that the TPMS lattice is significantly useful and could be efficiently used in high-performance structures such as cryogenic structures. In addition, the hexagonal lattice structure also facilitated the AM for the manufacturing support structure.

- The proposed design-development workflow facilitated the entire CAD-CAE processes with continuous improvements based on the feedback received time to time from different outputs such as manufacturing, assembly, and further requirements by the stakeholders. The list of requirements was also found significantly useful while pursuing the entire product development process. This workflow also helped to translate the list of requirements successfully into the design, manufacturing, and assembly phases, and thus it coupled efficiently the design process with the manufacturing and assembly, to fulfil all the requirements (imposed by the list of requirements). It was also concluded that the proposed workflow pushed every process to achieve the desired target values.

- The AM also provided a great support to develop the complex topologies of the wafer holding ring with its limited working cylinder. It also provided the design flexibility to facilitate the new design with complex geometry, in particular the TPMS lattice.

9.3. Future Work

The current research work has the capacity to be extended and further improved. In this regard, the following activities are suggested as future research work.

- The volume of the wafer holding ring can be increased to generate a larger design space for the employment of lattice structure and then investigate the structural performance.

- In the case of larger volume, topology optimization can be used to define the optimal design space for the design of the lattice structure.

- Other types of TPMS, as well as hybrid lattice can also be introduced for further investigations.

- The proposed design can be developed with an AM machine having a larger diameter of the working cylinder to reduce the efforts for the design of the build direction and support structure, and further investigate the structural performance.

List of Figures

Figure 1-1. *Cellular Structures.* *1*

Figure 1-2. *Classification of Lattice Structure.* *3*

Figure 1-3. *Beam Lattice (generated with nTop).* *4*

Figure 1-4. *Surface-based Lattice (generated with nTop).* *5*

Figure 1-5. *Examples of Regular Replication Patterns (generated with nTop).* *7*

Figure 1-6. *Examples of Hybrid Replication Patterns: Unit Cells Variation (generated with nTop).* *7*

Figure 1-7. *Examples of Pseudo-regular Pattern Replications (generated with nTop).* *8*

Figure 1-8. *Examples of Stochastic Replication Patterns (generated with nTop).* *9*

Figure 1-9. *Query Results from Scopus.* *12*

Figure 3-1. *Original 3D Design of the Detector Assembly.* *28*

Figure 3-2. *DA inside the Cryogenic System.* *29*

Figure 3-3. *Electronics of the Detector Holder.* *30*

Figure 3-4. *Details of the Stakeholders.* *30*

Figure 4-1. *Heat Conduction.* *33*

Figure 4-2. *Free Vibration.* *33*

Figure 4-3. *Workflow.* *35*

Figure 4-4. *Design Details of the New Design.* *37*

Figure 4-5. *Manufacturing Details of the New Design.* *37*

Figure 5-1. *Optimized Design of the Wafer Holding Ring.* *39*

Figure 5-2. *Optimized Design of the Wafer Holders.* *41*

Figure 5-3. *Optimized Design of the Thermalization Rods.* *42*

Figure 5-4. *Optimized Design of the Lower Al Casing.* *43*

Figure 5-5. *Optimized Design of the Upper Al Casing.* *45*

Figure 5-6. *Optimized Design of the Al Casings' Bolt.* *45*

Figure 5-7. *Details of the Cryogenic Device Mounting Plates.* *46*

Figure 5-8. *Design Modification of the Cryogenic Device Mounting Plates.* *47*

Figure 5-9. *Assembly Workflow.* *48*

Figure 5-10. *Wafer Assembly.* *48*

Figure 5-11. *DA Stage-1.* *50*

Figure 5-12. *DA Stage-2.* *51*

Figure 5-13. *Final Assembly-Exploded View.* *51*

Figure 5-14. *Final Assembly: Stage 1.* *52*

Figure 5-15. *Teflon Spacers.* *53*

Figure 5-16. *DA Stage-1-Exploded View.* *53*

Figure 5-17. *Final Assembly: Stage 2.* *55*

Figure 6-1. *FEA Workflow.* *56*

Figure 6-2. *2D and 3D Meshing Details.* *58*

Figure 6-3. *Mesh Quality Criterion and Failure Check.* 59
Figure 6-4. *Load and Boundary Condition for Structural and Modal Analysis.* 60
Figure 6-5. *Structural Analysis: Applying the Loads and Boundary Conditions* 63
Figure 6-6. *FEA Results of the Structural Analysis.* 64
Figure 6-7. *Modal Analysis: Activation of EIGRL Card* 64
Figure 6-8. *FEA Results of the Modal Analysis* 65
Figure 6-9. *Thermomechanical Analysis: Coupling the Thermal Load Case with Structural Load Step.* 66
Figure 6-10. *FEA Results of the Thermomechanical Analysis: Original DA Design* 68
Figure 6-11. *FEA Results of the Thermomechanical Analysis: New DA Design* 70
Figure 6-12. *Transient Thermal Analysis: Temp-Time Curve* 71
Figure 6-13. *Transient Thermal Analysis Setup.* 71
Figure 6-14. *Results of Transient Thermal Analysis: Original DA on the left side; New DA on the right side.* 73
Figure 7-1. *AM (SLM) Mahine: SISMA MYSINT100 PM/RM.* 75
Figure 7-2. *AM (via SLM).* 76
Figure 7-3. *Postprocessing through Sand Blasting Machine.* 77
Figure 7-4. *First Prototyping Via AM (SLM).* 78
Figure 7-5. *Subsequent Prototyping via AM (SLM).* 79
Figure 7-6. *Prototyping via Conventional Manufacturing* 81
Figure 7-7. *First Stage of Physical Assembly.* 82
Figure 7-8. *Second Stage of Physical Assembly.* 82
Figure 7-9. *Deviation Analysis from CAD Model.* 84
Figure 7-10. *Distortion Issues in the Physical Assembly* 85
Figure 8-1. *Design Space for the Lattice Design.* 86
Figure 8-2. *TPMS Gyroid Lattice.* 87
Figure 8-3. *Modeling of the TPMS Gyroid Lattice.* 87
Figure 8-4. *New Design with TPMS Lattice.* 88
Figure 8-5. *FEA Model: New Design with Lattice.* 89
Figure 8-6. *FEA Results of the Structural Analysis: New Design with Lattice.* 90
Figure 8-7. *FEA Results of the Modal Analysis: New Design with Lattice.* 90
Figure 8-8. *FEA Results of the Thermomechanical Analysis: New Design with Lattice.* 91
Figure 8-9. *Results of Transient Thermal Analysis.* 92
Figure 9-1. *Structural Analysis: Comparison of the Results.* 93
Figure 9-2. *Modal Analysis: Comparison of the Results.* 94
Figure 9-3. *Thermomechanical Analysis: Comparison of the Results.* 95
Figure 9-4. *Thermal Transient Analysis: Comparison of the Results @ 850 Sec.* 96
Figure 9-5. *Comparison of Total Mass.* 97

List of Tables

Table 1-1. *Applications of Lattice Structures by Field of Expertise.* *13*
Table 2-1. *Overview of the Lattice Structures via Traditional Manufacturing Methods.* *19*
Table 2-2. *Overview of the Lattice Structures via Additive Manufacturing (AM) Methods.* *20*
Table 2-3. *3D CAD Modelling of Lattice Structures.* *21*
Table 3-1. *Case Study: Assembly Details.* *28*
Table 4-1. *List of Requirements.* *31*
Table 4-2. *Case Study: Material Properties.* *34*
Table 4-3. *Case Study: DA Mass Details.* *34*
Table 5-1. *Mass Details of the New DA (without Lattice).* *55*
Table 6-1. *Material Properties.* *57*
Table 6-2. *DA Assembly Details by Material.* *57*
Table 6-3. *Meshing Details.* *58*
Table 6-4. *Loads and Boundary Conditions.* *60*
Table 6-5. *Details of Contact Surfaces.* *60*
Table 6-6. *Results of Structural Analysis.* *63*
Table 6-7. *FEA Results of the Modal Analysis.* *65*
Table 6-8. *Thermomechanical Analysis of the Original DA Design.* *67*
Table 6-9. *Thermomechanical Analysis of the New DA Design.* *68*
Table 7-1. *AM (SLM) Process Parameters.* *76*
Table 7-2. *Additional Requirements.* *83*
Table 8-1. *Results of Structural Analysis: New Design with Lattice.* *89*
Table 8-2. *Results of Modal Analysis: New Design with Lattice.* *90*
Table 8-3. *Thermomechanical Analysis.* *91*
Table 9-1. *Structural Analysis: Comparison of the Results.* *93*
Table 9-2. *Modal Analysis: Comparison of the Results.* *94*
Table 9-3. *Thermomechanical Analysis: Comparison of the Results.* *95*
Table 9-4. *Comparison of Total Mass.* *97*

List of Symbols and Acronym

3D:	3 Dimensional.	**TPMS:**	Triply Periodic Minimal Surface.
FCC:	Face-centered Cubic.	**BCC:**	Body-centered Cubic.
FCCZ:	Face-centered Cubic with z-strut.	**BCCZ:**	Body-centered Cubic with z-strut.
AM:	Additive Manufacturing.	**TO:**	Topological Optimization.
CAD:	Computer Aided Design.	**DH:**	Detector Holder.
Al:	Aluminium.	**B-Rep:**	Boundary Representation.
FEA:	Finite Element Analysis.	**SLM:**	Selective Laser Melting.
DA:	Detector Assembly.	**WA:**	Wafer Assembly.
TPMS:	Triply Periodic Minimal Surface.	**CAE:**	Computer Aided Engineering.
ICM:	Implicit CAD Modeling.	**FFD:**	Free Form Deformation.
TCD:	Twin Curve Division Method.	**AD:**	Arc Division Method.
CD:	Curvature Division Method.	**NURBS:**	Non-Uniform Rational B-Splines
NFFD:	NURBS Free Form Deformation Method.	**B-Splines:**	Basis Splines.